FABRICATION AND CHARACTERIZATION OF NANO-TiO_2 THIN FILMS FROM LOCAL MINERAL PRECURSORS

MAHDI EZWAN MAHMOUD

DISSERTATION SUBMITTED IN FULFILLMENT OF THE REQUIREMENTS FOR THE DEGREE OF MASTER OF ENGINEERING SCIENCE

FACULTY OF ENGINEERING
UNIVERSITY OF MALAYA
KUALA LUMPUR
APRIL 2012

UNIVERSITI MALAYA

ORIGINAL LITERARY WORK DECLARATION

Name of Candidate: MAHDI EZWAN MAHMOUD (I.C/Passport No:

Registration/Matric No: KGA100070

Name of Degree: MASTERS OF ENGINEERING SCIENCE

Title of Project Paper/Research Report/Dissertation/Thesis ("this Work"):

FABRICATION AND CHARACTERIZATION OF NANO-TiO2 THIN FILMS FROM LOCAL MINERAL PRECURSORS

Field of Study:

I do solemnly and sincerely declare that:

(1) I am the sole author/writer of this Work;
(2) This Work is original;
(3) Any use of any work in which copyright exists was done by way of fair dealing and for permitted purposes and any excerpt or extract from, or reference to or reproduction of any copyright work has been disclosed expressly and sufficiently and the title of the Work and its authorship have been acknowledged in this Work;
(4) I do not have any actual knowledge nor do I ought reasonably to know that the making of this work constitutes an infringement of any copyright work;
(5) I hereby assign all and every rights in the copyright to this Work to the University of Malaya ("UM"), who henceforth shall be owner of the copyright in this Work and that any reproduction or use in any form or by any means whatsoever is prohibited without the written consent of UM having been first had and obtained;
(6) I am fully aware that if in the course of making this Work I have infringed any copyright whether intentionally or otherwise, I may be subject to legal action or any other action as may be determined by UM.

Candidate's Signature Date 14 SEPTEMBER 2012

Subscribed and solemnly declared before,

Witness's Signature Date

Name:
Designation:

ABSTRACT

Ilmenite is a tin mining byproduct that contains the radioactive element Uranium (U) and Thorium (Th). Although present in minute amounts (300-400 ppm), Malaysian law (Act 304) stipulates that it is radioactive, and is therefore a schedule waste, and need to be dealt with accordingly. The disposal cost is too high, prompting the companies involved to reprocessed ilmenite into synthetic rutile via hydrometallurgy, a low grade TiO_2 intermediate compound. Synthetic rutile contains mostly TiO_2 in the rutile phase, iron, silicon and other impurities, making it highly impractical for any high-end usage. Due to this fact, its cost is quite low.

TiO_2 is a common compound that is most famous for use as white pigmentation in paints, due to its whitish colour. In the nanosize region, its applications are much more diverse, including self-cleaning coatings, electrochromism, and photocatalytic applications. It also comes in many forms such as tubes, particles, and spheres. TiO_2's flexibility allows it to be processed from many methods, such as solgel, hydrothermal, solvothermal and sonochemical method, with each method producing unique products that is suitable for differing applications.

There are two objectives to this work, the first objective is utilize a tin mining byproduct (ilmenite) to produce anatase nano-TiO_2 particles, and the second objective is to use these particles to produce nano-TiO_2 thin films. The processing methods to produce both the particles and thin films will be modified from conventional methods in order to suit the nature of the intended precursors.

We intend to use low grade synthetic rutile, derived from ilmenite, as a precursor to produce anatase nano-TiO_2 particles. The method that is going to be utilized is the

hydrothermal method, although, due to the nature of the precursor, the method needs to be modified. The product from this process will in turn be used as a precursor to produce nano-TiO_2 thin film, utilizing the solgel method. This solgel method also needs to be slightly modified due to the presence of impurities in the sample.

The properties that needs to be analyzed is the chemical composition of the samples, the crystallite size of the particles, its surface area, morphology for the nanoparticles, and the film thickness, transparency, morphology, topography, and phases for the thin film. To this end, characterization methods such as the XRD, SEM, BET, AFM, UV-Vis, and the surface profiler will be used. A control nanoparticle sample, purchased from American Elements, will be compared to our nanoparticles, for the thin films, data from literature will be used as comparison.

The proposed methods manage to produce both the nanoparticles and thin films successfully. We also discovered that in some aspects, such the crystallite size and surface area, it is better than the commercial product.

The thin film's morphology and surface profile (rough), low thickness and relatively high transmission indicates its suitability for photocatalytic and self-cleaning applications. The films are also relatively pure, with TiO_2 dominating the content of the films.

The results indicate that it is possible to convert a low quality waste product into a high quality usable nanomaterial with a multitude of potential applications. The resulting product is in some ways superior to commercial products, and the processing method is cheap, environmentally friendly and easily customizable.

ABSTRAK

Ilmenite ialah bahan sampingan perlombongan bijih timah yang mengandungi elemen radioaktif Uranium (U) dan Thorium (Th). Sungguhpun elemen-elemen radioaktif ini merupakan hanya sebahagian kecil (300-400 ppm) dari bahan sampingan perlombongan, undang-undang Malaysia (Akta 304) menganggap bahan sampingan ini bahan radioaktif, dan merupakan bahan buangan terkawal, danperlu diuruskan mengikut prosedur-prosedur yang terkandung di dalam akta tersebut. Kos pemprosesan dan pembuangan bahan sampingan perlombongan ini agak tinggi, dan ini menyebabkan syarikat perlombongan yang terlibat memproses ilmenite kepada bahan yang dikenali sebagai rutile sintetik, menggunakan kaedah yang dikenali sebagai hidrometalurgi. Rutile sintetik ini merupakan titanium dioksida bergred rendah. Ia juga mengandungi elemen-elemen lain seperti Ferum, Silikon dan elemen-elemen lain yang menyebabkan ia tidak boleh digunakan untuk penggunaan berkualiti tinggi. Ini meyebabkan kos rutile sintetik menjadi agak rendah berbanding dengan bahan titanium dioksida yang lain.

Titanium Dioksida (TiO_2) merupakan bahan yang agak meluas penggunaannya, contohnya, ia digunakan sebagai pemutih di dalam cat. Apabila saiz partikelnya mencapai tahap nano, applikasinya dalam bidang sains dan teknologi menjadi lebih meluas, dan contoh applikasi menggunakan bahan ini merangkumi bidang-bidang seperti salutan mudah bersih, peralatan elektrokromik, dan applikasi fotokatalitik. TiO_2 juga boleh dihasilkan dalma pelbagai bentuk contohnya tiub, partikel dan sfera. Sifatnya yang agak fleksibel juga membolehkan TiO_2 dihasilkan dari pelbagai kaedah pemprosesan, contohnya kaedah solgel, hidroterma, solvoterma, dan teknik kimia sono. Setiap kaedah ini menghasilkan produk-produk yang unik, yang boleh diguna pakai untuk applikasi yang berlainan.

Kajian ini mempunyai dua objektif, iaitu menggunakan bahan sampinga perlombongan bijih timah untuk menghasilkan partikel anatase nano-TiO_2, dan objektif kedua ialah menggunakan partikel-partikel nano ini untuk menghasilkan fuilem nipis TiO_2. Kaedah pemprosesan untuk menghasilkan partikel nano dan filem nipis perlu diubahsuai dari kaedah yang biasa digunakan kerana sifat bahan permulaan proses ini agak unik dan berlainan dari bahan yang selalu digunakan.

Bahan permulaan yang akan digunakan merupakan rutile sintetik yang dihasilkan dari ilmenite melalui kaedah hidrometalurgi, untuk menghasilkan partikel nano-TiO2 anatase. Kaedah yang akan digunakan merupakan kaedah hidroterma. Walaubagaimanapun, kaedah ini harus diubahsuai kerana rutile sintetik mengandungi elemen-elemen lain yang mungkin akan memudaratkan sifat-sifat partikel nano yang akan dihasilkan. Partikel-partikel nano ini pula akan digunakan untuk menghasilkan filem nipis, menggunakan kaedah solgel. Kaedah solgel ini juga mungkin perlu diubahsuai, bergantung kepada partikel nano yang akan digunakan.

Sifat-sifat yang akan dikaji termasuk komposisi kimia sampel, saiz Kristal partikel nano, luas permukaannya, morfologi, ketebalan filem, sifat lutsinar filem, topografi, dan fasa sampel. Kaedah-kaedah yang akan digunakan bagi kajian termasuklah teknik XRD, SEM, BET, AFM, UV-Vis, dan profil permukaan. Sampel kawalan, merupakan partikel nano yang dibeli dari syarikat American Elements, akan digunakan untuk perbandingan dalam kajian ini.

Kaedah yang dicadangkan berjaya menghasilkan partikel nano dan filme nipis. Kajian ini juga menunjukkan yang dari beberapa aspek, seperti luas permukaan dan saiz kristal, produk yang dihasilkan dalam kajian ini adalah lebih baik dan sempurna lagi.

Morfologi filem nipis dan profil permukaan (kasar), ketebalan yang rendah dan tranmissi yang tinggi menunjukkan kesesuaiannya untuk applikasi fotokatalitik dan alatan elektrokromik. Filem nipis yang dihasilkan juga mempunyai ketulenan yang tinggi.

Keputusan kajian menunjukkan yang bahan sampingan yang berkualiti rendah boleh ditukarkan kepada bahan nano berkualiti tinggi yang boleh digunakan untuk pelbagai applikasi bertahap tinggi. Produk yang dihasilkan dari bahan sampingan ini adalah lebih baik dari bahan komersial dari beberapa segi, dan proses yang digunakan juga merupakan proses yang berkos rendah, fleksibel, dan kurang pencemaran alam sekitar.

ACKNOWLEDGEMENT

I express my ever deepening gratitude to the Almighty for my good health and mind that enabled me to successfully complete this work with minimal obstacles.

First and foremost, I am deeply appreciative and indebted to my supervisor, Prof. Mohd. Hamdi Abd. Shukor for his directions, assistance, guidance and support, of which if I was without, would have rendered this work catastrophically incomplete.

I would also like to express my gratitude to the Department of CAD/CAM, Faculty of Engineering, University Malaya, for its support and assistance throughout the completion of this work. Big or small, it is almost impossible to complete this work without their collective contribution.

I would also like to thank my family, especially my parents, for their unending support and faith in me when I am pursuing my studies and completing this work. Their support kept me emotionally stable, especially when faced with difficulties throughout this work.

Finally, this work would not have been possible without financial support from the Malaysian nuclear agency (Nuclear Malaysia), under the Pre-Qualification Research and Development funds (NM-R&D-11-09), and also financial support from IPPP postgraduate research grant (University Malaya)

Mahdi E. M.
Faculty of Engineering,
University of Malaya,
13th September 2012

CONTENTS

TITLE PAGE

ABSTRACT ii

ACKNOWLEDGEMENT vii

LIST OF FIGURES xii

LIST OF TABLES xiv

CHAPTER 1: INTRODUCTION 1

1.1 Research Background 1

1.2 Problem Statement 4

1.3 Scope of Research 5

1.4 Research Objectives 11

1.5 Research Methodology 12

1.6 Thesis Organization 15

CHAPTER 2: LITERATURE REVIEW 16

2.1 Introduction 16

2.2 Nanotitania 16

2.3 Hydrothermal Method for Nanoparticle Synthesis 20

2.3.1 Fusion 20

2.3.2 Autoclave 21

2.3.3 Precipitation and Collection 22

2.3.4 Characterization and Example from Previous Research (Nano-TiO_2 Particles) 22

2.4 Solgel Method of Nano-TiO_2 Thin Films Fabrication 25

2.4.1 Sol-Solution Synthesis 26

2.4.2 Depostion 26

2.4.2.1 Spin Coating 27

2.4.3 Characterization and Examples from Previous Research (Nano-TiO_2 Thin Films) 28

2.5 Chapter Summary 30

CHAPTER 3: MATERIALS AND METHODS 31

3.1 Introduction 31

3.2 Nano-TiO_2 Particles (Modified Hydrothermal Method) 31

3.2.1 Alkaline Fusion 34

3.2.2 Washing and Filtration 36

3.2.3 Leaching 38

3.2.4 Post Processing of Nano-TiO_2 particles 41

3.3 Thin Film Nano-TiO_2 (Solgel) 42

3.3.1 Solution Creation 44

3.3.2 Substrate Preparation 45

3.3.4 Spin Coating 47

3.3.5 Post Processing Annealing 48

3.4 Characterization 50

3.5 Chapter Summary 51

CHAPTER 4: RESULTS AND DISCUSSION (NANO-TiO_2 PARTICLES) 52

4.1 Introduction 52

4.2 X-Ray Diffraction (XRD) 52

4.3 Energy Dispersive X-Ray Fluroscence (EDXRF) 58

4.4 N_2 Adsorption Desorption (BET) and Particle Size Analyzer (PSA) 61

4.5 Scanning Electron Microscope (SEM) 64

4.6 UV-Vis-NIR 67

4.7 Chapter Summary 72

CHAPTER 5: RESULTS AND DISCUSSION (NANO-TiO_2 THIN FILMS) 73

5.1 Introduction 73

5.2 Grazing Angle X-Ray Diffraction (GAXRD) 73

5.3 Scanning Electron Microscope /Energy Dispersive X-Rays Analysis (SEM/EDX) 78

5.4 Atomic Force Microscope 81

5.5 UV-Vis-NIR Analysis 87

5.6 Chapter Summary 96

CHAPTER 6: POTENTIAL APPLICATIONS 97

6.1 Introduction 97

6.2 Photocatalysis 97

6.3 Electrochromic Devices 101

6.4 Photovoltaic Applications 104

6.5 Chapter Summary 107

CHAPTER 7: Conclusions and Recommendations 108

REFERENCES 109

PUBLICATIONS AND AWARDS 119

APPENDIX 122

LIST OF FIGURES

FIGURE	TITLE	PAGE
1.1	Example of Nano-TiO_2 particles synthesized via the hydrothermal method from a) Hussein (2008) and b) Seo (2008)	7
1.2	Examples of Nano-TiO_2 thin films fabricated via the solgel method using titania rich precursors	10
1.3	Methodology	14
2.1	Nano-TiO_2 particles produced by previous researchers	17
2.2	Potential applications of nano-TiO_2 particles	18
2.3	TiO_2 thin films from the works of a) Kajitvichyanukul *et al* 2005; b) Jazra *et al* 2004; and c) Okimura 2001	19
2.4	Potential Applications of TiO_2 thin films	19
2.5	Nano-TiO_2 particles production via hydrothermal treatment	20
2.6	XRD of nano-TiO_2 particles synthesized from the hydrothermal method from the works of a) Jonville 2004; b) Mu *et al* 2010; and c) Chen *et al* 2009	24
2.7	SEM/TEM of nano-TiO_2 particles from hydrothermal synthesis from the work of a) He *et al* 2011; b) Zhao *et al* 2007; and c) Hidalgo *et al* 2007	25
2.8	Solgel Synthesis of nano-TiO_2 thin films	26
2.9	Schematics of the spin coating deposition process	27
2.10	XRD of nano-TiO_2 thin films via the solgel spin coating deposition from the works of a) Martyanov *et al* 2004; b) Wen *et al* 2001; and c) Wang *et al* 1999	29
2.11	SEM of nano-TiO_2 thin films spin coated onto various substrates taken from the works of a) 25Ahn *et al* 2003; b) Ogden *et al* 2008; and c) Suciu *et al* 2009	30
3.1	The development of nano-TiO_2 particles and thin films from	31

precursor derived from local minerals

3.2 Modified hydrothermal treatment for nano-TiO_2 particle 33

3.3 Sodium Titanate compound from alkaline fusion of synthetic rutile and NaOH pellets (scale: 1 mm : 5 mm) 36

3.4 Setup for a) Washing and b) Filtration of the alkaline fusion product 38

3.5 Leaching of sodium titanate complex using sulfuric acid 40

3.6 Figure 3.6 Nano-TiO_2 particles 41

3.7 Modified Solgel method to produce nano-TiO_2 thin film 43

3.8 The steps in sol-solution preparation with a) the constituent chemicals and b) Mixing and spinning in a sealed bottle 45

3.9 Substrate preparation for nano-TiO_2 thin film deposition with a)Glass/ITO substrate, b) washing and cleaning the substrate, c) determining which layer is glass or ITO and d) glass is the chosen deposition surface, with it being marked with colored tape 47

3.10 Spin Coating nano-TiO_2 thin film, with a) dripping the sol-solution during spinning onto the substrate and b) a single layer of deposited sol-solution 48

3.11 Post processing annealing of Nano-TiO_2 thin films 49

3.12 Thin Film TiO_2, post annealing 50

4.1 XRD Diffraction Peaks of ilmenite synthetic rutile and nano-TiO_2 particles 53

4.2 XRD Diffraction Peaks of commercial nano-TiO_2 and nano-TiO_2 particles 57

4.3 SEM of the a) commercial nano-TiO_2 and b), c) and d) nano-TiO_2 particles produced by modified hydrothermal method taken at 40kx magnification 65

4.4 Absorbance Spectrum of nano-TiO_2 particles and the commercial sample 68

4.5 Transmission Spectrum of nano-TiO_2 particles and the commercial sample 69

5.1 Setup for GAXRD analysis of thin film samples 74

5.2	XRD Diffraction peaks for m_{TiO2} = 0.05 g thin films	75
5.3	XRD Diffraction peaks for m_{TiO2} = 0.4 g thin films	75
5.4	XRD Diffraction peaks for m_{TiO2} = 1 g thin films	76
5.5	SEM Micrograph of nano-TiO_2 thin films at a) m_{TiO2} = 1 g, b) m_{TiO2} = 0.4 g and c) m_{TiO2} = 0.05 g at 40KX magnification	79
5.6	EDX analysis of nano-TiO_2 thin films at a) m_{TiO2} = 1 g, b) m_{TiO2} = 0.4 g and c) m_{TiO2} = 0.05 g	80
5.7	2D and 3D –AFM images (scanned area 1 μm x 1 μm) for nano-TiO_2 thin films deposited by spin coating at m_{TiO2} = 1 g	83
5.8	2D and 3D –AFM images (scanned area 1 μm x 1 μm) for nano-TiO_2 thin films deposited by spin coating at m_{TiO2} = 0.4 g	83
5.9	2D and 3D –AFM images (scanned area 1 μm x 1 μm) for nano-TiO_2 thin films deposited by spin coating at m_{TiO2} = 0.05 g	84
5.10	Relationship between concentration, thickness and surface roughness	86
5.11	Absorbance Spectrum of spin coated nano-TiO_2 thin films	89
5.12	Transmission Spectrum of Spin Coated nano-TiO_2 thin films	91
5.13	Tauc Plot for m_{TiO2} = 1 g sample for determination of optical bandgap	94
5.14	Tauc Plot for m_{TiO2} = 0.4 g sample for determination of optical bandgap	94
5.15	Tauc Plot for m_{TiO2} = 0.05 g sample for determination of optical bandgap	95
6.1	The mechanism of photocatalysis of TiO_2(taken from www.airrevolution.co.za/research)	98
6.2	The working mechanism of an Electrochromic Device using TiO_2 electrode (from Chen and Mao, 2007)	102
6.3	DSSC Schematics and working mechanisms (taken from Chen and Mao, 2007)	105

LIST OF TABLES

TABLE	TITLE	PAGE
1.1	Benefits and disadvantages of Hydrothermal Synthesis in nano-TiO_2 particle production	8
1.2	Benefits and disadvantages of Solgel Synthesis in nano-TiO_2 particle production	11
3.1	Sol-solution preparation parameters	44
3.2	Characterization Method for nanoparticles and nano-TiO_2 thin films	50
4.1	The evolution of crystallite size of TiO_2 phase from ilmenite to nano-TiO_2 particles	55
4.2	Comparison of crystallite size and crsytallinity of commercial and nano-TiO_2 particles produced by the modified hydrothermal method	58
4.3	EDXRF results of ilmenite, synthetic rutile and nano-TiO_2	60
4.4	Summary of Physical between ilmenite, synthetic rutile, nano-TiO_2 and Commercial nano-TiO_2	53
4.5	The optical bandgap of nano-TiO_2 particles and its commercial counterpart	70
5.1	Optical Transmission of UV-Visible light through nano-TiO_2 thin film deposited by the spin coating technique	91

CHAPTER 1: INTRODUCTION

1.1 Research Background

Malaysia is a country that is blessed with a variety of natural resources, whether in the form of minerals, oil and gas, or even flora and fauna. Various industries set up shop in Malaysia in order to exploit this opportunity, and since its independence, we literally see thousands of companies dealing with mining, deforestation, manufacturing and other lucrative business venture. What all these venture have in common is the generation of waste.

Malaysia generates many forms of waste from its various industries, and currently, only a few companies are equipped to deal with waste collection, management, recycling and reprocessing. From time to time, we hear about various wastes being dumped with impunity in rivers, unauthorized landfills, and other sensitive sites that is hazardous to the population. The government has launched a campaign promoting awareness among the Malaysian public regarding recycling and reuse of waste products; however, these calls are largely unsuccessful due to the enormous effort and costs required in these ventures.

Tin mining is a major industry in Malaysia. The mining industry is what industrialized Malaysia, turning this sleepy former British colony into an Asian economic powerhouse. The salient nature of this industry encourages the starting of many companies that deal with this venture at many levels, whether the mining itself, the separation and purification of the mining product, or the packaging and distribution of its end product. However, many byproducts are produced from tin mining, primarily among these is ilmenite, a low-grade iron based minerals, rife with impurities.

Ilmenite is a mildly magnetic mineral, consisting of a variety of transition metals, usually in the form of metal, intermetallic compounds, or oxides. Its content is location dependant

(Pownceby *et al* 2008,Li *et al* 2006) and its high level of impurities marks it as a low-grade mineral. Its abundance in certain locations, coupled with its relatively low grade and cost, makes it a potential viable source for metals and oxides. However, the extraction and purification processes involving ilmenite are numerous and complex, as detailed by various researchers (Li *et al* 2006;Yuan *et al* 2006;Kumari *et al* 2001). The processing of ilmenite produces many intermediate compounds, which, with further refinement, are equally useful, such as pseudorutile and synthetic rutile. Examples of these processing methods include acid leaching, carbothermic reduction, pyrometallurgy and hydrometallurgy, as detailed by Akhgar *et al* (2010), Mambote *et al* (2000), and Kucukkaragoz *et al* (2006). What these methods have in common is that it enables the modification of the product's properties by careful manipulation of the processing parameters. This facilitates the production of high quality products, almost equal to the ones in the market.

Synthetic rutile produced from ilmenite by Tor Minerals Sdn. Bhd is considered a low quality product; it contains 93% titania in the rutile phase, with various impurities such as silicon, manganese, zirconium, niobium and sulfur. The low quality nature of this product significantly reduces it cost, and it currently sells for MYR4.5/kg.

Titania (TiO_2) is a compound that is both familiar and abundant, having seen many applications in diverse areas such as cosmetics, coatings and water purification. This attribute is mainly due to the flexibility of titania as a compound, where it comprises of many unique phases and crystal systems that is responsible for its behavior in certain conditions. Titania comprises of eleven phases (some only exist in high pressure states), and four crystal systems (orthorhombic, monoclinic, tetragonal and cubic). Some common phases of titania are anatase (tetragonal), brookite (orthorhombic) and rutile (tetragonal). These phases occur naturally in minerals, and are regularly extracted and separated from

said ores in industrial settings. Sources of titania includes, but is not limited to, ilmenite ($FeTiO_3$), leucoxene ores, or rutile beach sand. Titania, as seen in its commercial form, is manufactured or processed from these sources using a myriad of methods, which includes the more common methods such as sol-gel method (widely used commercially), the hydrothermal and solvothermal methods, to the specialized and seldom used electrodeposition and the sonochemical method. The uniqueness of titania's attribute depends partly on its fabrication route, where we can see titania produced in different forms and shapes such as tubes (solvothermal) or rods (hydrothermal), segregated spheres (sol-gel), and smooth coatings (electrodeposition). These different forms of titania is crucial as its tailors to specific applications, for example, titania being applied for self cleaning applications needs to be coated on a surface/substrate, to allow a large surface area for it to act upon, whereas titania being used for photocatalytic applications needs to be in particle form, in order for it to be dispersed evenly in a medium (usually liquid), without upsetting the balance of the medium or introducing impurities that will contaminate the medium itself (Chen *et al* 2007).

The size of titania particles are also paramount in determining its characteristics and potential application. Due to its whitish color, titania is commonly used as white pigmentation in paints, with its own industrial code (E171), and this pigments are 1-10 μm in size. The smaller the particle gets, the more diverse its potential application can be. With today's focus on nanotechnology, interest in how titania can play a role in this field is being pursued by many scientist and researchers. As a result of this fervor, we see nanosized titania being used in areas previously thought unfeasible, such as electrochromic devices, electronic sensors and photovoltaic cells. The inclusion of titania into these devices produces effects such as lengthening of process cycles and increased efficiency. The

flexibility of titania as a compound also allows its fabrication method to be routinely modified to produce products that are deemed to be 'nano' in size, with determining factors such as crystallite/particle size and thickness being given special attention.

1.2 Problem Statement

Tor Minerals Sdn. Bhd. is a tin mining company based in Lahat, Perak. Their mining operation produces an abundance of ilmenite, and as ilmenite contains 300-400 ppm of Uranium and Thorium, it is classified as a radioactive material under Malaysian law (Act 304), which stipulates that any radioactive materials disposal be handled by the Atomic Energy Licensing Board (AELB), and certain waste management company that are licensed by the government to deal with this matter, along with licensed private contractors. Currently, Tor Minerals Sdn. Bhd. is sitting on 600,000 metric tons of ilmenite, and the cost of disposal is quite high, because it involves licensing and various other enforcement bureaucracies. This caused the company to reconsider, and using hydrometallurgy, they processed this ilmenite into synthetic rutile.

In short, the problems faced by the current tin mining process are listed below.

- Tin mining produces ilmenite, considered a scheduled waste due to its content of uranium and thorium
- The disposal cost is quite high and involves complex bureaucratic dealings, driving Tor Minerals to process it into synthetic rutile using hydrometallurgy
- Synthetic rutile caters to a niche market, making it difficult to sell

Even as a low quality mineral byproduct, synthetic rutile contains almost 90% TiO_2, which is quite a substantial percentage. However, the presence of impurities renders it unusable

for many applications involving TiO_2, although further processing will be able to rid it of its impurities and make it usable. Unfortunately, not many industries express interest in reprocessing these waste materials further due to its niche market potential and the need to channel more funds to make it viable. The successful reprocessing of this waste material into TiO_2 will however, transform this niche market with low commercialization potential, into a multipurpose material that caters to almost every industry ranging from academia to manufacturing.

1.3 Scope of Research

For the purpose of this research, the attention will be devoted to the production, and features of nanotitania, in line with current research interest. A significant number of methods to produce titania is mentioned in literature involves production of nanotitania, such as hydrothermal (Chen *et al* 2009; Sivaraju 2010;Sayilkan *et al* 2006), solvothermal (Supphasrirongjaroen 2008; Shen 2011; Wahi 2006) electrodeposition (Karuppuchamy *et al* 2002; Karuppuchamy *et al* 2006), and sonochemical methods (Guo *et al* 2003; Arami 2007). These methods are dominated by certain parameters, which makes it a relatively simple affair to manipulate the process to produced customized nanotitania. The research aims to produce two forms of titania, therefore, focus will be on two methods, hydrothermal (nanoparticles), and solgel (thin films). These two methods are established methods, with a body of research involving them published in literature (Hidalgo *et al* 2007;Oh *et al* 2006;Akarsu *et al* 2006; Ou *et al* 2007;Suciu *et al* 2009; Gaur *et al*2011;Valtierra *et al* 2006). However, room for improvement still exists, as some

cumbersome technique embedded in the method can be simplified or eliminated altogether, but still produce products that are similar in features and properties. Similarly, certain precursor chemicals and equipments are deemed expensive and its elimination or replacement can significantly curtail production costs.

The strong interest in the hydrothermal method is mainly due to its relative simplicity for large-scale synthesis of titania in a single reaction process. The process is efficient in terms of productivity and cost, and produces high quality titania particles and nanoparticles. This is iterated by various researchers such as Ou *et al* (2007) and Lasheen (2008). Basically, the hydrothermal method begins with fusing a precursor with a solvent at a set amount of time, temperature and pressure. Precursors to the process are usually Titanium Butoxide, TTiP or Titanium Butoxyl, and the chemical solvents are usually acid such as sulfuric or hydrochloric acids, or other organic solvents such as ethanol or methanol. The next step involves placing this mixture in an autoclave, set at a high temperature and pressure environment to facilitate the fusion of the chemicals and the precursor and the precipitation of particles/nanoparticles. The settings of the autoclave varies, but literature points to an average temperature of about 200-500°C, with the variation of time and pressure too large to draw an average. After this process, the mixture is removed and cleaned with a neutralizing agent, and dried either in air or in a furnace, usually at temperatures such as 70-150°C. Further processing might be needed, with milling of the product common in order to achieve uniformity. This summarizes the hydrothermal process conducted by Chen *et al* (2009), Sivaraju (2010), Sayilkan *et al* (2006), Liu *et al* (2005), Zárate *et al* (2008), and most, if not all, researches follow this standard rule when using the hydrothermal method, although some researchers will vary parameters such as time, temperature and pressure to study the effect it has on the titania nanoparticles. For comparison purposes,

Kim *et al* (2007) conducted hydrothermal treatment at 300°C, and studied the effect it has on the surface area/crystallinity of the particles, while Sayilkan *et al* (2006) and Kontos *et al* (2005) used Titanium Isopropoxide and Titanium Oxide Degussa P25 respectively to synthesize TiO_2 nanoparticles to study the changes in the physical and chemical properties of the formed nanostructures. Below are some SEM images of titania nanoparticles produced by the hydrothermal method.

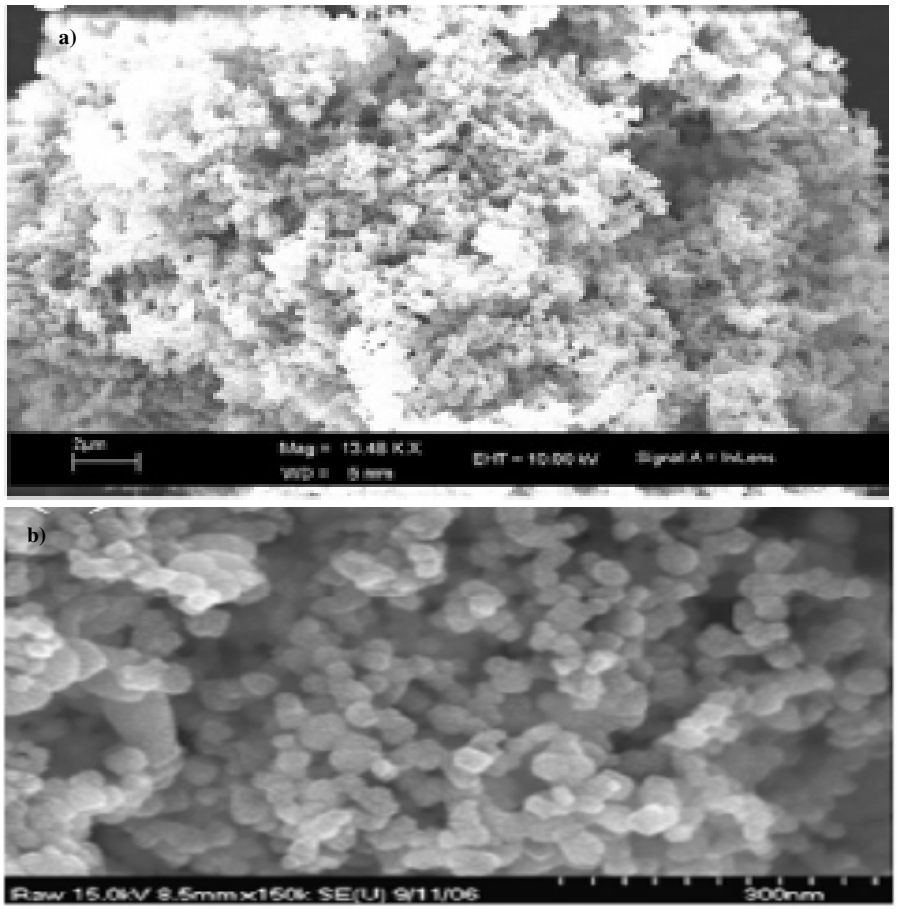

Figure 1.1 Example of Nano-TiO_2 particles synthesized via the hydrothermal method from a) Hussein (2008) and b) Seo (2008)

As can be seen from Fig. 1.1, the product of the hydrothermal process is uniform, and quite small in size. Products from the hydrothermal process are used for photocatalytic

applications, where nanoparticles are dispersed in liquid medium to act as purifiers (due to their detoxifying capabilities).

The hydrothermal method of producing nanotitania, although effective, suffers from several issues. Firstly, the cost of the process is quite high, especially considering the precursors, chemical solvents, the use of autoclave, and the time devoted to the process. It is mainly a batch process, and produces only a small amount of product per cycle, typically in grams. The parameters also need to be tightly controlled, as variations in parameters will alter the physical and chemical properties of the product, requiring a repeat of the process. The table below summarizes the benefits and disadvantages of the hydrothermal process of producing nanotitania.

Table 1.1 Benefits and disadvantages of Hydrothermal Synthesis in nano-TiO_2 particle production

Hydrothermal Process/Treatment to produce nano-TiO_2 particles	
Benefits	**Disadvantages**
Simple	The use of autoclave drives up the cost
Parameters easily adjusted and tailored	The use of synthetic and toxic chemicals greatly hamper the process
Low chance of failure due to seal nature of process	It is a slow process, taking time to precipitate nano-TiO_2 particles

This work will attempt to address these issues and modify the hydrothermal method to make it simpler, easy to control and cost effective.

The next method that will be addressed is the solgel method to produce thin film titania. The solgel method is widely used commercially, due to its simplicity and high quality products. Researchers such as Kajitvichyanukul *et al* (2005), Ahn *et al* (2003) and Mechiakh *et al* (2011),utilized the solgel method to produce thin film titania from various sources for various applications. The solgel method involves the fabrication of a titania containing precursor from any viable sources, and this solution is then deposited on a substrate using a variety of method such as spin or dip coating, or thermal evaporation. The films produced by this method are relatively thin/thick, opaque, and consist of particles on a substrate. The figure below show some example of thin film nanotitania coated on a substrate using the solgel method.

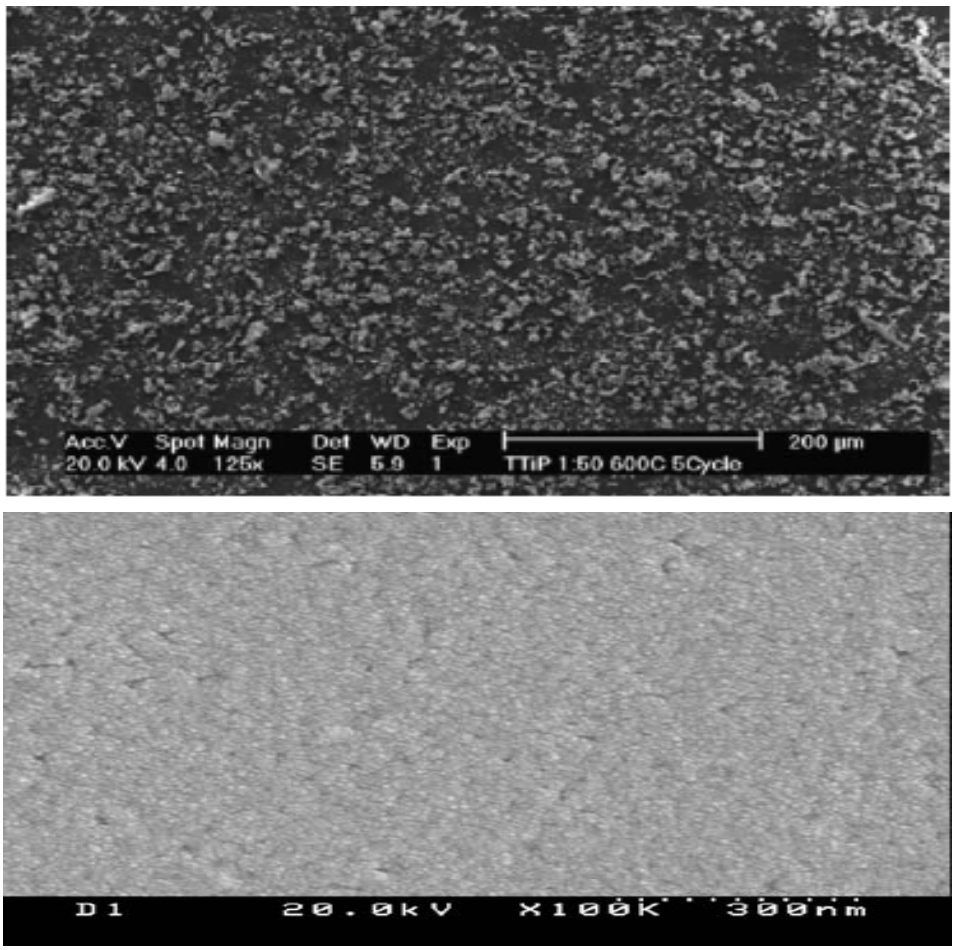

Figure 1.2Examples of Nano-TiO_2 thin films fabricated via the solgel method using titania rich precursors

Fig. 1.2 clearly shows the existence of particles on the surface, with its grain clearly defined, with uniform size throughout the substrate. Depending on the deposition method (whether spin coat, dip coat, electrodeposition or thermal evaporation), the quality of the films will vary.

The disadvantages of this method include expensive precursors, certain parameters that are difficult to control and predict such as aging time and coating speed and frequency, and the general rough nature of the films, making it unsuitable for applications that require high transmission of light. Table 1.2 summarizes its benefit and disadvantages.

Table 1.2 Benefits and disadvantages of Solgel Synthesis in nano-TiO_2 particle production

Solgel to produce nano-TiO_2thin films	
Benefits	**Disadvantages**
Simple and uses commercially available chemicals	Takes a significant amount of time and trial-and-error to discover the suitable combination of precursor and chemical reagants
Parameters are limited, and therefore easily controlled	High cost of precursors
Various deposition method available	The films are generally opaque and its surface rough, making it unsuitable for certain applications

This work will attempt to address these issues by modifying the method in a way that produces products that are similar, but far easier to control and manipulate.

1.4 Research Objectives

In short, the objective of this work is as follows

- Utilize synthetic rutile as a precursor to produce high quality anatase nano-TiO_2 particles

- Utilize a new hydrothermal method to suit our current resources and equipments to produce anatase nano-TiO_2 nanoparticles
- Characterize and compare this nano-TiO_2 particles with its commercial counterpart
- Use the nano-TiO_2 particles to produce thin films using a modified solgel method that addresses its disadvantages

The goal of this work is to use synthetic rutile, derived from ilmenite, as a precursor to produce nano-TiO_2 particles and nano-TiO_2 thin films. The success of this work will provide a viable alternative to the current abundance of ilmenite, as a high quality end product (whether nano-TiO_2 particle or nano-TiO_2 thin films) that is on par with commercial product will allow us to adapt it for mass production and enable this precursor to replace its more expensive counterpart in the nano-TiO_2 production scene.

1.5 Research Methodology

The block diagram shown in Fig. 1.3 outlines the methodology used in this work. It is divided into three stages; the preliminary stage involves the identification of precursors, nanoparticle synthesis methods, and thin film fabrication methods. The feasibility of a few conventional methods will be thoroughly researched and the most suitable method in accordance with the chosen precursor will be selected.

The next step is the experimental work and setup involving both the nanoparticle and thin film fabrication. The selected method will be employed, and the product will be visually

inspected and characterized to determine whether the product is feasible, if it is not, the method will be repeated with varying parameter to produce a good product.

The third stage is the results collection and analysis. Both the nanoparticles and thin films will be characterized, and the results will be compared with commercial products and published results to determine applicability. At the end of the analysis, the potential applications for the thin films will be discussed.

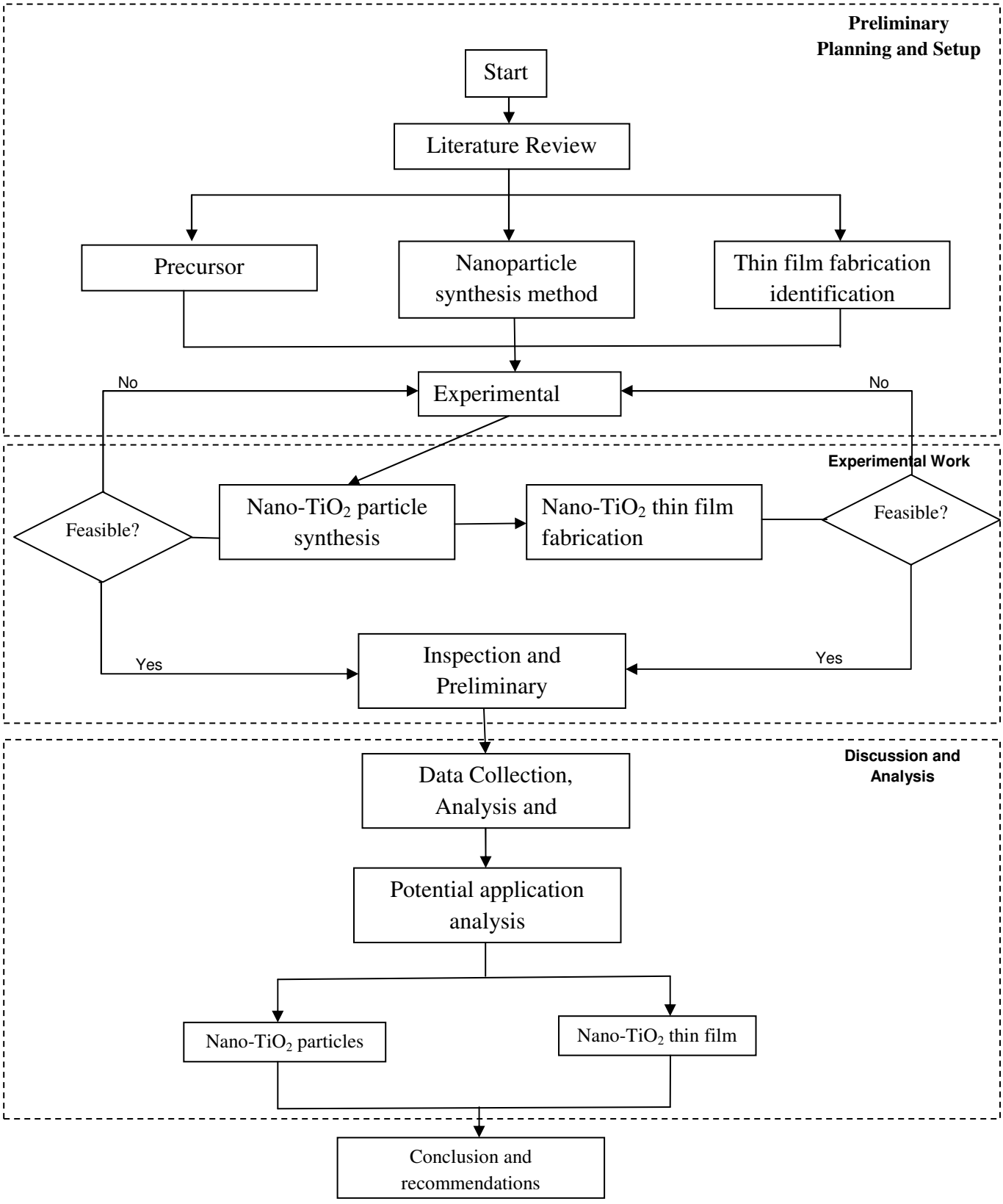

Figure 1.3. Methodology

1.6 Thesis Organization

This thesis is divided into sevenchapters; each chapter will deal with issues that are pertinent to this work in great detail. The first chapter, the introduction, will introduce the subject matter; discuss related work, and outline objectives and hypothesis of this work. The second chapter, the literature review, will discuss in great length previous work by various researchers, discuss their findings, and the methods that they employ to obtain their results. Comparisons will be drawn between these works, and their benefits and shortcomings will be highlighted in detail. The third chapter, the experimental method, will detail the proposed method in our work, the materials and equipment used, and the characterization methods employed and the underlying reason for each characterization method used. The fourth chapter, aptly called the results and discussion (Nano-TiO_2 particles), will attempt to analyze our proposed method, its similarity and differences with conventional method, the product produced form the proposed method, the comparison with commercial products, the benefits of our method over conventional ones, of the nano-TiO_2 particles. The next chapter will discuss the same aspects, but relating to the nano-TiO_2 thin films instead of the nano-TiO_2 particles. The sixth chapter discusses the potential application of both products, and comparisons are drawn with literature in order to justify our arguments. The final chapter, chapter seven, will conclude this work, and recommend some further studies involving the products. A list of references, appendix, awards and publications pertinent to this work will be showcased at the end of this thesis.

CHAPTER 2: LITERATURE REVIEW

2.1 Introduction

This chapter will outline the two forms of nano-TiO_2 that will be fabricated during the course of this work, nanoparticles and thin films, along with describing both the established method for producing nano-TiO_2 and nano-TiO_2 thin films from various precursors. The method that will be discussed in detail will be the hydrothermal method of synthesizing nano-TiO_2 particles, and the solgel method and spin coating deposition technique for nano-TiO_2 thin film fabrication. The intricacies of both techniques will be detailed, along with the various parameters involved. The end product of both methods will be shown here for future comparison purposes.

2.2 Nanotitania

The previous section describes titania in terms of its shape and sizes, synthesis method, and common applications. This section aims to delve deeper, and more specific aspects of nanotitania will be explored, in the form of particles and thin films.

Nanotitania is nanosized titania in any form. The definition of sizes vary according to the nature of the titania itself; particulates are considered 1-D nanostructures if it is less than 100 nm in size, while thin films are considered 2-D nanostructures.

Nanotitania is unique in many senses, in that it opens up a wide array of potential applications for this previously underutilized oxide. We now see nanotitania being used as water splitting agents and electrochemical electrodes. The evolution of this material

into something extraordinary is only made possible with the scaling down of its size to the nano-region.

In order to demonstrate this point, we will be discussing nano-TiO_2 particles and nano-TiO_2 thin films. Nano-TiO_2 is considered as such if its primary particle size (crystallite size) is less than 100 nm. This definition is explained in length in ISO CPD 10678. This small size is indicative of a large reactive surface area, with improved structural, chemical, and optical properties. Nano-TiO_2 particles are usually homogenous and uniform in distribution. Literature reports various particle size of nano-TiO_2, from an average of 10 nm (Akarsu *et al* 2006; Rao *et al* 2007) to 100 nm (Nguyen *et al* 2006). Fig. 2.1 shows examples of nano-TiO_2 particles that are produced by various researchers (Lu *et al* 2008; Arami *et al* 2007; Morgado *et al* 2006).

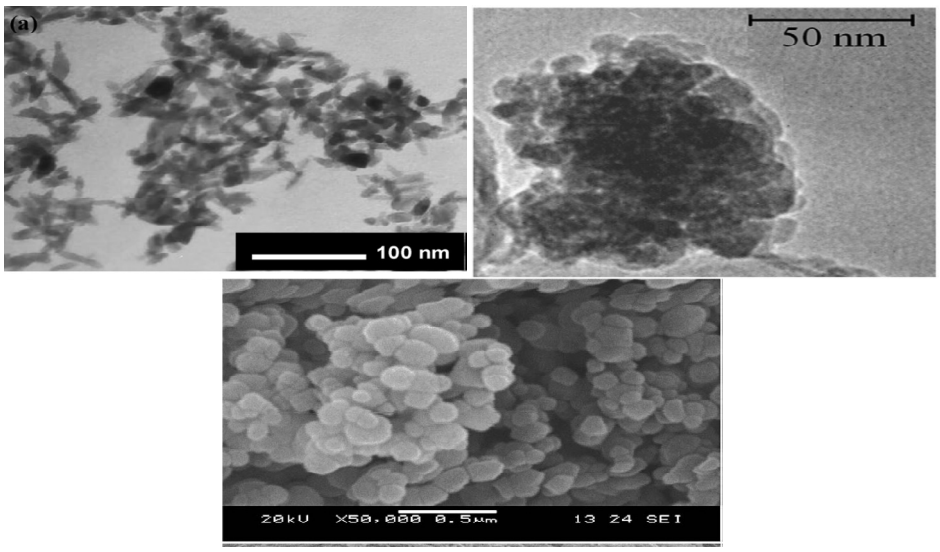

Figure 2.1. Nano-TiO_2 particles produced by previous researchers

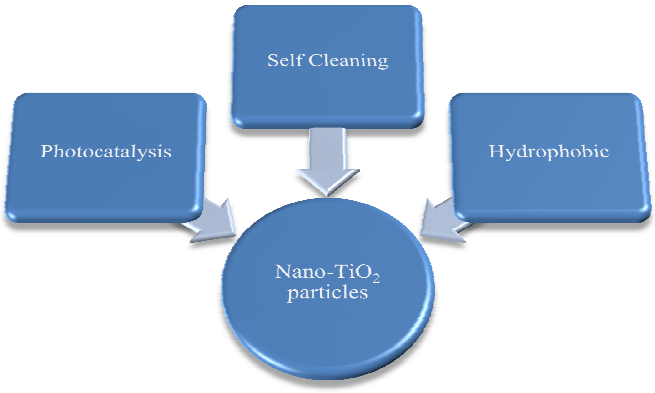

Figure 2.2 Potential applications of nano-TiO_2 particles

Methods that are capable of producing nano-TiO_2 particles are usually methods that are common in literature, such as hydrothermal, solvothermal, solgel and sonochemical. These methods are usually slightly modified in order to accommodate the production of nano-TiO_2 particles. Due to the intricate nature of the product from these processes, the parameters need to be carefully controlled and monitored in order to ensure the integrity of the processes. This is due to the fact that the structural and chemical properties of nano-TiO_2 are very much dependent on its processing parameters. The methods are elaborated upon in various published works such as Shen *et al* 2011, Wahi *et al* 2006, and Ou *et al* 2007.

TiO_2 also exist as thin films, commonly being applied as sensors and electrodes. Thin film TiO_2 is fabricated from various TiO_2 containing precursors such as titanium butoxide, titanium alkoxide and Degussa P25 (Karuppuchamy *et al* 2002; 2005; Wang *et al* 1999). These thin films are considered nanostructures due to its thickness and nanosized grains and particles that form the coating itself. Again, the nature of TiO_2 thin films is outlined in ISO CPD 10678. Fig. 2.3 shows some examples of TiO_2 thin film fabricated via various routes.

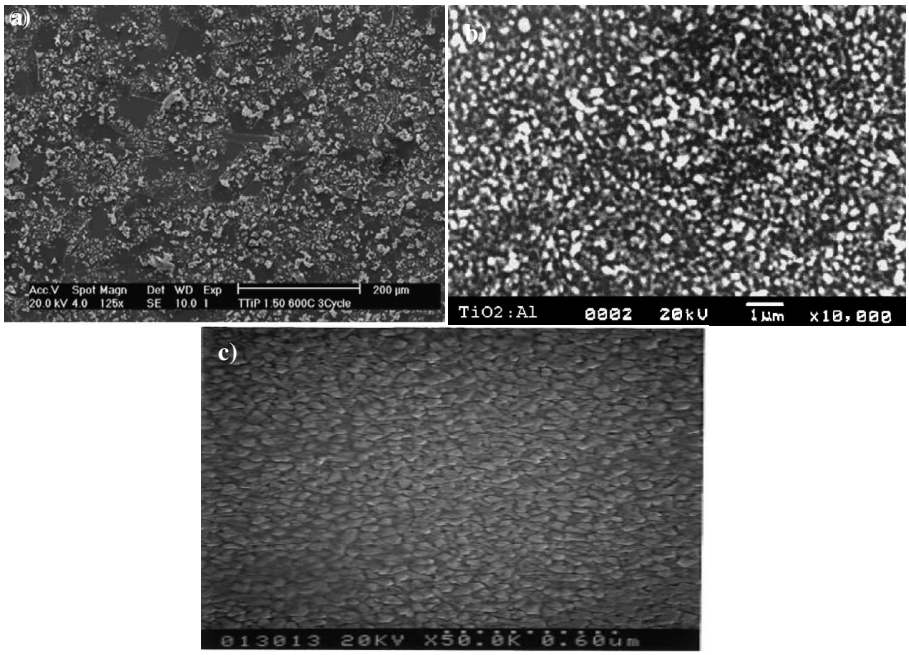

Figure 2.3. TiO_2 thin films from the works of a) Kajitvichyanukul *et al* 2005; b) Jazra *et al* 2004; and c) Okimura 2001

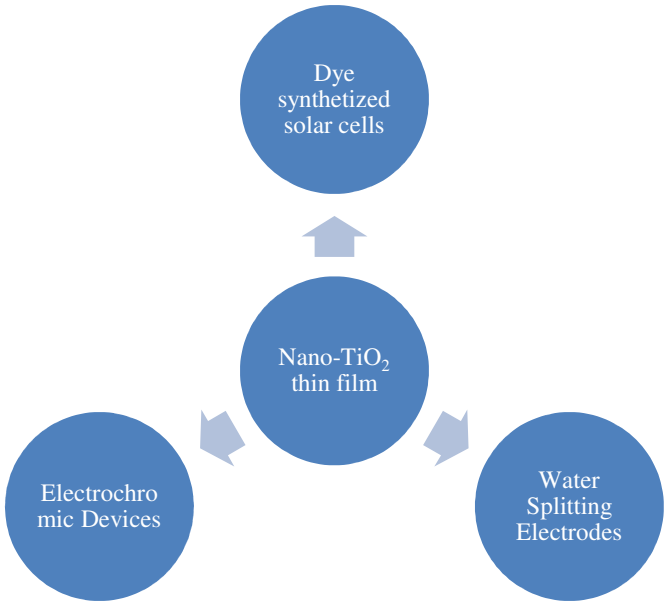

Figure 2.4. Potential Applications of TiO_2 thin films

Similar to nano-TiO_2 particles, TiO_2 thin films can be fabricated using a variety of methods such as solgel, the hydrothermal method, or electrodeposition. Due to the sensitive nature of the final product, the process needs to be tightly controlled in order to ensure that the films are not deformed in any way.

2.3 Hydrothermal Method for nanoparticle synthesis

This section is devoted to exploring the hydrothermal synthesis to produce nano-TiO_2 particles conducted by previous researchers. As mentioned in the previous chapter, the hydrothermal synthesis is an established method, especially when it comes to producing nano-TiO_2 particles (Malinger 2011; Castro 2008), nano-TiO_2 thin films (Zhao 2007) and titania nanotubes (Morgado 2006). The reason of its popularity is mostly due to its simplicity, and its capability in producing large amounts of product per cycle of process. The hydrothermal method involves the crystallization of particles from an aqueous solution in high pressure and high temperature environments. In order to create this extreme environment, this method requires an autoclave, which is an inert chamber lined with structurally stable materials such as steel or Teflon. The hydrothermal method is especially suitable in producing crystallographic materials, especially nanomaterials and nano-oxides. Due to its nature, it is also suitable in the production of nano-TiO_2 particles, due to its crystalline nature and its small sizes. Fig. 2.5 summarizes the approach of the hydrothermal method for producing nano-TiO_2 particles.

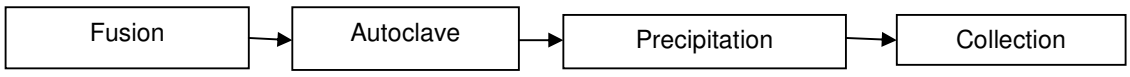

Figure 2.5 Nano-TiO_2 particles production via hydrothermal treatment

2.3.1. Fusion

The first step in this method is the selection and mixing of a precursor and its chemical solvent. In the hydrothermal method, the precursors are usually compounds that have a

significant amount of TiO_2, and the solvent(s) are mostly water-based chemical solvents. The mixing can be done physically using a glass rod, or mechanically using an overhead stirrer, depending on the medium of the precursors and solvents. The mixing is done to ensure that the surface of both the precursors and solvents are in maximum contact with each other, in order to ensure a complete and smooth reaction during the next step. The mixing is done at ambient temperatures, although it might be conducted under more extreme settings. The solution is either left to settle or used immediately, again, depending on the approach favored by individual researchers. This stage is crucial, as it plays a significant role in the determination of the physical and chemical properties of the final product. Researchers, such as as Hidalgo *et al* (2007), uses TTiP mixed with Isopropanol, and HCl with distilled water, Oh *et al* (2006), uses titanium butoxide mixed with 2-butoxyethanol and acetic acid, and Akarsu *et al* (2006) uses tetrabutylorthotitanate ($Ti(OBu^n)4$) mixed with HCl, while Sayilkan *et al* (2006) uses $Ti(OPr^i)_4$,dissolved in n-propanol as a precursor, with this solution was added to HCl (aq) and an alkoxide solution. Most of the mixing in these cases was done physically, using a glass rod.

2.3.2. Autoclave

After the mixture is primed and deemed ready, the next step is placing it in the autoclave to initiate and complete the chemical reactions that will precipitate nanoparticles. The parameters involved at this stage of the process are the temperature, time and pressure in the autoclave, which are all automated. To accelerate the rate of reactions, the temperatures are increased, although in some cases, a lower temperature is preferred in order to preserve certain structural characteristics of the precipitate. Chen *et al* (2009) uses a Teflon lined autoclave to perform hydrothermal treatment at 200°C from 3-36 hours to produce nano-TiO_2 particles, Sivaraju *et al* (2010) uses a stainless

steel Teflon line autoclave for the hydrothermal treatment at 150ºC – 200°C, at 12-48 hours, and similarly, Akarsu *et al* (2006) used Stainless Steel Teflon lined autoclave preheated at 200°C for 1 hour. The methods are similar, but as shown by these three researchers, even though their products are nanoparticles, there are some variations in their physical/structural properties.

2.3.3. Precipitation & Collection

There are various ways to collect the precipitate formed in the previous step of the process, Mu *et al* (2010) recovered the nano-TiO_2 particles from the hydrothermal treatment via filtration and repeated washing with deionized water, Malinger *et al* (2011) used centrifuging to recover their nanoparticles, and Kim *et al* (2007) used filtration and washing with water and ethanol to obtain their nanoparticles. Another viable method of precipitation and collection of the precipitates is centrifuging, where it involves placing the solid-liquid mixture containing the nanoparticles in a centrifuge, and spinning the solution at high frequencies to induce phase separation. The liquid portion is then removed. Filtration is also common, and can be done a number of ways, but mostly involves a vacuum pump and a fine sieve to separate the solids from the liquid. The washing is optional, and is done after filtration/centrifuging in order to ensure that no impurities or ions remain on the surface of the nanoparticles.

2.3.4. Characterization and examples from previous research (nano-TiO_2 particles)

In order to verify that the final product of the hydrothermal treatment is indeed nanoparticles, most researchers employ characterization techniques such as the XRD, EDXRF, SEM, and PSA. These techniques provide details such as particle size, crystallite size, homogeneity, and particle distribution in the sample, allowing to

researcher to confirm the actual status of their nanoparticle. As an example, Jonville (2004) compiled a report regarding the usage of TEM and image processing analysis to characterize TiO_2 nanoparticles.

Researchers frequently conduct XRD analyses on nanoparticles. Mostly, their findings focus on the crystallite sizes of the sample, with crystallite sizes of less than 100 nm sufficient to prove that their samples are actually nanoparticles. The phases of the nanoparticles are equally important, and this is evident in the work of Kim *et al* (2007), Sivaraju *et al* (2010), and Oh *et al* (2006).

SEM and TEM analyses are also capable of determining particle size, and again, the criteria that is looked for is that the particle size is less than 100 nm. Using built in software applications, researchers such as Hidalgo *et al* (2007), succeeded in determining the size of their particles. Their analysis showed a sufficiently small particle size, distributed uniformly throughout the sample, with its homogeneity intact.

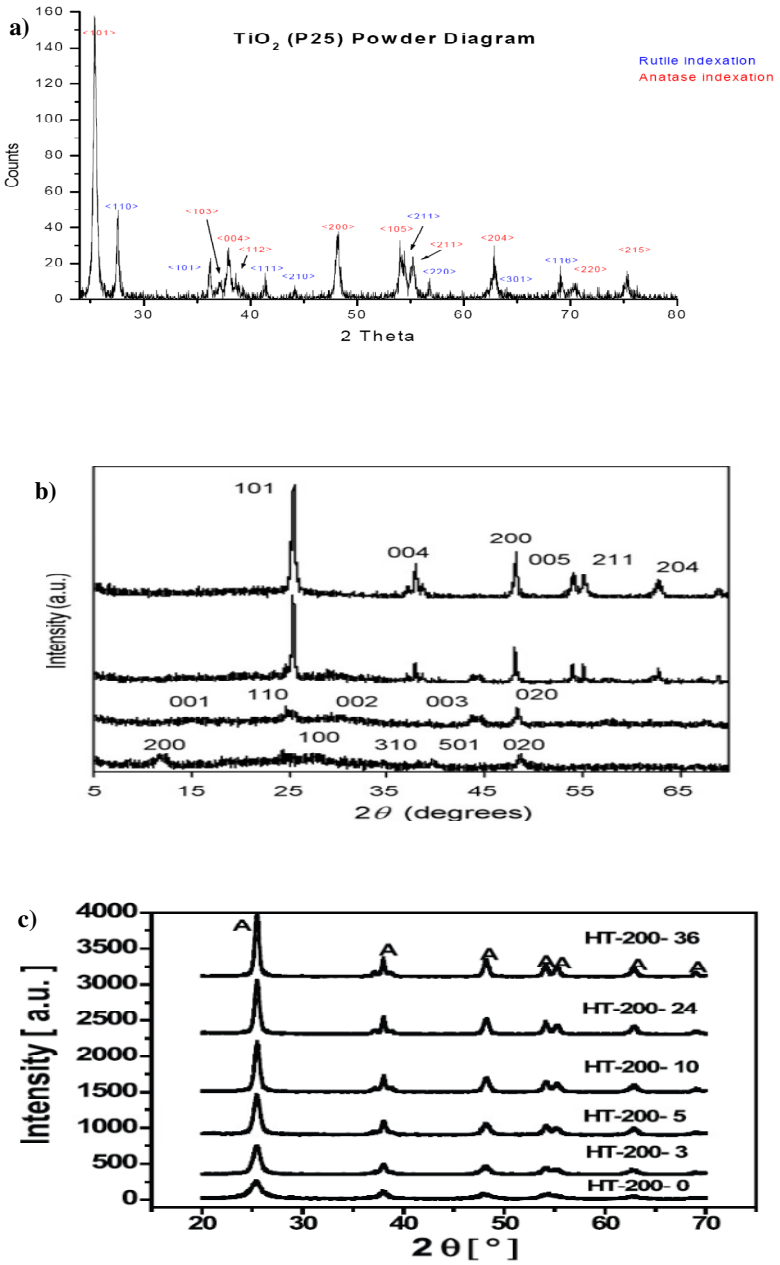

Figure 2.6 XRD of nano-TiO_2 particles synthesized from the hydrothermal method from the works of a) Jonville 2004; b) Mu *et al* 2010; and c) Chen *et al* 2009

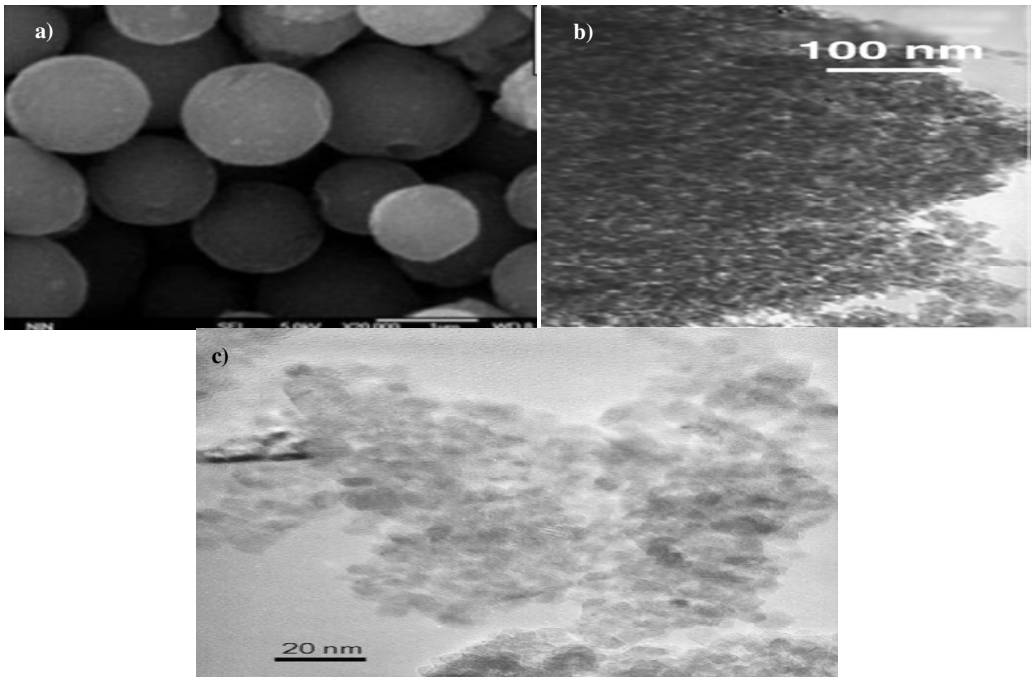

Figure 2.7 SEM/TEM of nano-TiO_2 particles from hydrothermal synthesis from the work of a) He *et al* 2011; b) Zhao *et al* 2007; and c) Hidalgo *et al* 2007

2.4. Solgel Method of nano-TiO_2 thin film fabrication

The subject of nano-TiO_2 thin films is especially abundant in literature due to its applicability in many fields. Some detailed work on nano-TiO_2 thin film synthesis using the solgel method includes the work of Suciu *et al* (2009), Valtierra *et al* (2006), and Ahn *et al* (2003). The approach by these researchers might be slightly different, but generally, they follow the same set formula. The first step of the solgel method is the sol-solution synthesis. This involves dissolving a titania rich precursor in a liquid medium such as acid, alkali, water or alcohol. The dissolving method include aging at room temperature, using an autoclave or high temperature stirring in a sealed case. The solution will then be deposited using a variety of methods such as spin coating and dip coating onto a substrate, which might be glass/ITO, stainless steel or any other viable

material, and it might also be annealed for structural integrity, depending on its intended application. Fig. 2.8 summarizes the solgel synthesis of nano-TiO_2 thin films.

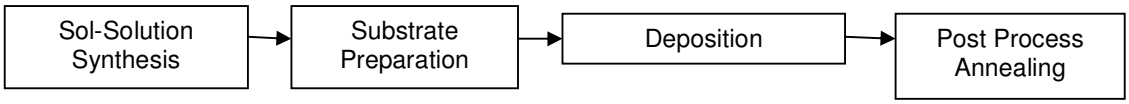

Figure 2.8. Solgel Synthesis of nano-TiO_2 thin films

2.4.1 Sol-Solution synthesis

Sol creation in the solgel method involves fusing precursors with chemical reagants to create new compound that are more susceptible manipulation using other methods. Some example of precursors include Titanium Butoxide, Titanium Alkoxide, TTiP, while some common chemical reagants include mild acids, alcohol, and hydrocarbons (Kajitvichyanukula *et al* (2005); Yu *et al* (2001); Sonawane *et al* (2002); Garzella *et al* (2000); Blount *et al* (2001); Francioso *et al* (2003)). The precursors and chemical reagants are mixed and sealed under various conditions to ensure maximum reaction rates between them. In contrast with the hydrothermal synthesis, this method actually dissolves the titania rich precursor in the solution, which will produce a solution rich in titania, instead of precipitating titania solids.

2.4.2. Deposition

The deposition process is a process where the sol-solution is deposited onto a cleaned and prepared substrate. The substrate needs adequate cleaning and preparation to ensure that no impurities, dust or water molecules are on its surface, that will affect the adhesion of the sol-solution on the substrate. There are various ways of depositing sol-

solution onto a substrate; among them spin coating (Lin *et al* 2012), dip coating (Strawbridge *et al* 1986), doctor's blade (Lee *et al* 2010), printing (Ito *et al* 2007) and capillary coating (Weill *et al* 1986). Each method has their advantages and disadvantages, and the application of each method depends on the final product a user is trying to make. However, for the purpose of this work, the spin coating technique will be discussed in detail.

2.4.2.1 Spin coating

The spin coating method is quite popular in literature, and its details are outlined in various works by Meyerhofer (1978), Saleema (2009), Kitsuka (2009) and Lin (2012). It involves spinning a substrate on an axis perpendicular to the coated surface area. A schematic of this process is shown below.

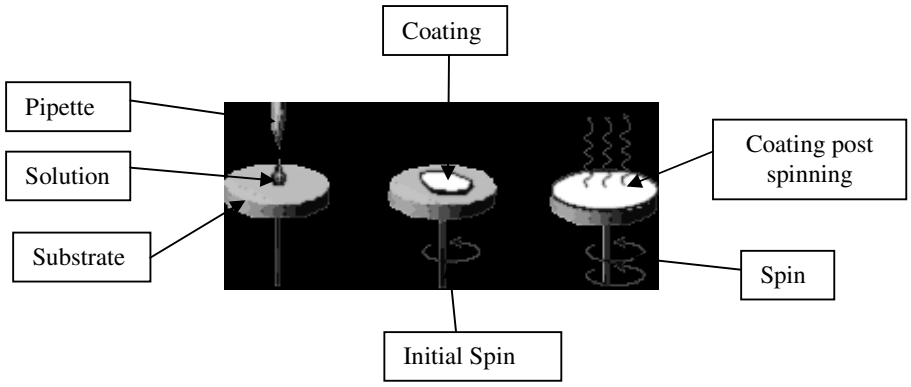

Figure 2.9. Schematics of the spin coating deposition process

The solution is carefully dripped onto a substrate in a spin-coater, and the substrate is spun on an axis, and the centrifugal force generated will spread the liquid around the substrate into a uniform coating. The quality of the coating depends on rheological parameters of the solution, and operates within the Newtonian context. Other variables include the Reynolds Number of the surrounding atmosphere, with a high Reynolds

number indicating turbulences in the atmosphere inside the spin-coater, which will affect the optical quality of the coating on the substrate. Spin coating is a fully automated process, and the speed and rate of deposition can be fully controlled using programmable controllers attached to the spin coaters. The thickness of coating from this technique varies, but thicknesses from 100 nm to 10 um have been reported in literature. The coating's thickness is governed by equation 2.2.

$$h = \left(1 - \frac{\rho_A}{\rho_{A_o}}\right).\left(\frac{3\eta m}{2\rho A_o \omega^2}\right)^{1/3} \quad (2.2)$$

where h is the thickness, ρ_A is the mass of volatile solvent per unit volume, ρ_{Ao} is the initial value of ρ_A, m is the evaporation rate of the solvent, and ω is the angular speed of the axis, η is the viscosity of the solvent.

This method is favored as it can be automated, produces a highly homogenous coating, and conducted using a spin coater in a controlled environment, therefore minimizing the possibility of errors. The solution prepared by the solgel method is deposited onto the spin coater, and a centrifugal force generated by the spin coater at high speeds will coat the substrate with the solution.

2.4.3 Characterization and examples from previous research (nano-TiO_2 thin films)

Due to its delicate nature, the characterization of nano-TiO_2 thin films is a tedious affair. Most works in literature (Kajitvichyanukula *et al* 2005; Yu *et al* 2001; Sonawane 2002) details the synthesis and characterization of nano-TiO_2 thin films, and the

methods used are seldom conventional, in a sense that certain alterations is needed in order to accommodate the samples. For example, due to the low thickness of nano-TiO_2 thin films, when characterizing using the XRD method, the low grazing angle method is required to be used instead of powder diffraction analysis. This is similar in AFM analysis of nano-TiO_2 thin films, where a contact mode analysis of the nano-TiO_2 thin film is not feasible, due to its delicate and sometime structurally flimsy nature. Therefore, the non-contact mode is preferred.

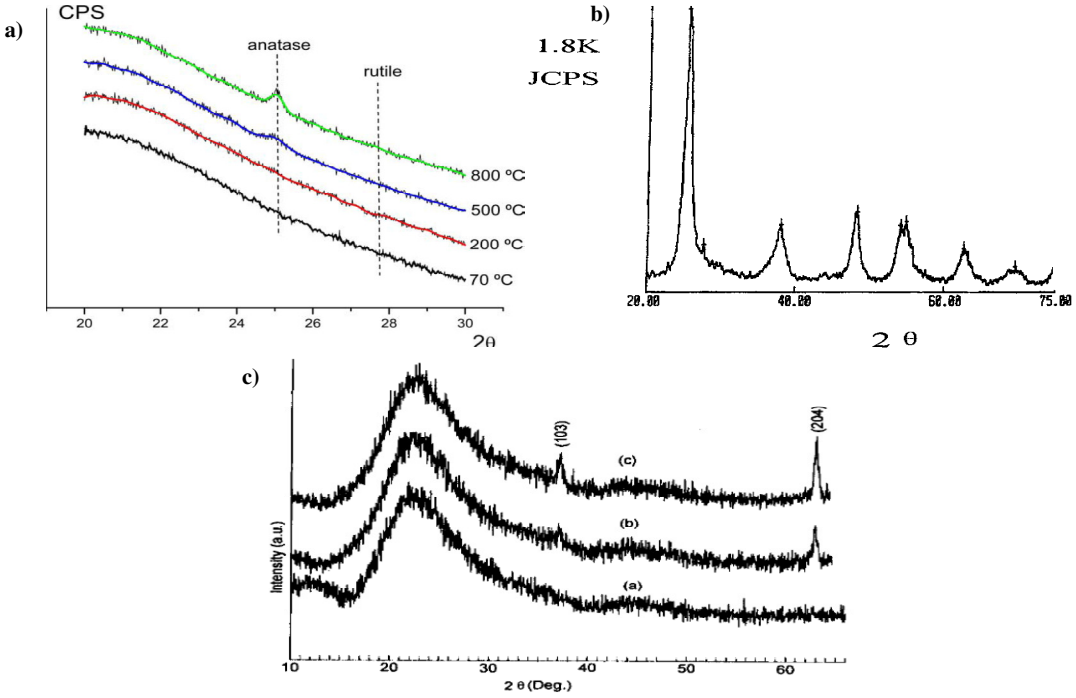

Figure 2.10 XRD of nano-TiO_2 thin films via the solgel spin coating deposition from the works of a) Martyanov *et al* 2004; b) Wen *et al* 2001; and c) Wang *et al* 1999

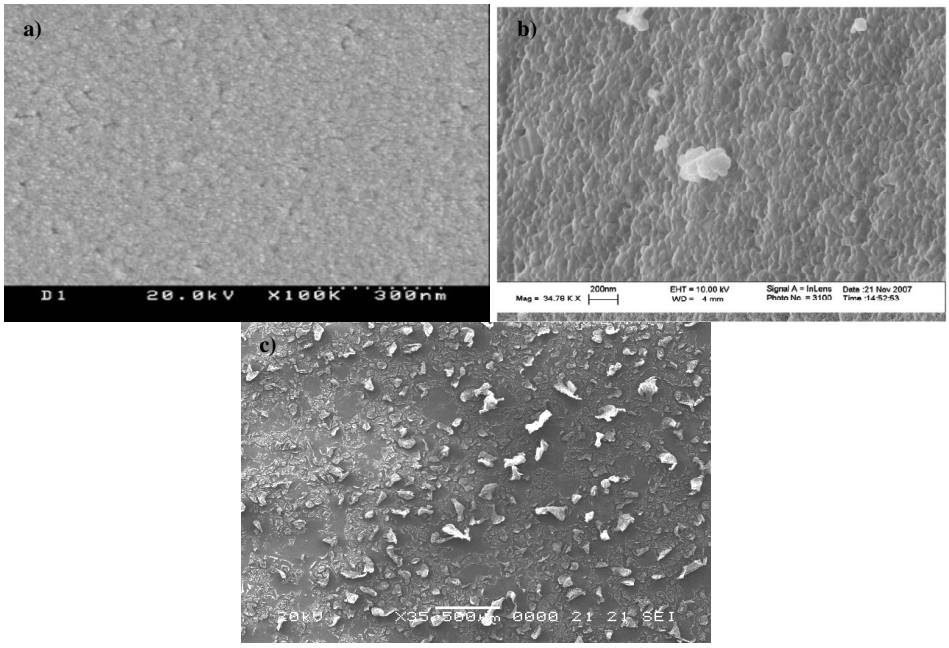

Figure 2.11 SEM of nano-TiO_2 thin films spin coated onto various substrates taken from the works of a) Ahn *et al* 2003; b) Ogden *et al* 2008; and c) Suciu *et al* 2009

2.5. Chapter Summary

This chapter attempts to familiarize the reader with previous works in regards to nanotitania in the form of particles and thin films, the hydrothermal method of producing nano-TiO_2 particles, and the solgel method of producing nano-TiO_2 thin films. Multiple published works was used to form a basis that explains the nature of nanotitania, along with the processing method. This chapter serves as a platform to the next chapter, where we will discuss the method we developed to produce nano-TiO_2 from local mineral precursors using slightly modified version of the methods, described above.

3. EXPERIMENTAL METHODS

3.1 Introduction

This section will explain the methods used in this work to produce nano-TiO_2 particles and nano-TiO_2 thin films from local mineral precursors. The previous section explained in details previous work regarding both materials, and using these works as a basis, we will adapt and develop new methods to suit our precursors, which are synthetic rutile, derived from ilmenite. Many factors need to be taken into consideration, such as chemical reagants, the total cost of the whole process, the relative purity of the product, and its potential application with regards to structural and chemical properties. Fig. 3.1 summarizes our route in obtaining nano-TiO_2 thin films.

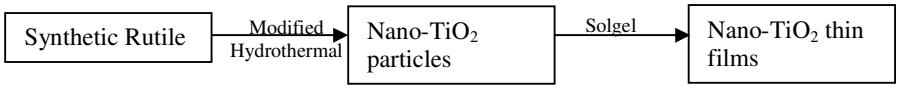

Figure 3.1. The development of nano-TiO_2 particles and thin films from precursor derived from local minerals

3.2. Nano-TiO_2 particles (modified hydrothermal method)

Due to the nature of our precursor (synthetic rutile), it is imperative that we find a suitable method that can effectively produce anatase nano-TiO_2 particles. The conventional hydrothermal treatment (Malinger 2011; Castro 2008), although effective, requires extensive modifications in our case, due to the unique nature of synthetic rutile compared to other common TiO_2 precursors. In effect, problems with the conventional hydrothermal method involving synthetic rutile are:

- The highly impure nature of synthetic rutile, which might react with chemical reagents and form compounds that embed themselves into the nano-TiO_2 particles
- Usage of the autoclave, which significantly drives up the cost of the operation and will also drive up the cost of the product
- The usage of highly toxic chemicals, such as TTiP, that necessitates the process being done in a controlled environment, unnecessarily complicating this lab scale process

The aim, with regards to this process is to eliminate the use of an autoclave and costly toxic chemicals, and lower the processing temperature as much as possible, in other words, make it green and as environmentally friendly as possible. A new process, outlined in Fig. 3.2, is proposed, which is a modification to the conventional hydrothermal synthesis.

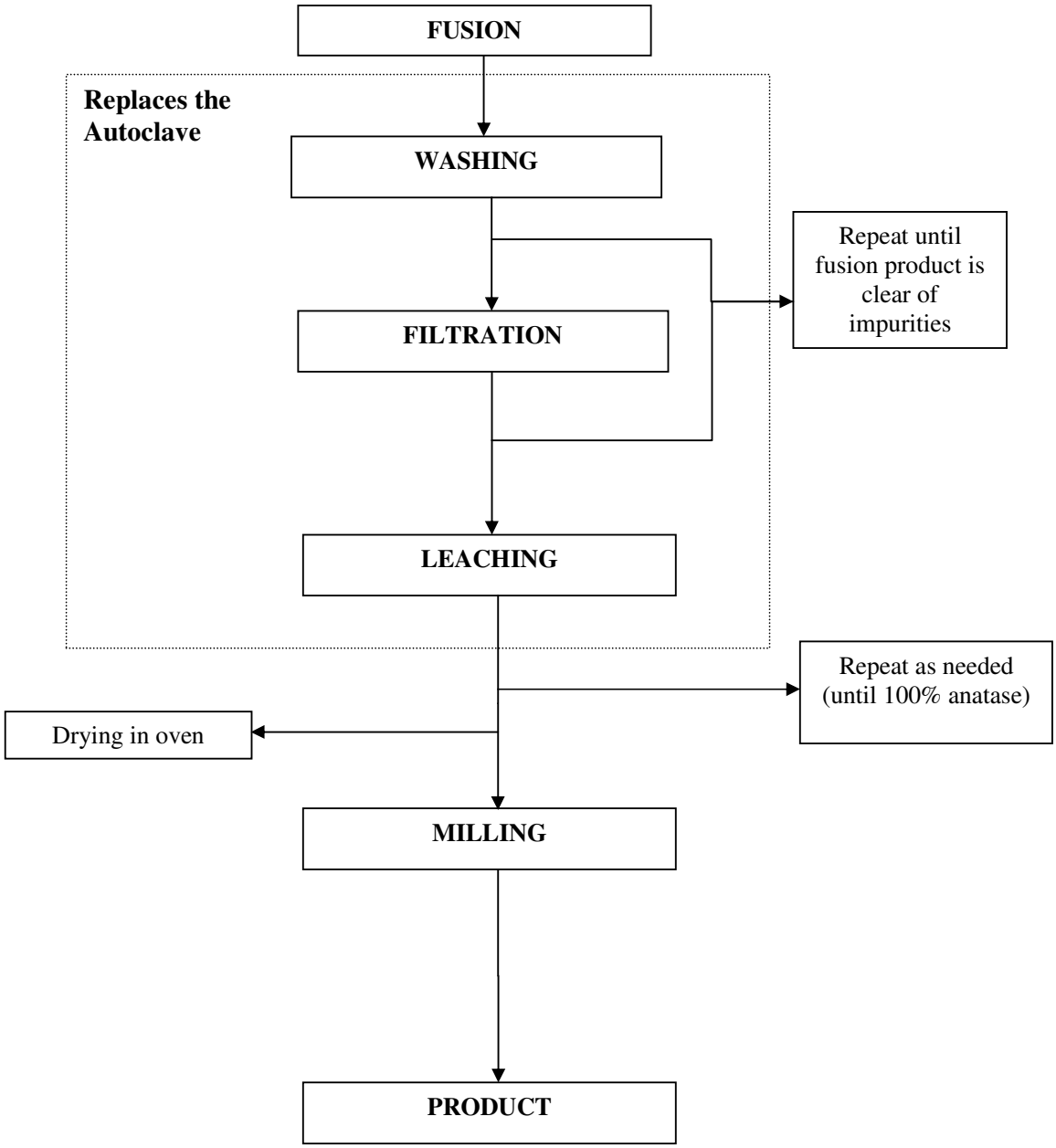

Figure 3.2 Modified hydrothermal treatment for nano-TiO_2 particle

Fig. 3.2 details our proposed method in producing nano-TiO_2 particles. This method is modified from the conventional hydrothermal method, shown in Fig. 2.5. We chose to keep the fusion step; however, the precursor used was synthetic rutile, instead of costly synthetic chemical used by other researchers mentioned in the previous chapter. This precursor is derived from a low-grade mineral, ilmenite, and has a significant amount of impurities (~8%). Therefore, the autoclave hydrothermal treatment was eliminated, and washing and filtration of the fused product was used instead, in order to remove these impurities. The autoclave treatment would have irrevocably fused the TiO_2 with the impurities, contaminating the product. In order to produce nano-TiO_2 particles, we decided to uses mild acid leaching, as the method is effective, efficient and environmentally friendly, while being cost effective. The implications of these steps are that instead of using an autoclave for hydrothermal treatment, the process is divided into two steps, the washing and filtration, and the acid leaching. These relatively inexpensive techniques significantly reduces the processing cost of nano-TiO_2 particles, and is easily monitored and controlled, as it is conducted in the open, without requiring the construction of a deliberate control chamber. One of the weakness of autoclave usage in the hydrothermal method is the inability for the researcher to observe the reactions when it is happening, which will allow them to stop the process or alter the parameters if it is not turning out as it should be. This modified hydrothermal method allows us to do just that, as mild acid leaching takes place in a reactor round flask, which is transparent. Each step will be explained in detail in the following subsections.

3.2.1 Alkaline Fusion

The first step in the modified hydrothermal method is alkaline fusion. This fuses an alkaline based chemical compound with our precursors via heat treatment. The ratio of

the mixture varies, but for the purpose of this work, we chose a 1:2 ratio, where 1 part of synthetic rutile is matched by 2 parts of NaOH pellets. The product from this process is a sodium titanate compound, which makes it easier to process into other forms of TiO_2, such as nanotubes and nanoparticles. There is precedent for this in literature, such as the work of Mazzocchitti *et al* (2009), and Manhique *et al* (2011). However, there is a marked difference between the work by these researchers, and our proposed method. For example, the work of Manhique *et al* (2011) involves extracting TiO_2 from ilmenite concentrates using alkaline fusion and heat treatment, with the products of the process being micron-sized TiO_2 particles, in excess of 1-10 um, while the work of Mazzocchitti *et al* (2009) uses hydrometallurgy to remove silicon and aluminium from ilmenite concentrates to obtain ferrotitanium, and an intermediate TiO_2 precursor. Our work will use synthetic rutile as a precursor to produce nano-TiO_2, surpassing the intermediate compounds formed in both process mentioned previously, to directly forming anatase nano-TiO_2 particles.

The weighed synthetic rutile and NaOH pellets will be thoroughly mixed using a glass rod, and each pellet of NaOH needs to be coated with synthetic rutile. The mixture will then be loaded into an alumina crucible, and placed in a furnace, set at 550ºC for 3 hours. Repeated experiments have shown that this parameter is the best, and how we arrived at this conclusion will be further discussed in Chapter 4.

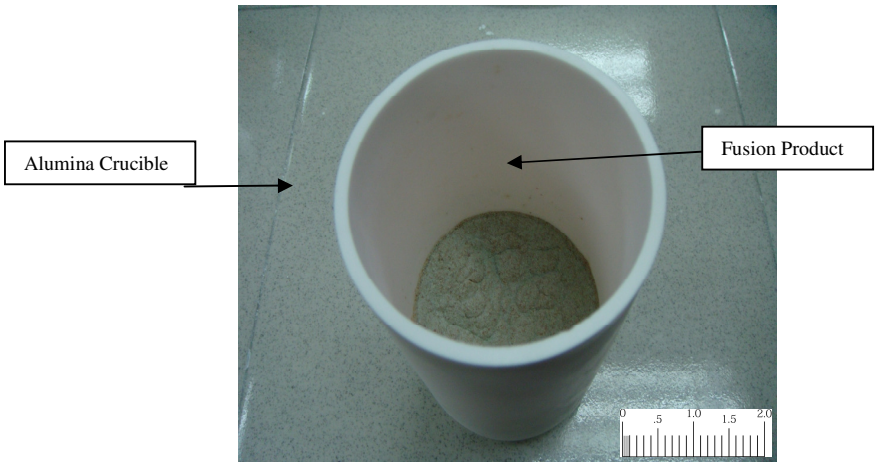

Figure 3.3 Sodium Titanate compound from alkaline fusion of synthetic rutile and NaOH pellets (scale: 1 mm : 5 mm)

As can be seen in Fig. 3.3, the sodium titanate compound is brownish-blue, but the clear indication of the success of this process is the thorough dissolving of synthetic rutile and NaOH pellets in each other. Anything less indicates an incomplete process, and the step needs to be repeated, either by increasing the processing temperature, or heating time.

3.2.2 Washing and filtration

This step involves washing and filtering the fusion product produced from the previous step using deionized water and an overhead stirrer. The washing and filtration process is quite common, and is present in virtually every form of TiO_2 processing, usually as an intermediate step. This step is crucial as it washes away the impurities in the fusion product, along with excessive sodium ions from the NaOH in the previous step. The elimination of these elements will ensure the maximum purity of the end product, and will also ensure that these impurities will not embed themselves in the nano-TiO_2 that will be formed during the next step. The impurities will be washed into the liquid

medium of deionized water, and the filtration and separation of this liquid medium from the solid precipitate will ensure that these impurities are eliminated.

This step starts by placing the fusion product into a 10 L beaker, and filling it to its capacity with deionized water. An overhead stirrer, set at 450 rpm, is positioned on the top, and ran for 3 hours, as shown in Fig. 3.4 (a). After that time, the solution is allowed to settle, which will allow us to see two distinct layers, a solid precipitate and its liquid byproduct. The liquid is carefully filtered for removal using a filtration setup shown in Fig. 3.4 (b), which consists of a ceramic funnel, conical flask and a vacuum pump. This step needs to be repeated at least once, in order to ensure that all the impurities that are present are eliminated from the fusion product. In our case, we conduct this process for a minimum of two times before using this washed and filtered product for the next step, acid leaching.

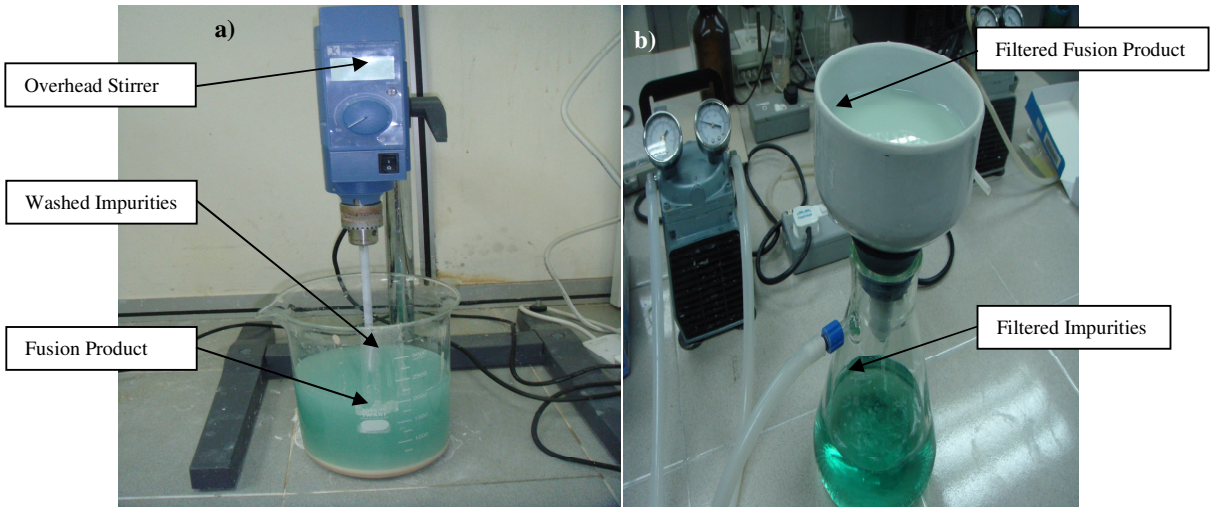

Figure 3.4 Setup for a) Washing and b) Filtration of the alkaline fusion product

3.2.3 Leaching

Leaching is basically a separation process that serves to isolate useful compounds from undesirable elements that constitutes the whole ore/mineral/element. This process is widespread in the mining and metallurgical industries, where the mined ore or metals are riddled with impurities and other undesirable elements/compound that makes up the whole material. Usually, a chemical solvent, such as an acid or alkali is used. The concentrations of these solvents are usually strong, and they serve as a medium that collects all these impurities in liquid form. The solution containing the impurities will then be filtered away and washed, leaving the precipitate that will be used.

The work of Sayan *et al* (2000, 2001) deals with leaching TiO_2 from clays and titania-containing ore using sulfuric acid. However, the product from this process is not nano-TiO_2 particles, but intermediate TiO_2 compounds that need further refinement for it to be of any practical use. Taking a page from his work, we use sulfuric acid (H_2SO_4) as a leaching agent to leach nano-TiO_2 particles from the sodium titanate compound formed during the fusion process. The sulfuric acid leaching agent will provide protons and

sulfate ions that interact with the sodium titanate compound, and these ions will serve to separate the sodium from the sodium titanate compounds, leaving TiO_2. This will leave the TiO_2 compound in an unstable state, and in order to achieve energy stability, the Ti-O matrix will reorient itself by shortening bond lengths and while keeping its tetragonal configuration in order to achieve the lowest and most stable energy configuration. This process is aided by the presence of the sulfate ions, which acts as a catalyst in the process, encouraging new crystallite formation. Once the sulfate ion is depleted, the formation of new crystallites ceases, and these crystallites are what make up the nano-TiO_2 particles in the form of a solid precipitate. The impurities, sodium and other undesirable elements are trapped in the liquid layer, making filtration a necessity in order to remove elements that might affect structural and chemical properties of the newly formed nano-TiO_2 particles. This mechanism is analogous to the ones presented in the work of Ou *et al* (2007), where the author(s) reviewed various mechanisms that produce titania nanotubes and nanoparticles, with methods such as the solgel method and the hydrothermal method being discussed extensively.

The parameter used in this leaching process to produce nano-TiO_2 particles are T=80ºC, t=4 hours and H_2SO_4 (aq) = 2 M. These parameters are determined to be the most suitable through extensive literature review and trial and error experimentation. Processing temperatures below 100ºC will minimize agglomeration of the particles, allowing it to retain its nano sizes, and remain in the anatase phase, without the risk of forming large particles or converting to the rutile phase. High temperatures will also destroy the nanostructures formed during the process, and might also integrate impurities into the nano-TiO_2 particles, as the extra energy introduced into the process might encourage the amalgation of impurities into the Ti-O matrices. A highly acidic leaching agent will also introduce too much protons and sulfate ion, where the sulfate

ion acts as a catalyst encouraging crystal growth to the point where it surpasses the nano-region. Also, the excess sulfate and protons will integrate themselves into the Ti-O matrix, forming compounds that might affect the structural and chemical properties of the nano-TiO_2 particles. Finally, the leaching time of 4 hours seems ideal, since surpassing this time will destroy the nanostructures and form agglomerates of TiO_2, due to prolonged exposure to heat and leaching agents, while shorter leaching time will not drve the process to completion, in that we will see rutile and anatase phases in the nano-TiO_2 particles. Fig. 3.5 shows the setup of the leaching process in detail.

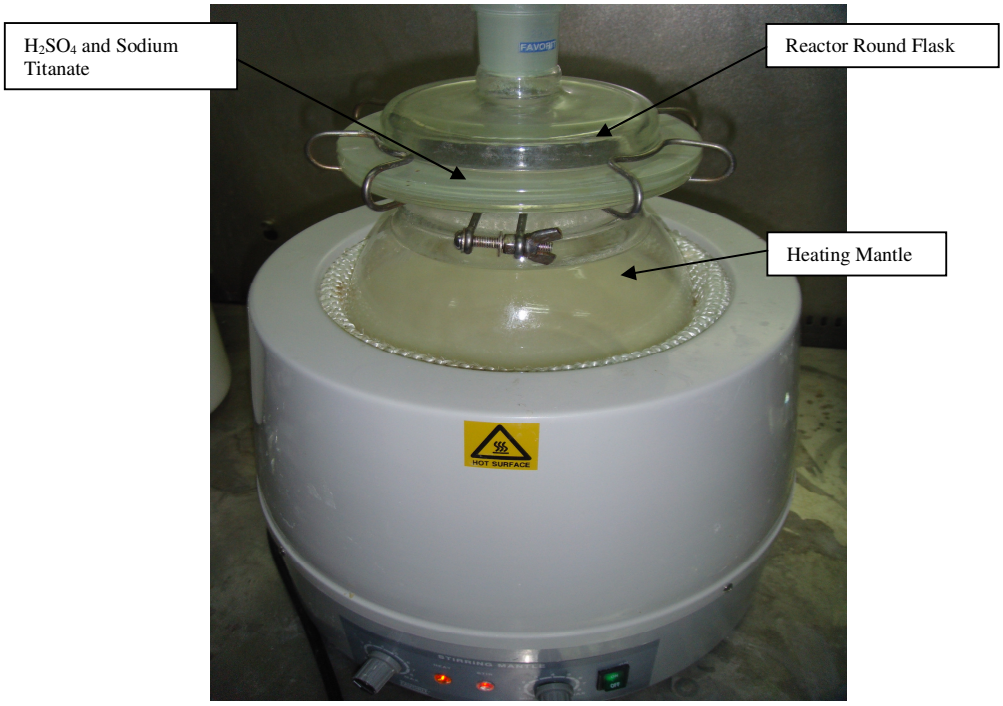

Figure 3.5 Leaching of sodium titanate complex using sulfuric acid

3.2.4. Post processing of nano-TiO_2 particles

After the leaching and filtration process that removes impurities and collect the nano-TiO_2 precipitate, post processing in the form oven drying, milling or mortar and pestle needs to be conducted. This is done in order to dry the precipitate and get nano-TiO_2 particles in powder form, and to remove any excess moisture and making sure that the nano-TiO_2 particles has a uniform distribution. In this work, we use the mortar and pestle to grind the nano-TiO_2 precipitate to form nano-TiO_2 particles. The final product is shown in Fig. 3.6.

Figure 3.6 Nano-TiO_2 particles

3.3. Thin Film nano-TiO_2 (Solgel)

Section 3.2 deals with the formation of nano-TiO_2 particles from synthetic rutile. This section, in turn, will explain how these nano-TiO_2 particles are used to form nano-TiO_2 thin films using the solgel process. Nano-TiO_2 particles will serve as the precursor to the process. For details regarding the solgel process, please refer to section 2.4.

In this work, we will use the solgel method to produce nano-TiO_2 thin films. The goal of this process is to utilize the nano-TiO_2 particles as precursors, avoid the use of toxic chemical reagants to ensure that the process remains environmentally friendly, and keep the overall processing cost low and simple. To this end, we have developed a method, outlined in the block diagram of Fig. 3.7.

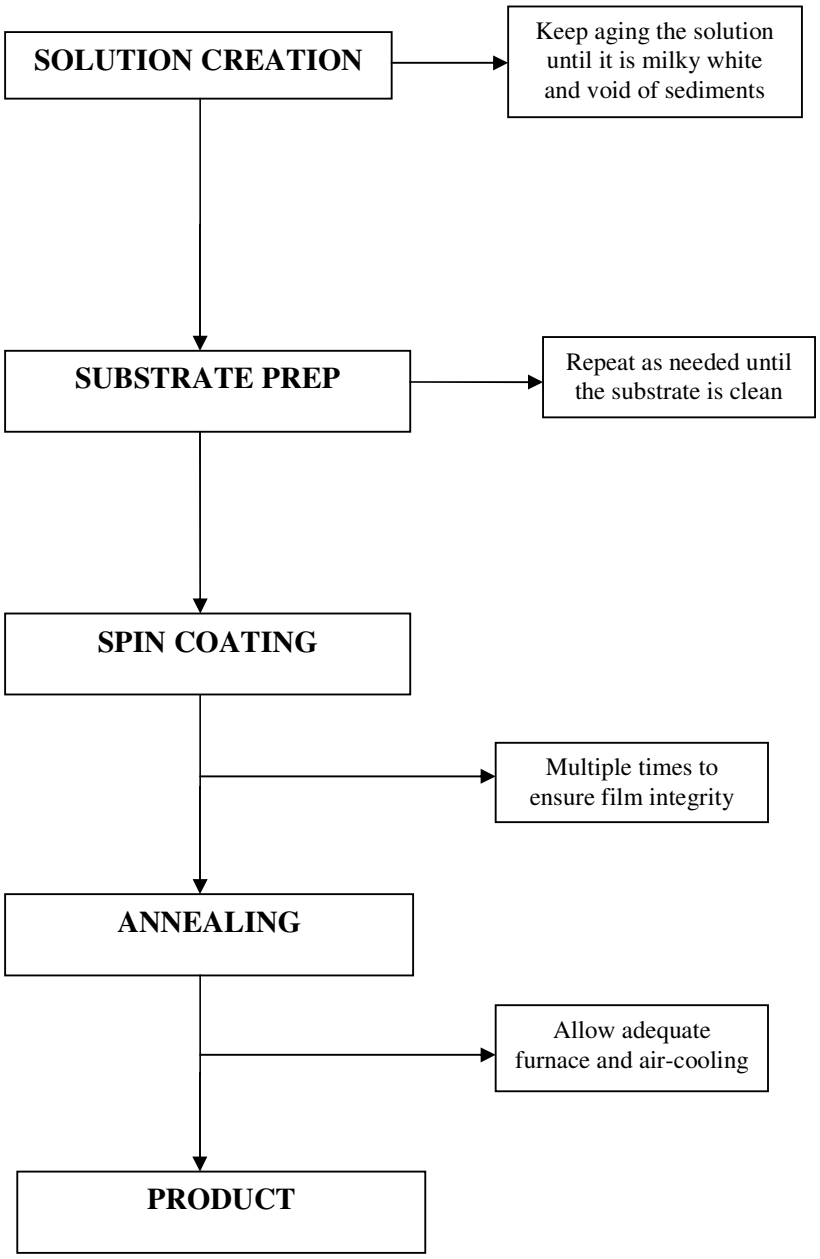

Figure 3.7. Modified Solgel method to produce nano-TiO_2 thin film

The steps presented in Fig. 3.7 are fairly analogous to the ones in literature, the only difference being the precursor. However, a trial and error approach is required to determine the best deposition speed and time, due to the fact that the precursor contains impurities, and is much smaller in terms of size than the usual precursors used in this process. The details of each step will be explained in the proceeding subsections.

3.3.1. Solution Creation

Solution creation is the staple of any solgel process. A solution is created by mixing a TiO_2 rich precursor with chemical reagants to form a TiO_2 rich solution. Details of previous work, along with the chemicals used in this process are available in section 2.4.1, along with a short summary of various previous researches.

In this work, nano-TiO_2 particles are mixed with 6 ml of acetic acid, and 30 ml of ethanol, in a sealed bottle. The mass of the nano-TiO_2 particles used were varied, from 0.01 g to 2 g. Table 3.1 summarizes the parameters of the sol-solution preparation.

Table 3.1. Sol-solution preparation parameters

Mass of nano-TiO_2 particles (g)	Volume of acetic acid (ml)	Volume of ethanol (ml)
2 1 0.4 0.1 0.05 0.01	6	30

A magnetic stirrer was introduced into the bottle and solution mixture, and it was stirred, without heating, for 20 hours. This will result in a TiO_2 rich solution, which is milky white in color. The time determination is done through trial and error, where 20 hours seem to be best, due to the fact that shorter times will result in the nano-TiO_2 particles not being dissolved in the solution, while stirring for more than 20 hours will destroy the uniformity and nano size of the particles. Fig 3.8 (b) shows the nano-TiO_2 sol-solution formed in this work.

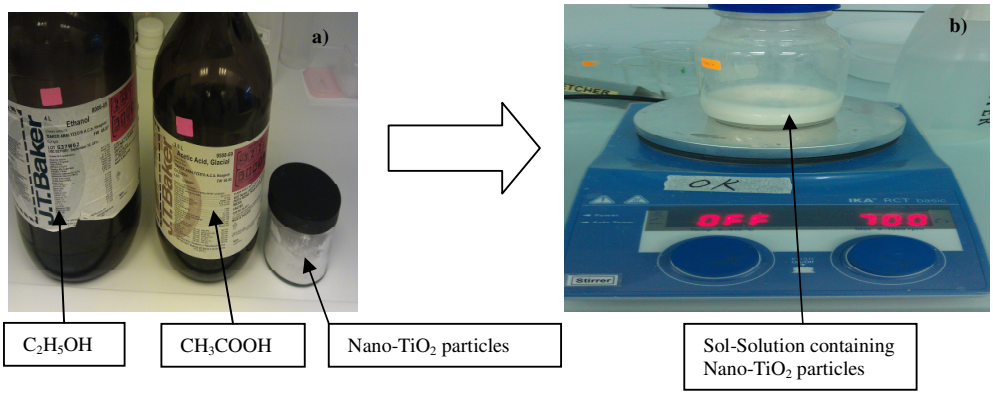

Figure 3.8. The steps in sol-solution preparation with a) the constituent chemicals and b) Mixing and spinning in a sealed bottle

3.3.2 Substrate Preparation

In this work, we are depositing the nano-TiO_2 sol-solution onto a glass/ITO substrate. The reason for us using this substrate is its relative inertness and its smooth and relatively flat surface. The substrate needs to be prepared and freed from any moisture or dust particles that might affect the adhesiveness of the film to the substrate, or might contaminate our thin films. Cleaning agents for substrates are acetone and deionized water, as these agents are relatively inert and easy to remove after washing.

We first place the substrate in a small beaker and sonicate it in a small sonicator for five minutes. After that, it is thoroughly cleaned using a soft cloth, dipped in acetone, to remove any dust or moisture that might be trapped on the glass/ITO surface due to surface tension or electrostatic bonds. In order to ensure maximum cleanliness of the surface, this step is repeated thrice. After the ethanol cleaning process, it is allowed to settle for less than a minute and air dried to ensure that the acetone is completely evaporated from its surface. Once the substrate seems clean and dry, it is immediately washed with deionized water and air dried by softly waving it in air until all the moisture disappears from its surface. Again, to ensure maximum cleanliness, this is repeated thrice. At the end of the washing and drying, a multimeter is used to determine the identity of each layer of the substrate. The deposition is to be done on the glass layer; hence, the layer, which shows a resistance value of infinite, will be the layer that the sol-solution deposition will be done on. This layer is marked with a small strip of color tape, in order to indicate the deposition layer. At this point, the substrate is ready for solution deposition. Fig. 3.9 summarizes the substrate preparation for nano-TiO_2 thin film deposition.

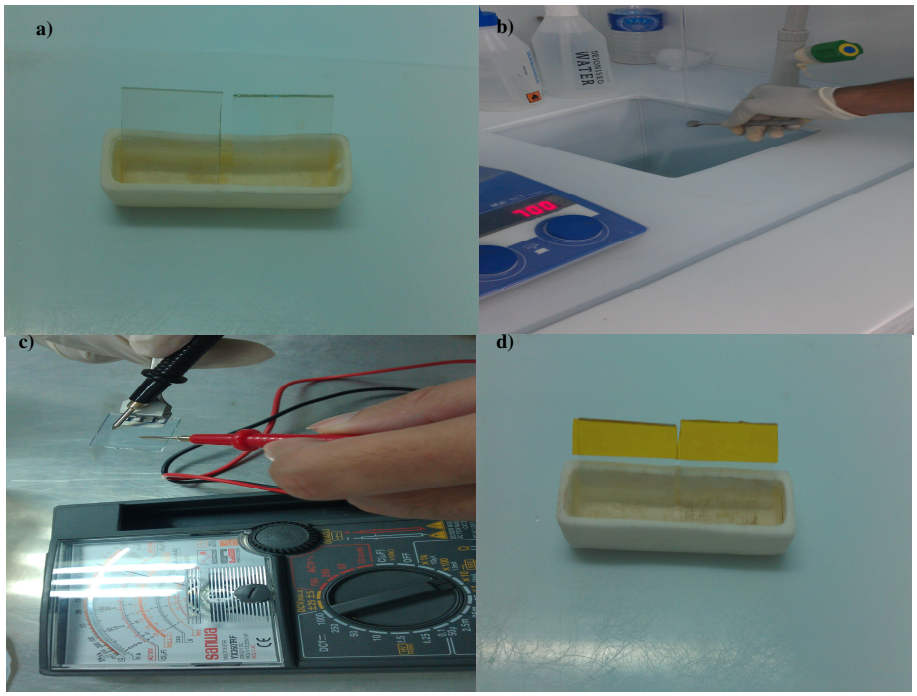

Figure 3.9. Substrate preparation for nano-TiO_2 thin film deposition with a) Glass/ITO substrate, b) washing and cleaning the substrate, c) determining which layer is glass or ITO and d) glass is the chosen deposition surface, with it being marked with colored tape

3.3.4 Spin Coating

Spin coating is a popular method for the deposition of sol-solution in the solgel process, and details of the process, as well as previous work(s) regarding this method are explained in detail in section 2.4.2.1. We will also use this method to deposit our solution onto the glass/ITO substrate.

We used a spin coater (Model WS-400B-6NPP Lite) for this process. This spin coater is equipped with a vacuum chamber, and the process is fully automated using a programmable controller (Laurell Tech Corp). The cleaned substrate is place at the center of the spin coater, and it is spun on its axis for 30 seconds at 1000 rpm. During this initial spinning phase, using a pipette (5 ml), the solution is carefully dripped onto

the substrate through an opening at the top of the spin coater, for a total amount of two drops. After the initial spinning phase, the speed is increased to 3000 rpm, and it is spun for a total of 1 minute. During this phase, three more drops are added to the substrate. At the end of the spin coating, the substrate is removed and placed in an incubator for five minutes at a constant temperature of 70ºC to enhance the integrity of the film. After this period, it is again spin coated using the same parameters for a total of ten times, or until the thickness and film is deemed sufficient enough via visual inspection. Once it is determined that the film is structurally sufficient, it is removed from the spin coater and again placed in the incubator at 70ºC for a total of 20 minutes. A pictorial representation of this process is shown in Fig. 3.10.

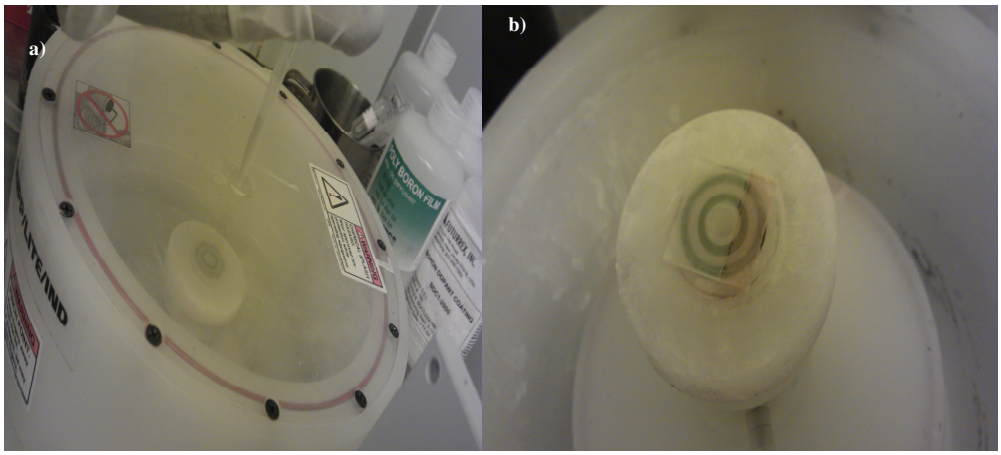

Figure 3.10. Spin Coating nano-TiO_2 thin film, with a) dripping the sol-solution during spinning onto the substrate and b) a single layer of deposited sol-solution

3.3.5. Post processing annealing

Once the deposition is completed, the thin films need to be annealed. The annealing of thin films are a matter of choice for the researchers, as some researchers eschew annealing, deeming their film uniform and strong enough, while other anneal their

films. Annealing serves to strengthen the adhesiveness between the substrate and coating, and also evaporates the extra solutions that skew the uniformity of the coating on the substrate. However, the annealing temperature needs to be carefully selected in order for it to just serve those two purposes without fundamentally altering any other properties or feature of the films.

In this work, we chose to anneal the films at 500ºC for 1.5 hours, using a furnace. The reason we chose these parameters is that TiO_2 change phases from anatase to rutile at 600ºC. The change of phase also indicates extensive agglomeration and the enlargement of crystallite sizes of the nano-TiO_2 particles, essentially destroying the very nature of the nanostructure. Keeping it below 600ºC will ensure that this does not occur. Also, this temperature completely vaporizes any remaining acetic acid or ethanol that might still be in the thin film, preserving the purity of the coating itself. Fig. 3.11 shows the furnace used for annealing.

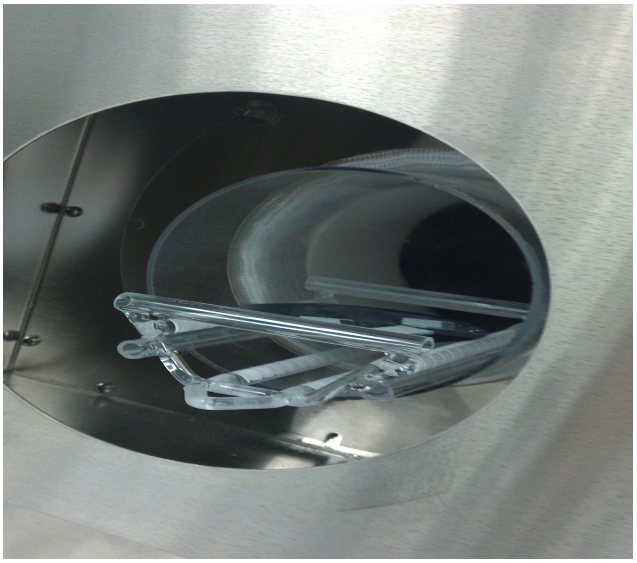

Figure 3.11. Post processing annealing of Nano-TiO_2 thin films

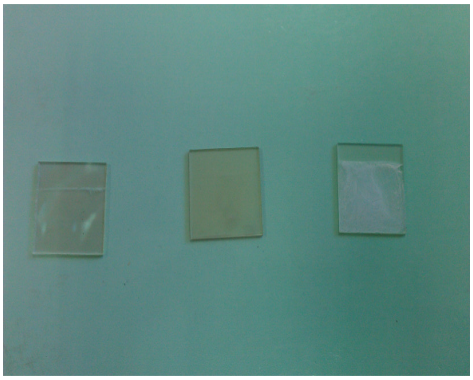

Figure 3.12. Thin Films TiO_2, post annealing

3.4. Characterization

Since the objective of this work is to determine the viability of derivatives of ilmenite as precursor to produce nano-TiO_2 particles and nano-TiO_2 thin films, extensive characterization of both products need to be carried out. Table 3.2 summarizes these characterization methods for both products.

Table 3.2 Characterization Method for nanoparticles and nano-TiO_2 thin films

Sample	Characterization Method	Properties
Nano-TiO_2 particles	XRD (PanAnalytical)	Crystallinity, Crystallite size
	EDXRF	Chemical composition
	BET/PSA (Quantachrome)	Surface Area/Particle Size
	SEM (FEI Quanta)	Morphology
	UV-Vis (UV3600 Shimadzu)	Optical Properties
Nano-TiO_2 Thin Film	XRD (Bruker)	Phases, Crystallinity
	UV-Vis	Optical Transmission
	AFM (XE-100 Park Systems)	Surface Profile, thickness
	SEM/EDX (FEI Quanta)	Morphology, chemical content
	UV-Vis (UV3600 Shimadzu)	Optical Properties

The results from these characterization methods will be compared to data from commercial products, or published results in literature, to determine whether it is viable as nano-TiO_2 particles and thin films. The viability of these products will enable us to identify its potential applications.

3.5. Chapter Summary

This chapter details the processing method used to produce both the nano-TiO_2 particles and nano-TiO_2 thin films. The methods used in this work are the amalgation of many established works and techniques, with slight modifications in some steps, and this is done to accommodate our unique precursors. The products are characterized for a variety of properties such as crystallite sizes, morphology, surface profile, film thickness, and optical properties in order to determine its viability as nanoparticles and thin films. The next chapter will discuss in detail the results of these characterization techniques, and any other anomalies or advantages that are the result of this process.

CHAPTER 4: RESULTS AND DISCUSSION (NANO-TiO_2 PARTICLES)

4.1 Introduction

This chapter will extensively discuss the characterization results of the nano-TiO_2 particles synthesized from the modified hydrothermal method. The characterization techniques used are outlined in Table 3.2, in the previous chapter. This work focuses on the structural properties such as the particle's crystallinity and crystallite size, its surface area and particle size, its morphology and surface profile, and its chemical composition, and its optical properties, such as absorbance and transmission. These properties are given special attention due to the fact that the criteria that determine whether the product is considered nano-TiO_2 hinges on these properties, as outlined in ISO CPD 10678. At the end of this chapter, with our results and analysis, we will establish our product as nano-TiO_2 particles, and its potential impact on the formation of nano-TiO_2 thin films.

4.2 X-Ray Diffraction (XRD)

We used the XRD technique to analyze our nano-TiO_2 particles, and the nano-TiO_2 particles purchased from American Elements, as a control sample. The X-Ray Diffraction (XRD) analysis was performed using a PANalytical PW3040/60 X'Pert PRO apparatus. The voltage and anode current used were 40 kV and 30 mA, respectively. The CuK_α = 0.15406 nm and the scanning range was from 20^o to 80^o. The reason we used the XRD technique to analyze our samples is listed below.

- To identify the elements present in our samples, ensuring that TiO_2 forms the majority, if not all, of our samples, and
- To determine the crystallite size (Scherrer Equation) and crsytallinity (Full Width Half Maximum) of the TiO_2 peak in our samples

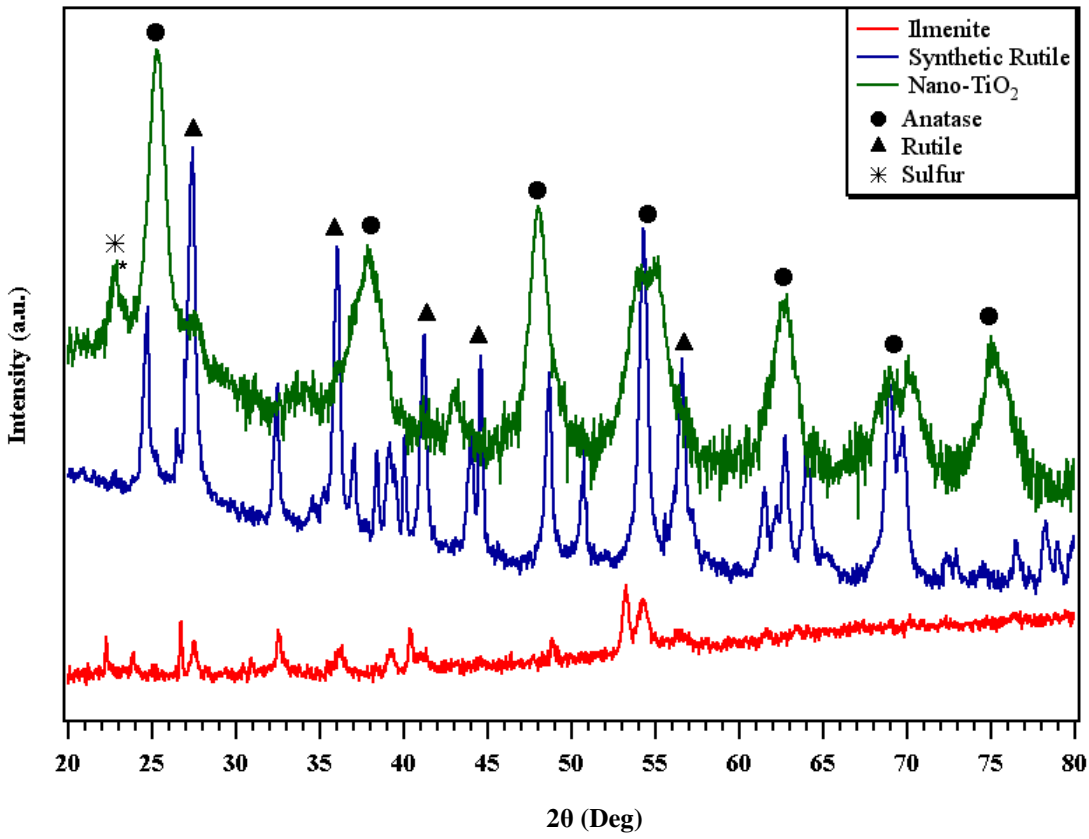

Figure 4.1. XRD Diffraction Peaks of ilmenite synthetic rutile and nano-TiO_2 particles

Fig. 4.1 outlines the evolution of the TiO_2 phase from ilmenite, a low-grade mineral, to synthetic rutile, the hydrometallurgically synthesized product, to nano-TiO_2 particles produced by our modified hydrothermal method. Ilmenite showed many peaks, which consist of Iron, Silicon, magnetite and other compounds. After ilmenite is processed via hydrometallurgy, we see TiO_2 peaks in the rutile phase emerging prominently among the many peaks present, although some other peaks, such as silicon, is still present, although

barely perceptible. Using this synthetic rutile as a precursor, the modified hydrothermal method is used to synthesize nano-TiO_2 particle, and in the XRD diffraction peaks of Fig 4.1, we see that only the TiO_2 phase remains, with remnants of sulfur, although the presence is quite small to warrant any significant effect on the structural properties of nano-TiO_2. Overall, casual visual inspection of the peaks, especially in the region of 26-30°, shows that the Full Width Half maximum value of the TiO_2 peaks also increases from ilmenite, to synthetic rutile, to nano-TiO_2 particles, indicating a significant decrease in the crystallite sizes of the TiO_2 peaks from one process to another. This is also indicative of another structural property of the samples, which is its crystallinity. The crystallinity of the sample is determined by the sharpness of the peaks, with sharper peaks representing more crystalline samples. This is also the case shown in the works of Oh *et al* (2007), where they used the hydrothermal method to synthesize nanosized TiO_2 powders, and analyzed it using the XRD technique. Their XRD peaks are present in four positions, at (101), (004), and (200) and (105), and are broad, indicating small crystallites, with it determined to be 11.2 nm. Table 4.1 outlines the crystallite size evolution from ilmenite to nano-TiO_2 particles, with the Scherrer Equation (Equation 4.1) used to calculate the crystallite size from the XRD diffractogram.

$$D = \frac{K*\boldsymbol{\lambda}}{\theta_{\frac{1}{2}}\cos\theta_B} \tag{4.1}$$

where K* is a constant (ca. 0.9), λ the X-ray wavelength (1.5418 Å), θ_B the Bragg angle and $\theta_{1/2}$ the pure diffraction broadening of a peak at half height, due to crystallite dimensions.

Table 4.1. The evolution of crystallite size of TiO_2 phase from ilmenite to nano-TiO_2 particles

TiO_2 peak of (at crystallographic orientation of (101))	**Crystallite sizes (nm)**	**FWHM (a.u.)**
Ilmenite	29.5	0.3897
Synthetic Rutile	41.6	0.2922
Nano-TiO_2 particles	15.6	0.4546

The comparison between the peaks are only done at the (101) crystallographic orientation due to the fact that it is only at this crystallographic orientation where all three elements show a clear TiO_2 peak, allowing us to compare and draw conclusions from them. If it were taken from any other crystallographic orientation, the comparison would be one sided and inconclusive, because it may be present in one element but not the other. For example, at $2\theta = 41°$, there is an anatase peak and rutile peak at both the nano-TiO_2 particle and synthetic rutile respectively, but no such peak is present in ilmenite, not allowing us to compare all three samples at this position.

Ilmenite contains a substantial, although minority amount of TiO_2, and according to literature, depending on its location, it is a more iron rich mineral (Pownceby *et al* 2008; Li *et al* 2006). The low TiO_2 presence accounts for the small crystallite size of the particles, due to the limited sensitivity of the XRD machine in detecting the small amounts of TiO_2. The smaller the weight percent of TiO_2 in the sample, the more difficult it would be to detect during XRD scans.

The hydrometallurgy process expels the majority iron and its derivatives from ilmenite and collects all the TiO_2 present in the sample, encouraging agglomeration and particle fusing between the TiO_2 particles. This inadvertently results in larger crystallites of TiO_2, as seen in Table 4.1, growing in size from 29.5 nm to 41.6 nm. However, the modified hydrothermal method on synthetic rutile significantly decreased the crystallite size of TiO_2 at the (101) crystallographic orientation, to a point where it is even smaller than the crystallite size of TiO_2 in ilmenite, while also forming the clear majority of the elements present. The modified hydrothermal method produces nano-TiO_2 particles that are smaller in crystallite size, and managed to remove residual impurity present in ilmenite, as shown in this XRD analysis.

Fig. 4.2 compares our nano-TiO_2 particles with commercial nano-TiO_2 particles purchased from American Elements.

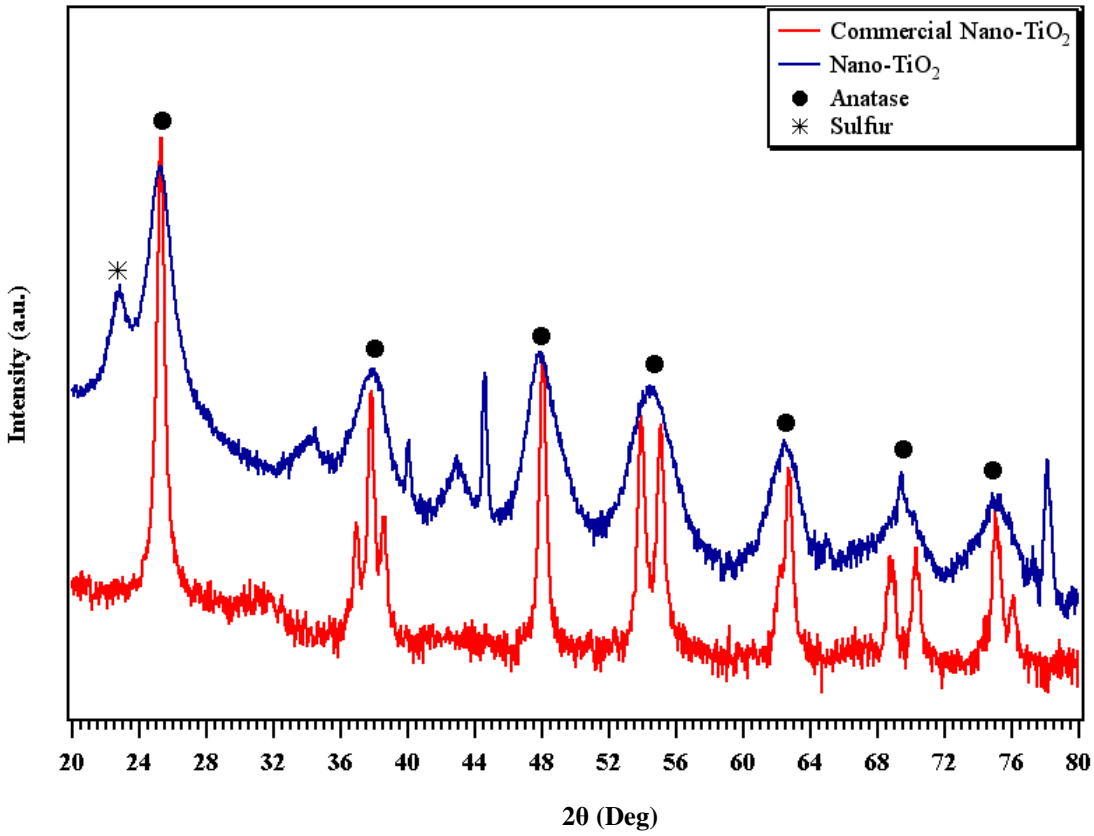

Figure 4.2. XRD Diffraction Peaks of commercial nano-TiO_2 and nano-TiO_2 particles, with * indicating the presence of sulfur

Fig. 4.2 clearly shows that our product is similar to the commercial product, the only difference being its crystallite size and the crystallinity. First, all the peaks present are identified as anatase TiO_2, indicating that the rutile phase has been successfully converted to anatase. This is also confirmed by the presence of anatase phase in the commercial samples, as the company (American Elements) indicated that their product is 100% anatase TiO_2. The crystallite size of our product is also clearly much smaller than the commercial product's, while our crystallinity is also much lower than the commercial product. Table 4.2 compares the value of our crystallite size and the FWHM of our sample, and the commercial sample.

Table 4.2. Comparison of crystallite size and crsytallinity of commercial and nano-TiO_2 particles produced by the modified hydrothermal method

Samples (at 101)	Crystallite size (nm)	FWHM (a.u.)
Nano-TiO_2 particles	15.6	0.4546
Nano-TiO_2 particles (American Elements)	40.0	0.2273

The structural feature of our product is clearly superior in terms of crystallite size and crsytallinity compared to the commercial product, although the determination of superiority or inferiority of a certain feature is largely dependent on the intended application. Various works reported small crystallites of TiO_2 produced from the hydrothermal method, such as Byrappa *et al* (2000), Watanabe *et al* (2010) and Chen *et al* (1995).

4.3. Energy Dispersive X-Ray Fluorescence (EDXRF)

The EDXRF is a method commonly used to determine the chemical composition of an unknown sample in terms of weight or atomic percent, depending on the setting and brand of the machine. This method is beneficial, as it requires minimal sample preparation, is relatively easy to use, and it also provides a rapid and non-destructive method for the analysis of trace and major elements in a sample. In short, in this work, EDXRF is used to

- Identify the elements present in the nano-TiO_2 particles

- Determine the weight percent of each element that is present in the nano-TiO_2 particles

All measurements were carried out under vacuum conditions, using an EDAX International DX-95 EDXRF spectrometer with a Mo target, equipped with a liquid- nitrogen-cooled Si(Li) detector. The incident and take-off angles were 451, with a Be window thickness of 12.5 mm. The distance between the sample (exposed diameter of 22 mm) and the detector was 4.5 cm. The energy resolution was 0.16 keV. The concentrations of elements from Sodium to Uranium were measured, although, lighter elements such as O and F will be virtually undetectable due to its light weight and bond with metals, therefore, in this analysis, the metals that are detected are assumed to be bonded with oxygen, forming oxides.

Most of the work in literature depended on the Energy Dispersive X-Rays attached to Scanning Electron Microscopes for chemical composition analysis, as seen in the work of Balachandra (2011) and Alexandrescu *et al* (2004), however, we opted for EDXRF, as the EDAX technique only scans a small area, and the samples involved were too little, whereas EDXRF involves a large amount of samples, and is more inclusive of the whole compound.

Table 4.3 summarizes the results from our EDXRF analysis of ilmenite, synthetic rutile, and nano-TiO_2 particles.

Table 4.3 EDXRF results of ilmenite, synthetic rutile and nano-TiO_2

	Elements (in wt %)					
Sample	**Ti**	**Zr**	**Nb**	**S**	**Fe**	**Si**
Ilmenite	67.94	NA	0.92	NA	29.00	NA
Synthetic Rutile	93.80	0.34	1.05	0.08	2.32	2.09
Nano-TiO_2 particles	95.07	0.49	0.36	2.83	0.09	NA

The results of EDXRF is supported by the XRD analysis from section 4.2, where the evolution from ilmenite to nano-TiO_2 shows the gradual removal of impurities, and the increase in terms of weight percent of TiO_2 phase in the samples. Ilmenite had only 67.94% of Ti/TiO_2, while synthetic rutile, after undergoing hydrometallurgy, increased to 93.8% TiO_2. After the synthetic rutile undergoes modified hydrothermal method, the TiO_2 phase increased to 96%. Major impurities that were present in the sample such as iron (29%), after undergoing two processes, were nearly negligible in the nano-TiO_2 particles stage. However, metals such as Zirconium and Niobium, is present at all stages of the process. Its amount is just below 1%, making it a viable dopant; however, the scope of this work does not cover the dopant effect in the structural and optical properties of the nano-TiO_2 particles. However, one anomaly that is worth mentioning is the emergence of sulfur in the nano-TiO_2 particles. It is surmised that the sulfur was a residual from the leaching process, where the reaction was saturated before the sulfate ions were depleted, allowing them to be

present in the sample in the form of ions or compounds. Its percentage is about 3%, and it is significant enough to be detected by the XRD and EDXRF analysis. In this work, we attempt to remove sulfur by washing and filtration of the leached product; however, repeated washing and filtration might destroy the integrity of the nanostructure, and encourage aggolomeration. Therefore, we limited washing and filtration of the leached product to twice, at the very most. However, it is worth noting that despite the presence of sulfur in the nano-TiO_2 particle, its structural properties seems unaffected, as clearly shown in the XRD analysis of the samples. It is also worth noting that despite the presence of metallic impurities in the form of Zirconium, Niobium and Iron, the structural properties of nano-TiO_2 particles produced by the modified hydrothermal method is still significantly better than the commercial product, especially in terms of crystallite sizes.

4.4. N_2 Adsorption-Desorption (BET) and Particle Size Analyzer (PSA)

The N_2 Adsorption-Desorption Surface Analysis (BET) and Particle Size Analyzer (PSA) are used to measure the surface area of the samples and its average particle size, respectively. These methods are chosen due to its non-destructive nature, its simplicity, and the accuracy of its results. The BET analysis was conducted using Quantachrome 1.2 apparatus. Prior to each absorption-desorption measurements, the samples were degassed at 373 K, under P = 0.35509 mm Hg for 24 hours. The specific surface areas were determined using the linearized BET equation at $0 < P/P_o < 0.30$.

The Particle Size Analyzer used is Microtac X100 (USA). It determines particle sizes using the laser diffraction method, and the samples are mixed in deionized water for analysis.The

results are statistical, with a bell curve representing the size distribution of the sample. The measurement range of the analyzer is between 0.02 to 704 μm. In this work, the median value of the particle size is taken as the average particle size of the sample, as it is established that the median value represents the sample as a whole. Both the BET and the PSA method are used in this work in order to:

- Determine the reactive surface area of the nano-TiO_2 particles
- Determine the average particle size of the nano-TiO_2 particles
- Compare both values and the correlation between these two structural properties

Table 4.4 summarizes the results from these two techniques.

Table 4.4. Summary of Physical between ilmenite, synthetic rutile, nano-TiO_2 and Commercial nano-TiO_2

Samples	S_{BET} (m^2/g)	Particle Size (μm)
Ilmenite	5.9	232.5
Synthetic Rutile	3.9	298.2
Nano-TiO_2 particles	186.8	4.1
Commercial nano-TiO_2	41.9	27.9

As seen in Table 4.4, the evolution of surface area from one phase to another is almost exponential. Ilmenite has a surface area of 5.9 m^2/g, although this surface area is not TiO_2 exclusive, as it includes impurities such as iron. After undergoing hydrometallurgy and

converting to synthetic rutile, the surface area decreases to 3.9 m^2/g, and at this point, the sample is almost TiO_2 exclusive, with 93.78% Ti/TiO_2, as shown in Table 4.3. However, undergoing the modified hydrothermal method, the surface area became 186.8 m^2/g, an increase in surface area of about 46,897.8%, which is unprecedented, even in literature. Chen *et al* (2007) used the hydrothermal method to synthesize nanoparticles for dye-synthesized solar cells, with titanium (IV) *n*-butoxide as its precursor, and the surface area of these nanoparticles turned out to be 255 m^2/g. The difference with our work is that the precursor he used was highly pure, and their hydrothermal method involved autoclave usage, while we managed to produce nano-TiO_2 particles with a surface area of 186.8 m^2/g using precursors that is a fraction of their precursors in terms of price and purity. Also, the work of Akarsu *et al* (2006) produces nano-TiO_2 particles with a surface area of 40 m^2/g, using Tetrabutylorthotitanate as its precursor, and in this case, it is clear that the nano-TiO_2 particles produced by our work is superior, even though it is a much cheaper and simpler process. Our work proved that high surface area is achievable using mineral byproduct derivatives, which is cheap and readily available in Malaysia. Even the commercial nano-TiO_2 particles' surface area is at least seven times smaller than our samples, as shown in Table 4.4. Large surface area is one of the structural properties that are highly sought after in the field of nanomaterials, as it requires smaller amount of per weight materials that can work better than conventional materials. The potential implications of this is further discussed in Chapter 6.

The particle size analysis shows a tremendous reduction in particle size, from ilmenite to nano-TiO_2 particle. Processing of ilmenite into synthetic rutile increased the average particle size from 232.5 to 298.2 μm. In turn, the processing of synthetic rutile into nano-TiO_2 brought down the average particle size from 298.2 μm to 4.1 μm, a reduction of

71,731%. The average particle size of commercial nano-TiO_2 particles is 41.9 μm, which is ten times larger than our samples.

Both analysis techniques proved that nano-TiO_2 particles from synthetic rutile as its precursor produced by the modified hydrothermal method is superior to the commercial product in terms of crystallite size and surface area, and the improvement is not slight, but rather quite profound, making it viable for a multitude of applications which will be further discussed in chapter 6.

4.5. Scanning Electron Microscope (SEM)

The Scanning Electron Microscope is used due to its ability to obtain clear images of our samples, which is an an inorganic oxide, and the rather simple sample preparation, thus minimizing chances for error. It is also a staple in literature, especially when dealing with nanomaterials, as it is capable of showing the nanomaterials' details and features quite accurately. Quite a few works are present in this regard, as seen in the works of Hussain *et al* (2010) and Kang *et al* (2001), where the SEM technique is used to show the result of their studies. In short, the SEM technique is utilized in order to:

- Determine the morphology of the nano-TiO_2 particles
- Visually compare our product with the commercial product

The SEM used in this work is the FEI Quanta Scanning Electron Microscope (SEM). The power and working distance was varied to accommodate different samples, but generally, it

was set at 30 kV and 8.0 mm respectively. The samples were coated with gold in a thermal evaporator, a process that takes about an hour.

We analyzed our nano-TiO_2 particles and the commercial nano-TiO_2 particles. Various images were taken, but we chose only a few images in order to best demonstrate the features that we are trying to show in this work. Fig. 4.3 shows the SEM of both samples.

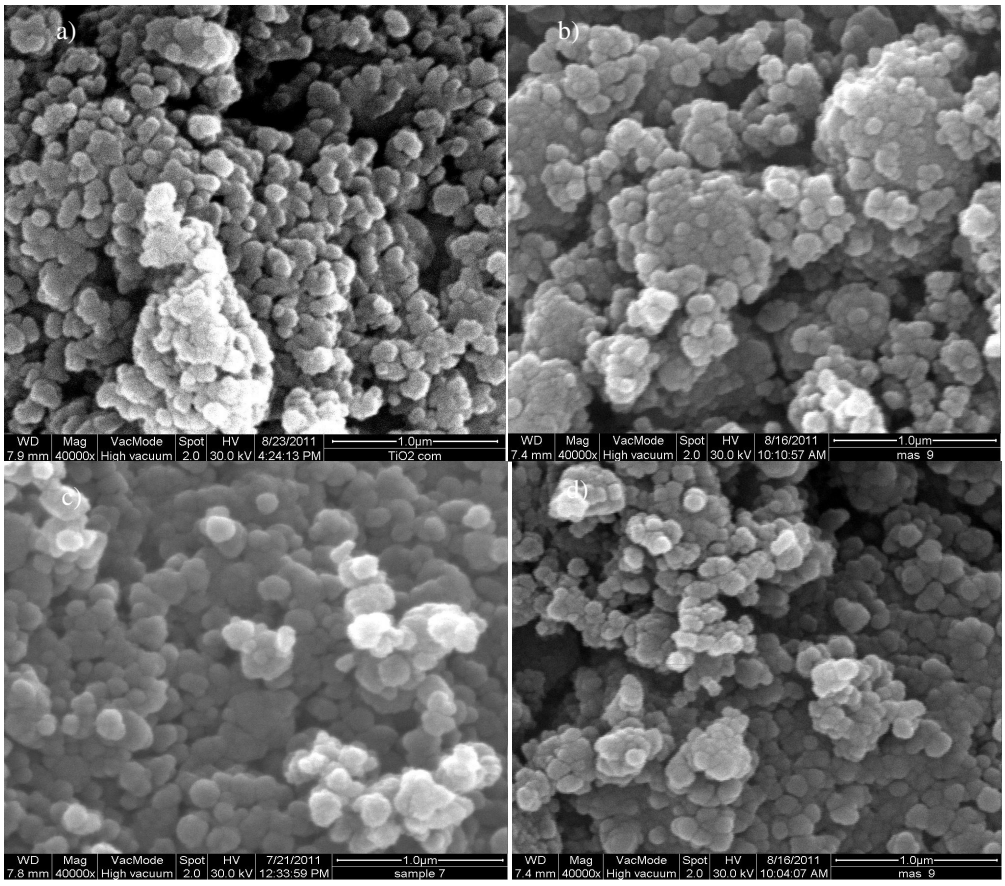

Figure 4.3. SEM of the a) commercial nano-TiO_2 and b), c) and d) nano-TiO_2 particles produced by modified hydrothermal method taken at 40kx magnification

As seen in the figure above, the morphology and the features of both samples differ in quite a few aspects. The most obvious difference is the rather uniform shape and distribution of the commercial sample, compared to our nano-TiO_2 particles. Another prominent difference is the size of the particles, where average size of the crystallite of the commercial sample is clearly larger than the majority of the crystallites that form our nano-TiO_2 particles. Another feature is the agglomeration in our nano-TiO_2 particles, whereas its existence in the commercial sample is negligible.

All of these features seen in our sample can be explained rather simply by its processing route and the parameters involved during processing. The distribution and uniformity of our nano-TiO_2 particles are rather skewed, due to the fact that its precursor, synthetic rutile, is rather uneven in size and distribution, and although the modified hydrothermal processing greatly improved this flaw, it is not capable of fully eliminating this anomaly, as it is still somewhat noticeable in nano-TiO_2 particles. The small crystallite sizes of our nano-TiO_2 particles is due to the reaction of the sodium titanate compound with the protons and sulfate ions during leaching, where the reorientation of bonds during leaching recreates smaller crystallites in order to minimize the total energy during processing. In a sense, the smaller crystallite sizes is a product of a system trying to stabilize itself by channeling the extra energy produced by the interaction of protons, sulfate, sodium titanate, and the extra heat during leaching into the titanate compounds that forces it to miniaturize itself. This mechanism is explained in detail in the works of Byrappa and Adschirri (2007). This phenomenon is also related to agglomeration, where agglomeration is the reaction of nanoparticles when it is provided with extra energy in the form of heat and chemical reactions. The excess heat and chemical reactions will bond the particles to each other to eliminate grain boundaries, as grain boundaries are where it is energetically most unstable.

The elimination of grain boundaries will merge these multiple nanoparticles into one large particle. This is clearly seen in our samples, where to a certain extent; agglomeration is quite visible, whereas the commercial sample shows little to no sign of agglomeration. The existence of excess energy in the system is also proven largely by the presence of sulfur in our nano-TiO_2 particles, as shown in Figs. 4.2 and 4.3. These excess sulfur showed that the system had more than enough sulfate ions to react with the sodium titanate compound to form nano-TiO_2 particles, with some left over, due to the amount left still being significant enough to be present in XRD scans.

4.6 UV-Visible-Near Infrared Analysis (UV-Vis-NIR)

The UV-Vis-NIR method is mainly utilized to determine the optical properties of the nano-TiO_2 particles. This method is nondestructive, highly accurate, inexpensive, and requires minimal sample preparation. It utilizes many modes such as reflectance and transmittance to determine the many optical properties inherent in the samples, by passing high intensity light through the samples, and gathering the feedback in the form of plots. In this work, the UV-Vis-NIR method is going to be used to:

- Determine the absorbance and the optical bandgap of the nano-TiO_2 particles and the commercial sample
- Determine the optical transmittance of the nano-TiO_2 particles and the commercial sample

The UV-Vis-NIR analysis in this work is carried out using Shimadzu UV3600 UV-Vis-NIR Spectrophotometer. The light source used in the scan has a scanning wavelength of 340 nm, and the scan range was from 200-800 nm, in 0.5 nm intervals. Two measurement modes were used in this study, which are the reflectance mode and the transmission mode. The results of the reflectance mode were converted to absorbance coefficient using the internal software supplied by Shimadzu, by utilizing the Kubelka-Munk equation.

The absorbances of the samples were first measured, and the results are shown in Fig. 4.4, while its transmission spectrum is shown in Fig. 4.5.

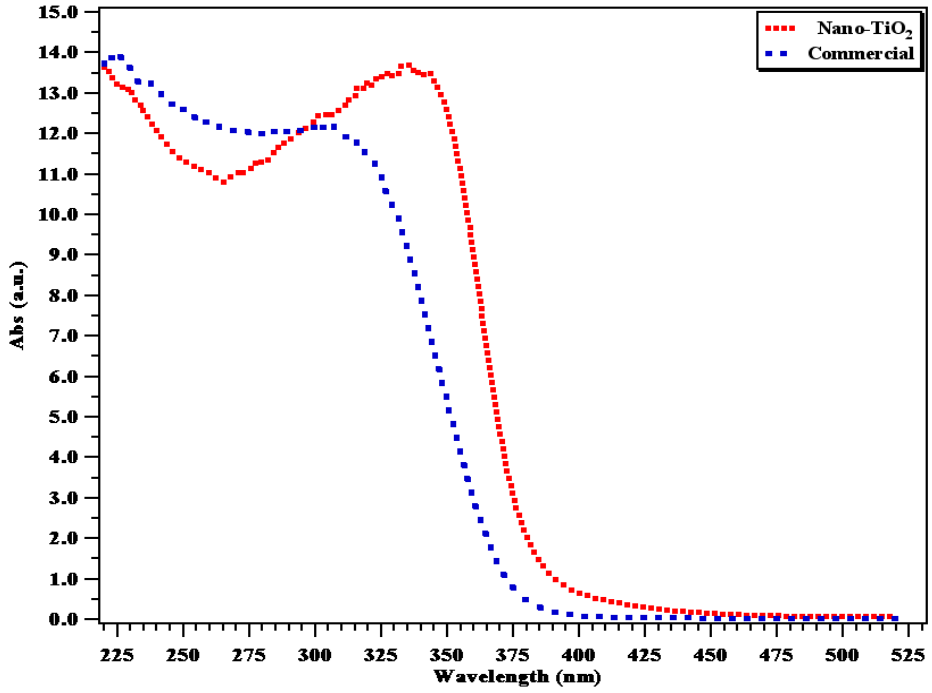

Figure 4.4. Absorbance Spectrum of nano-TiO_2 particles and the commercial sample

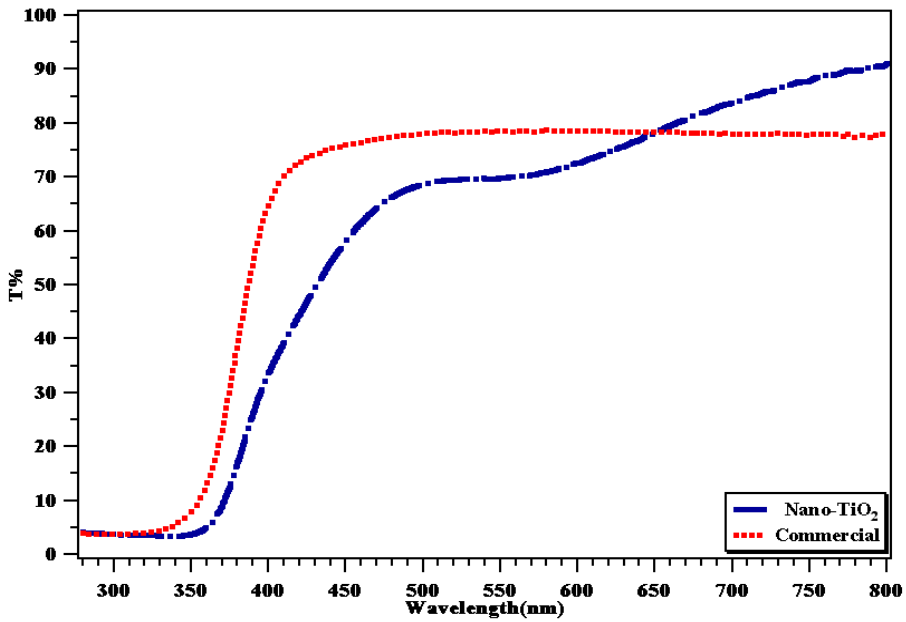

Figure 4.5. Transmission Spectrum of nano-TiO_2 particles and the commercial sample

The samples are prepared via packing it into a sample holder using a compressor to ensure highest packing density and even distribution of powdered sample. Hence, the chances of error or of skewed readings are extremely small, and these results are deemed as accurate with minimal error in this case.

The previous section discusses the structural properties of the nano-TiO_2 particles extensively. It is also well established in literature (Mu *et al* 2010; Fen *et al* 2011) that the structural properties have a tremendous influence on the optical properties of nanoparticles. Structural properties that affect the optical properties of the sample include crystallite/particle sizes, porosity, packing density and crystallinity. As established previously, our samples have smaller crystallite sizes, lower crystallinity, and higher packing density than the commercial sample. It is expected that the absorbance and optical transmission of nano-TiO_2 particles would be higher than its commercial counterpart, and

this is proven in Figs. 4.4 and 4.5. The most prominent absorption edge in the nano-particle absorption spectrum is shifting closer to the visible spectrum, nearing 400 nm, whereas the commercial sample's absorption edge is closer to 350 nm, still in the UV region. Table 4.5 summarizes the optical bandgap of both samples, calculated by extrapolating the absorption edges, and plugging the intercept into equation 4.2.

$$E_g = \frac{1240}{\lambda} \quad 4.2$$

where E_g is the optical bandgap, and λ is the wavelength corresponding to the relevant absorbance/transmission.

Table 4.5. The optical bandgap of nano-TiO_2 particles and its commercial counterpart

Sample	Optical bandgap (eV)
Nano-TiO_2 particles	3.23
Nano-TiO_2 particles (commercial)	3.30

The optical bandgap of the nano-TiO_2 particles are clearly smaller than the commercial sample, although by a small margin. The smaller nanoparticles, with its higher packing density and high specific surface area, as outlined in section 4.2 and 4.4, makes these particles absorb the passing UV radiation, and continue absorbing visible radiation close to the 400 nm region. In contrast, the absorbance displayed by the commercial sample is low due to its generally lower packing density, dispersed and larger nanoparticles.

The transmission spectrum is inversely proportional to the absorbance spectrum; where transmission is high, the absorbance is low, due to the fact that radiation that is transmitted

through the sample is not being absorbed. This is clearly evident in Fig. 4.5, where the transmission is lowest in the UV region (300-400 nm), and it rises up and stabilizes in the visible region (400-700 nm). The NIR region is beyond the scope of this work, and it shall not be elaborated upon here. The transmission of commercial sample is on average 78% between 400-600 nm, and the transmission of nano-TiO_2 particles is 68% in the same range. Due to its inverse relationship with absorbance, transmission is also affected by the same structural factors as absorbance, only differently. The smaller particles and high packing density of nano-TiO_2 particles generally prevents visible light radiation from passing through it, lowering its transmission. Instead, it encourages either absorption, as seen in Fig. 4.4, where the absorption of nano-TiO_2 particles is clearly higher, or it might be due to light scattering. XRD and EDXRF analysis in sections 4.2 and 4.3 respectively showed the presence of metallic and nonmetallic impurities. These impurities are detrimental to the optical transmission, as it scatters or reflect the incident light. The transmission of the commercial sample is almost 10% higher, and this is accounted for mostly by the less dense packing factor, the more homogenous and separated particles, and the absence of impurities. As a side note, larger particles also tend to scatter incident light, and this might account for the relatively low transmission of the commercial sample. However, the disadvantage of large particles is offset by its purity, which our sample clearly lacks.

4.7 Chapter Summary

This chapter presents and analyzes the results from various characterization techniques such as the XRD, EDXRF, BET, PSA, SEM and UV-Vis-NIR. All of these techniques are used to quantify and qualify the structural and optical properties of the nano-TiO_2 particles that were produced using the modified hydrothermal method. In short, it was found that the particles are indeed nano in size, as proven by the XRD and SEM, is crystalline instead of amorphous, as proven by the relatively sharp peaks in XRD analysis, contains in excess of 96% TiO_2 in the anatase phase, albeit with a few impurities such as iron, zirconium and niobium, as confirmed by the EDXRF and XRD, has an average particle size of well below 10 μm, and a reactive surface area of 186.8 m^2/g. The optical bandgap was determined to be 3.23 eV, and its optical transmission was 68%. It was noted that even with the presence of impurities, the structural property of the nano-TiO_2 particles is comparatively superior to the commercial nano-TiO_2 particles in almost all aspects, although these impurities seem to somewhat effect the optical properties, although not by a large margin. The optical and structural properties of nano-TiO_2 particles are heavily intertwined, and changing one will change the other. It is concluded at this point that the modified hydrothermal using synthetic rutile as its precursor is a viable method of producing high quality anatase nano-TiO_2 particles. These marvelous structural properties pave the way for many potential applications of these nano-TiO_2 particles, which will be further discussed in Chapter 6.

CHAPTER 5: RESULTS AND DISCUSSION (NANO-TiO_2 THIN FILMS)

5.1 Introduction

The previous chapter discussed the characterization results of nano-TiO_2 particles. In this chapter, we will discuss the results from characterizing the nano-TiO_2 thin films fabricated using the nano-TiO_2 particles as its precursor. The deposition method used to deposit the sol-solution onto the glass/ITO substrate was the spin coating method, detailed in section 3.2.4. In this work, many samples were prepared and analyzed; however, only three samples were selected to represent the nano-TiO_2 thin films in this thesis, due to the fact that other samples (2g, 01.g and 0.01 g) failed to adequately adhere to the substrate. At the end of the chapter, we will summarize the features, advantages and disadvantages of the thin films produced by this method.

5.2 Grazing Angle X-Ray Diffraction (GAXRD)

The thin films were analyzed using a specialized XRD technique, called the Grazing Angle XRD (GAXRD). This is due to the fact that powder diffraction XRD scans of a thin film deposited on a substrate will produce the diffraction peaks of the substrate, or even if the diffraction pattern of the thin film is actually present, it will be overshadowed by the much stronger peaks of the substrate, making it virtually undetectable, or at best, inconclusive. GAXRD allows the scanning of thin films with minimal contribution from its substrate in the diffraction peaks. Fig. 5.1 shows the basic schematic of a thin film analysis using the GAXRD technique, taken from Tanner *et al* (2004). The works of Lin *et al* (2012), Martyanov *et al* (2005) and Wen *et al* (2001)

showed usage of the GAXRD technique to analyze TiO_2 thin films fabricated by the solgel method and deposited by spin coating.

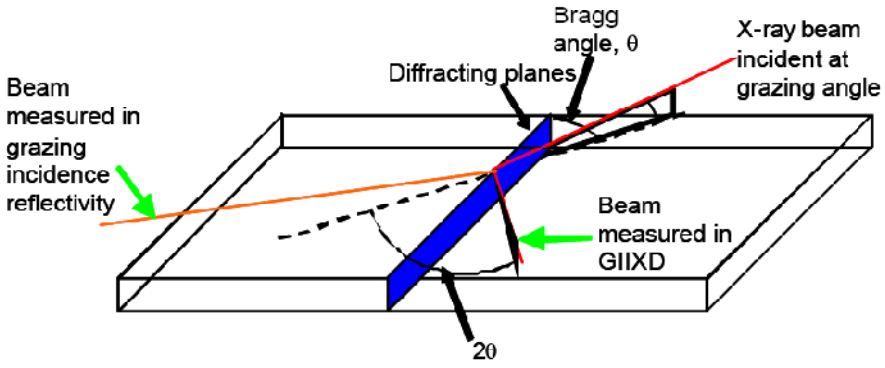

Figure 5.1. Setup for GAXRD analysis of thin film samples

The GAXRD analysis was performed using a Bruker D8 Advance XRD Diffractometer. The CuK_α = 1.54 Å, with a scanning range was from 20º to 80º. The scan setting was customized to the thin film setting with a step-mode of 0.5º.Within the scope of this work, the usage of the GAXRD technique is:

- To confirm the existence of TiO_2 in the thin film
- To determine the phase of the TiO_2 in the thin film

Fig. 5.2-5.4 details the XRD Diffraction peak of the nano-TiO_2 thin films deposited via the spin coating technique.

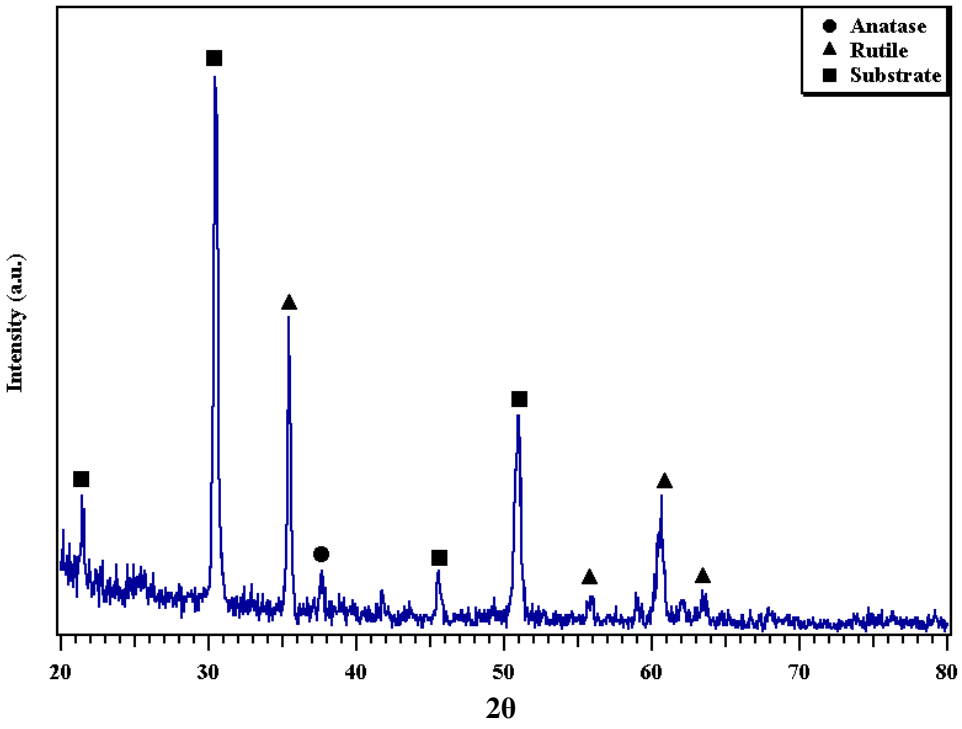

Figure 5.2. XRD Diffraction peaks for m_{TiO2} = 0.05 g thin films

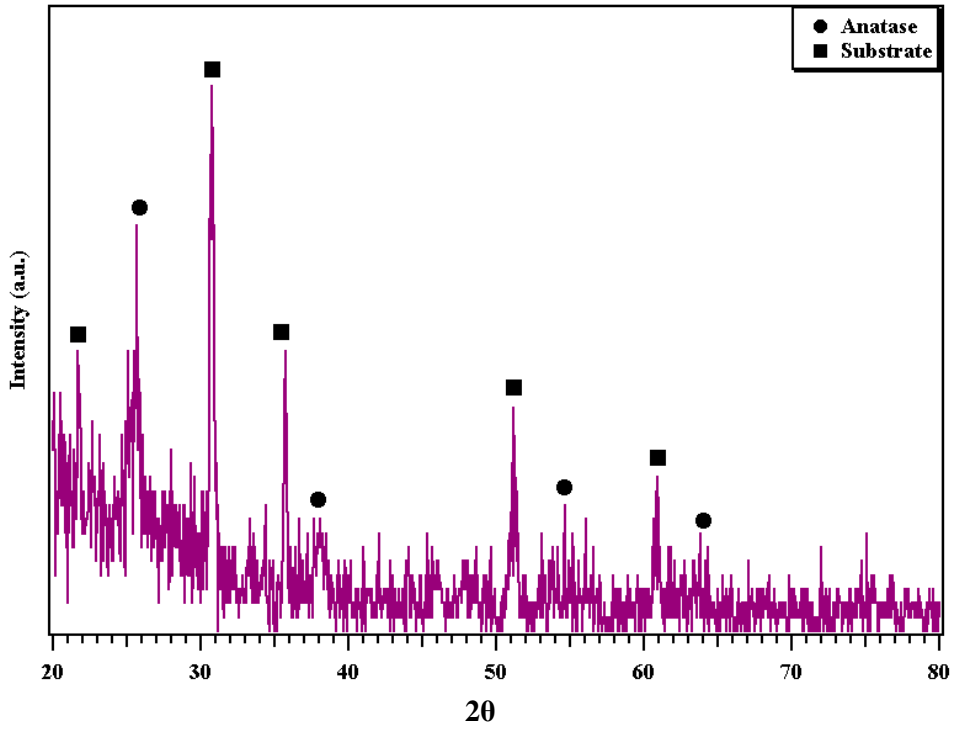

Figure 5.3. XRD Diffraction peaks for m_{TiO2} = 0.4g thin films

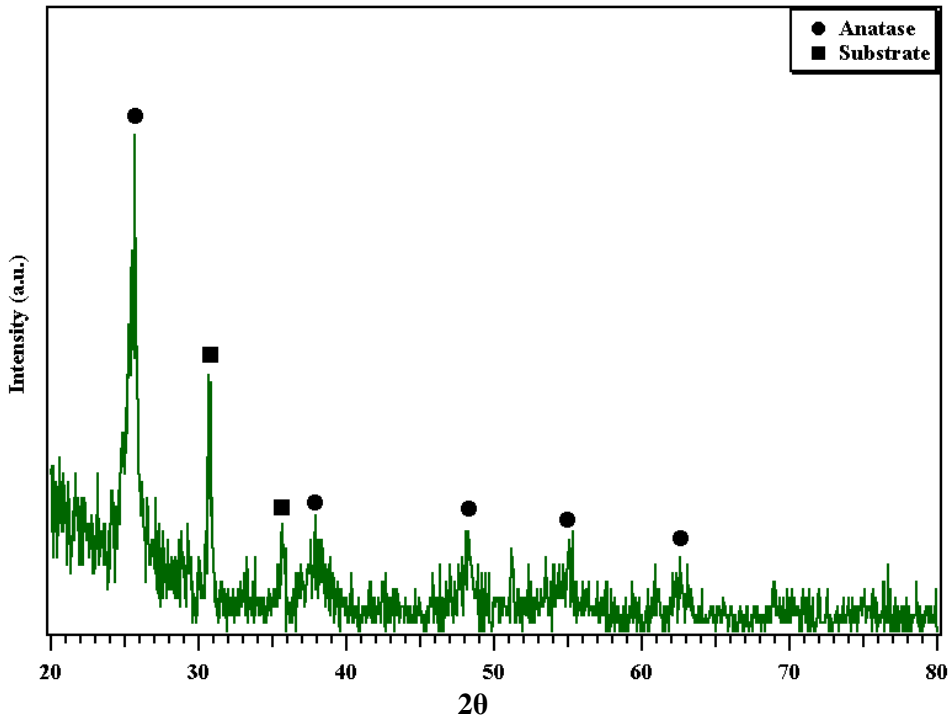

Figure 5.4. XRD Diffraction peaks for m_{TiO2} = 1 g thin films

All of the samples showed the presence of the anatase phase of TiO_2, with the m_{TiO2} = 0.05 g having rutile as its majority phase, although a small amount of anatase is still present, with varying degrees of intensity. The difference is attributed to the difference in concentration of nano-TiO_2 particles used during the preparation of the sol-solution before deposition. This is probably due to the concentration of the nano-TiO_2 particles used during the solution preparation, and the resulting thin films from the deposition. Visual inspection reveal that the m_{TiO2}= 1 g sample was nearly opaque, while the m_{TiO2} = 0.05 g was nearly transparent, and this corresponds to the concentration of the nano-TiO_2 particles used; the higher concentration of nano-TiO_2 particles used, the higher is its likelihood to be detected by GAXRD scans. The concentration also affects the sample's thickness and surface roughness, which will be discussed in subsequent sections. The substrate's presence in the m_{TiO2} = 0.05 g sample was stronger compared to the other two samples, as expected.

The presence of the rutile phase in the m_{TiO2} = 0.05 g sample is due to the fact that the low concentration of nano-TiO_2 particles in the deposited thin film allows the individual particles to absorb more energy during the annealing process of the fabrication (annealed at 500ºC). The same amount of energy that is supplied to a much larger concentration would be evenly distributed among the particles in order to ensure uniform recrystallization and particle growth. However, smaller concentrations of nano-TiO_2 particles will ensure that each particle gets a higher amount of energy, ensuring processes like recrystallization and particle growth takes place a lot faster than usual. However, the majority of the nano-TiO_2 particles remain in the anatase phase, with only a very small percentage of it converting into the rutile phase. Moreover, the presence of rutile does not seem to drastically affect the structural or optical properties of the thin films, which will be shown in subsequent sections.

The FWHM values for the peaks indicate the samples' crystallinity, with a smaller value indicating higher crystallinity. The anatase peaks of both the $mTiO_2$ = 0.05 g and 0.4 g have rather small FWHM values at position of 2θ = 35.61º, with both FWHM equaling to 0.2952. At the same position, the FWHM value for the m_{TiO2} = 1 g sample is 0.5904, which indicates a less crystalline sample. As the concentration of nano-TiO_2 in the solution decreases; it is much easier for the samples to reach thermodynamic stability with the same amount of energy during annealing. As shown in literature, annealing improves structural properties such as crystallinity (Ahn*et al* 2003). Keeping the annealing temperature constant at 500ºC, while varying the concentration of nano-TiO_2particles, will provide more energy per particle for the sample with smaller concentrations of nano-TiO_2 particles, allowing it to stabilize itself and at improve its structural, and subsequently, optical properties (Vishwas *et al* 2010).

The next section will discuss the analysis of the samples using the SEM/EDX technique. This will provide a clear visual representation of the samples at a microscopic level, and EDX will confirm the presence of TiO_2 in samples.

5.3 Scanning Electron Microscope/Energy Dispersive X-Rays (SEM/EDAX) Analysis

The Scanning Electron Microscope (SEM) and Energy Dispersive X-rays (EDX)are used in this work due to its ability to obtain clear images of our samples, and also for its ability for elemental analysis.It is quite a common analysis method, especially in literature, when it comes to detailing the morphology of samples such as particles, pellets and thin films, due to its simplicity of operations, ease of sample preparations, and the clarity of its images. Images of thin film TiO_2 thin film in literature is quite abundant, and can be seen in the works of Lin *et al* (2012) and Nam *et al* (2011), among others. In the scope of this work, the SEM/EDX is used in order to:

- Determine the morphological analysis of nano-TiO_2 thin films
- Determine the elemental analysis of nano-TiO_2 thin films

The reason we avoided using the EDXRF for elemental analysis in this case is the difficulty of sample preparation, where the readings from EDXRF will show prominent readings from the substrate instead of the nano-TiO_2 thin film, as it is more partial to the samples. EDX is a much more discrete method, and is capable of elemental analysis of thin films, making it quite suitable in this case. The SEM used in this work is the FEI Quanta Scanning Electron Microscope (SEM). The power and working distance was varied to accommodate different samples, but generally, it was set at 30 kV and 8.0 mm respectively. The samples were coated with gold in a thermal evaporator, a process which takes about an hour. Fig. 5.5shows the SEM micrographs of the nano-TiO_2 thin films, while Fig. 5.6 shows the EDX analysis of each sample.

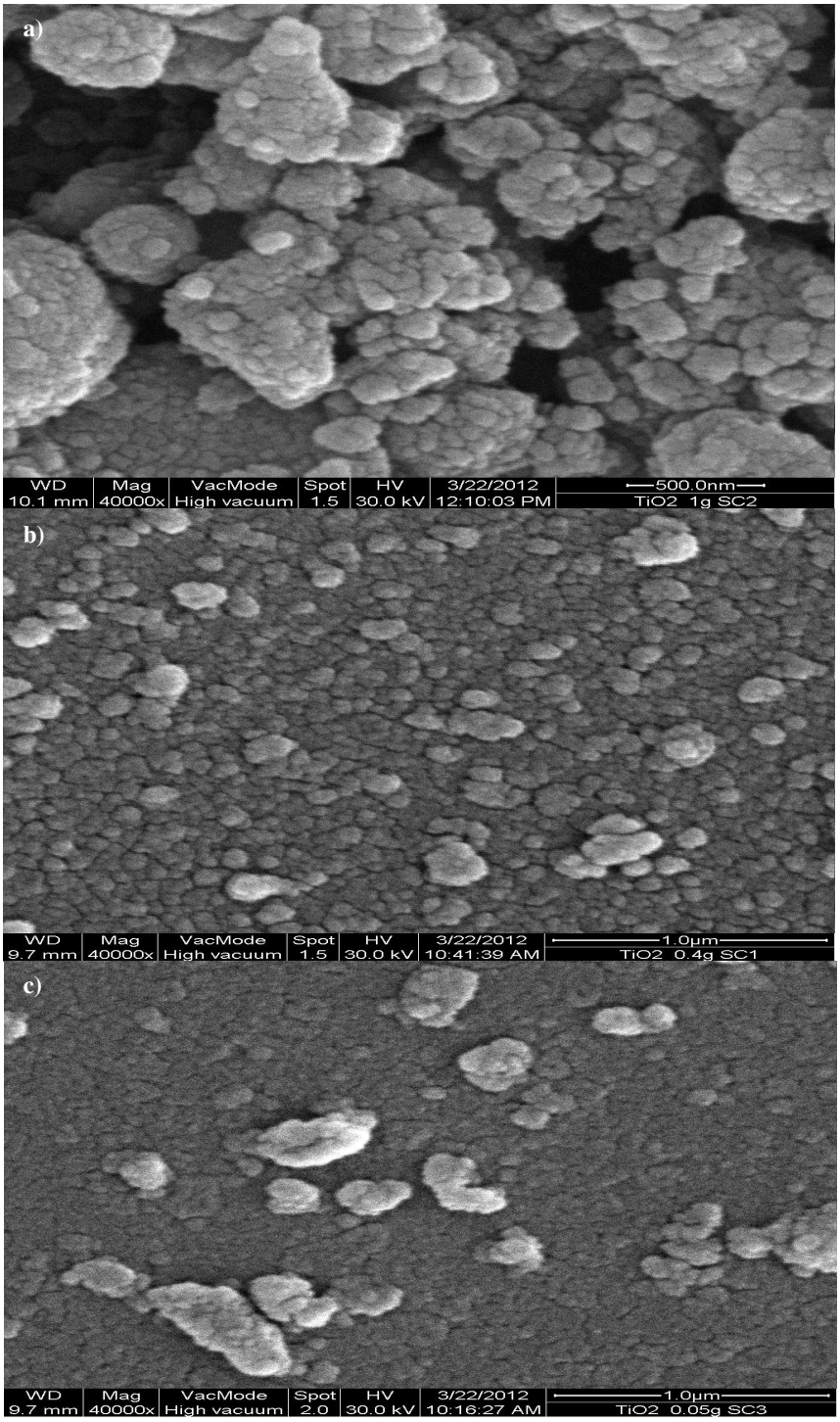

Figure 5.5. SEM Micrograph of nano-TiO_2 thin films at a) m_{TiO2} = 1 g, b) m_{TiO2} = 0.4 g and c) m_{TiO2} = 0.05 g at 40KX magnification

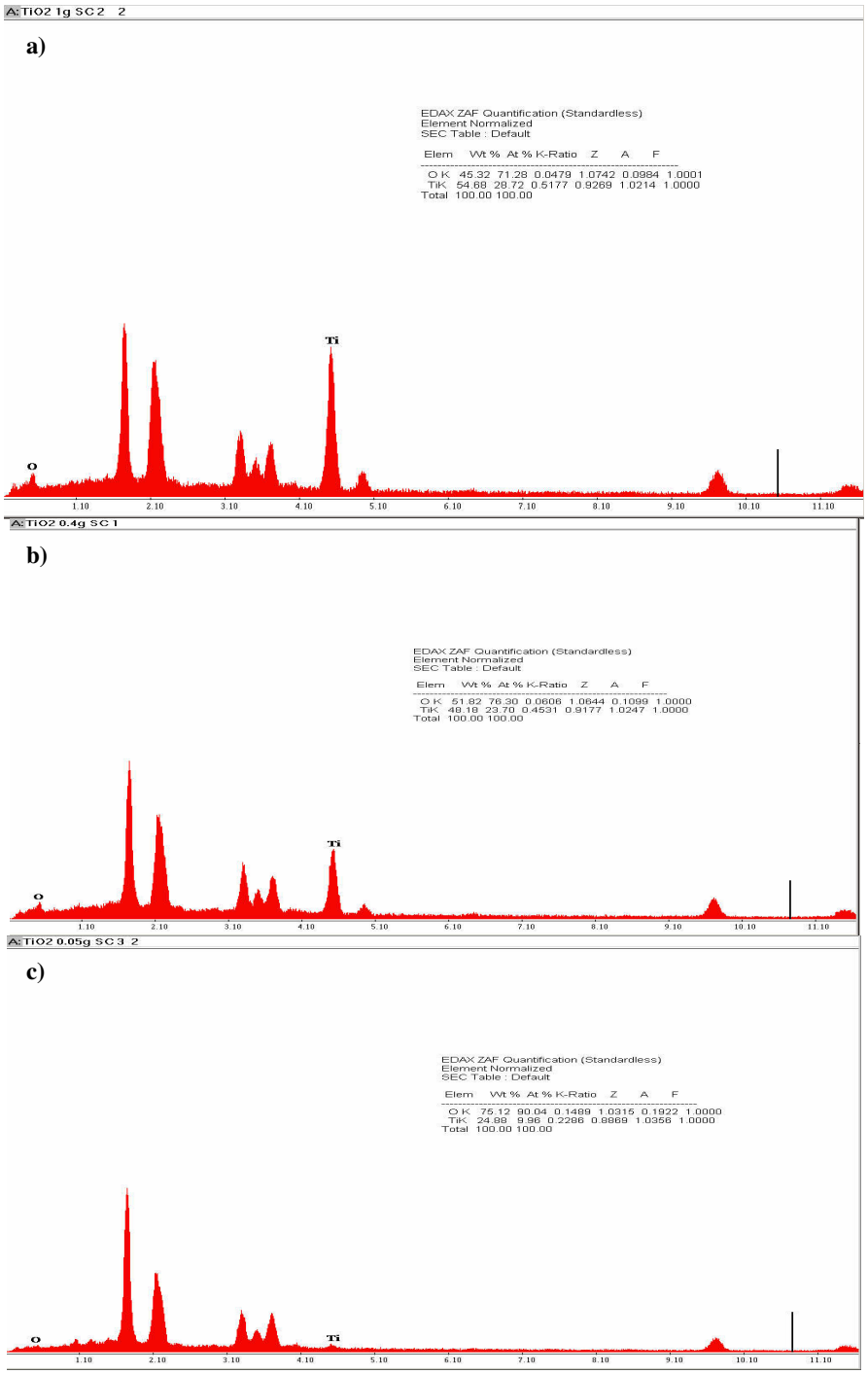

Figure 5.6. EDX analysis of nano-TiO_2 thin films at a) m_{TiO2} = 1 g, b) m_{TiO2} = 0.4 g and c) m_{TiO2} = 0.05 g

The thin films, with the exception of the m_{TiO2} = 1 g sample, showed rather good distribution and uniformity, with a few agglomerates remaining on the surface. The agglomeration shown in Fig. 5.5 (a), however, is indicative of the high concentration of the nano-TiO_2 particles. During spin coating deposition, the high angular velocity of the spin coater that rotates the substrate will forcefully separate the larger agglomerated particles from the smaller crystallites. These larger particles, gathering momentum from the anglular velocity of the spin coater, is then expelled from the surface of the substrate altogether during the deposition. However, the sample in Fig. 5.5(a) still showed extensive agglomeration among the nano-TiO_2 particles, proving that at this rotation speed (1000-3000 rpm) and deposition time (30s – 1 minute), it is still insufficient for the m_{TiO2} = 1 g sample. However, it is adequate for smaller concentrations of m_{TiO2} = 0.4 g and m_{TiO2} = 0.05 g, where it is observed the deposition is uniform, tightly packed, and almost free from agglomeration.

The EDX analysis showed that the samples are 100% TiO_2, confirming the XRD analysis conducted in the previous section for all samples, although it is markedly difficult to detect TiO_2 at low m_{TiO2}concentrations.

The next section will discuss the results obtained from the AFM analysis, and how does the SEM results correlate to the AFM results in terms of morphology and surface profile.

5.4Atomic Force Microscope (AFM)

The Atomic Force Microscope (AFM)is a method employed to analyze the topography of a surface. This is achieved via the interaction of a cantilever (made from Silicon or

other sensitive materials) interacting with a surface. It is capable of providing a 2-dimensional (2-D) and 3-dimensional (3-D) representation of the sample's surface. It is capable of operating in two modes, contact and non contact. The selection of the analysis mode depends largely on the samples itself; however, in order to minimize surface damage or scratching, the non-contact mode is preferred. The analysis is entirely non-destructive, and the sample preparation is relatively simple and straightforward. The works of Nam *et al* (2011) and Jahromi *et al* (2009) details analysis of solgel spin coating TiO_2 thin films using AFM. By using the AFM, we hope to:

- Determine the topographical feature of the samples
- Determine the relationship between surface roughness, thickness and concentration of nano-TiO_2 particles deposited by spin coating

The AFM used in this work is the XE100 Park systems (Jeol). Preliminary analyses in contact mode damaged the sample's surface and render the results unusable. Largely in part to this, the non-contact mode was chosen instead for subsequent analysis. Each sample were analyzed at three different points on the samples in order to obtain an average profile of the samples, however, only the best images were selected to be shown here. The data collected from the AFM analysis is the sample's thickness and roughness, along with its general topographical profile.In order to confirm the thickness of the samples, the thickness of the films were also measured using a surface profiler at many points on the samples (Alpha Step IQ Surface Profiler with Tencor). An average of the thickness will be taken, and this value will be used for any subsequent calculation or determination of film's thickness in this work.

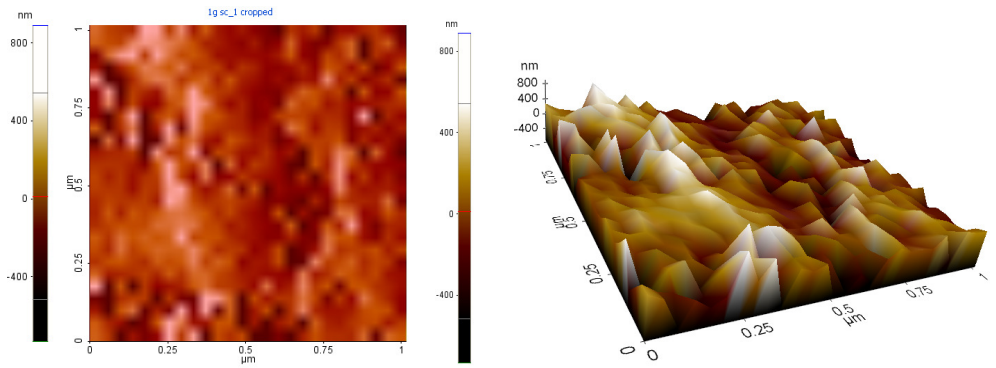

Figure 5.7 2D and 3D–AFM images (scanned area 1 µm x 1 µm) for nano-TiO_2 thin films deposited by spin coating at m_{TiO2} = 1 g

Fig 5.7 shows the 2-D and 3-D image of nano-TiO_2 thin films deposited by spin coating technique with m_{TiO2} = 1 g. As shown in the Fig. 5.7, the sample is on average 500 nm thick, and the value of thickness from the surface profiler is 459.08 nm, a 10% error margin between both samples. The sample has a rather prominent surface, with many prominent peaks perpendicular to the surface. This is consistent with Fig. 5.5 (a), where agglomeration of the nano-TiO_2 particles on the surface produces a second layer of uneven surface on the coating.

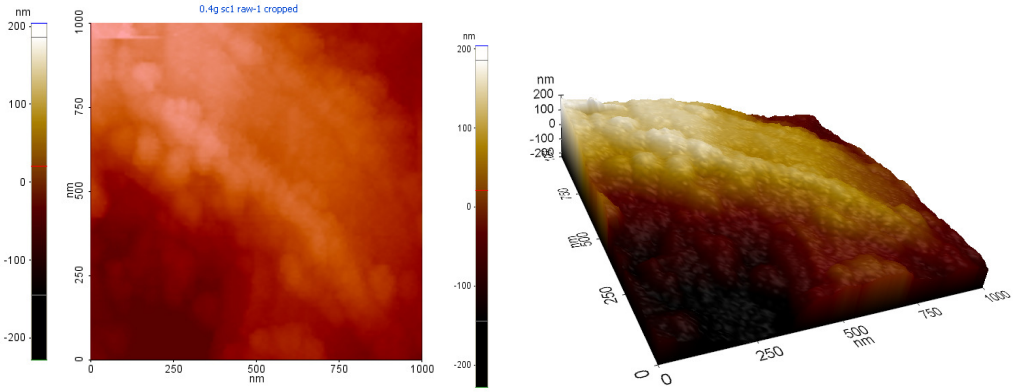

Figure 5.8 2D and 3D –AFM images (scanned area 1 µm x 1 µm) for nano-TiO_2 thin films deposited by spin coating at m_{TiO2} = 0.4 g

Fig. 5.8 shows the 2D and 3D image of nano-TiO_2 thin film deposited with m_{TiO2} = 0.4 g. In contrast to the previous sample, this surface is somewhat more even, with a lower average thickness of nearing 200 nm; however, the thickness for this sample obtained from the surface profiler is 61.64 nm, quite a large error margin. As seen in the Fig. above, the thin film is sloped, with one end of the sample thinner than the other. The thickness gradient is quite high, with one point having a thickness of below 100 nm, and the other point have a thickness nearing 200 nm. The surface profiler, takes an average reading from one end of the sample, and is more representative of the sample as a whole. In this case, the thickness value obtained by using the surface profiler will be used. A cursory visual inspection reveals a rather flat surface with no perpendicular peaks on the surface. It is speculated that the annealing merged the nano-TiO_2 particles in the sol-solution to form larger, more combined grains without converting into rutile, as shown in Fig. 5.3. It also seems to agree with Fig 5.5 (b), as the distribution of the nano-TiO_2 particles seems to be quite uniform with minimal agglomeration on the surface of the coating, creating a rather homogenous surface profile.

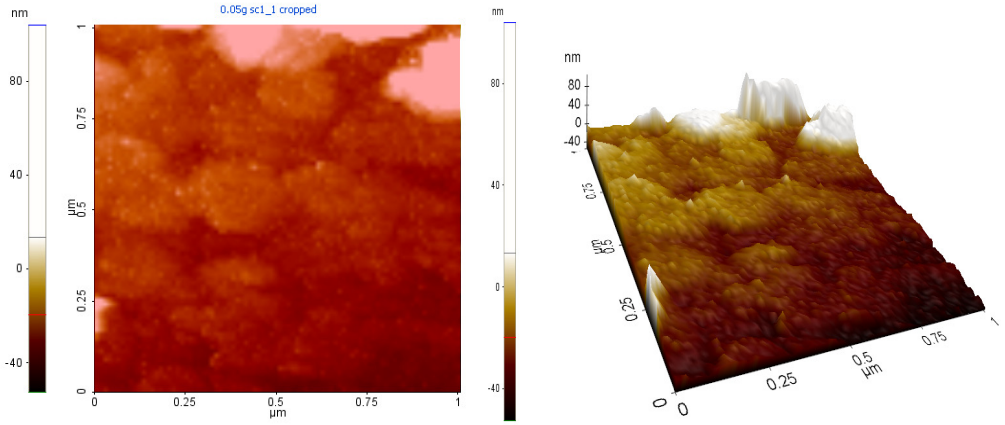

Fig 5.9 2D and 3D –AFM images (scanned area 1 µm x 1 µm) for nano-TiO_2 thin films deposited by spin coating at m_{TiO2} = 0.05 g

Fig. 5.9 shows the 2D and 3D image of nano-TiO_2 thin film deposited with m_{TiO2} = 0.05 g. Overall, this sample is even thinner, averaging out at 20 nm thickness measured by

the AFM and 19.2961 nm on the surface profiler, which is a very small error margin (>1%).The surface's thickness is small, and there are prominent peaks that are perpendicular to the surface, similar to the m_{TiO2} = 1 g samples, indicating that the annealing did not merge the nano-TiO_2 particles into larger grains but instead converted it into rutile, as shown in Fig. 5.2. Again, it agrees with Fig. 5.5 (c), where minimal agglomeration on the surface is observed. Also, it is noticed that the coating is form by smaller crystallites than the previous sample, accounting for the fine perpendicular grains seen in Fig. 5.9.

Figs. 5.7-5.9provide an overall picture of a rough surface with a thickness dependant on the concentration of nano-TiO_2 particles in the sol. The image of the roughness of the samples is also shown in the 3D image of the samples, namely, the m_{TiO2} = 1 g sample has a roughness of 270.4 nm, the m_{TiO2} = 0.4 g sample has a roughness of 84.3 nm, and the m_{TiO2} = 0.05 g has a surface roughness of 16.9 nm. The roughness is calculated from equation 5.1

$$R_q = \sqrt{\frac{1}{L}\int_0^L z^2\,(x)dx} \tag{5.1}$$

where L is the evaluation length, z is the height and x is the distance along the measurement.

Fig. 5.10 outlines the relationship between the thickness of the thin films, the concentration of nano-TiO_2 particles in the sol, and the surface roughness (R_q) of the thin films. Both thickness and R_q have a linear relationship with the concentration of nano-TiO_2 particles in the sol. This relationship can be used to predict the roughness and thickness of the deposited thin films based on the concentration of the nano-TiO_2

particles in the sol, provided the volume of the chemical reagants are kept constant. For example, if we were to use m_{TiO2} = 0.5 g, the thickness of the thin films will be 110 nm and the R_q will be 90 nm, provided that the volume of acetic acid and ethanol is kept constant at 6 ml and 30 ml, respectively, and the spin coating deposition speed and time is similar to the ones used in this work. Works by other researchers showed an inverse relationship between the spin coating speed and the thickness, however, literature on the relationship between the concentration of precursors with the thickness and roughness is rather scarce.

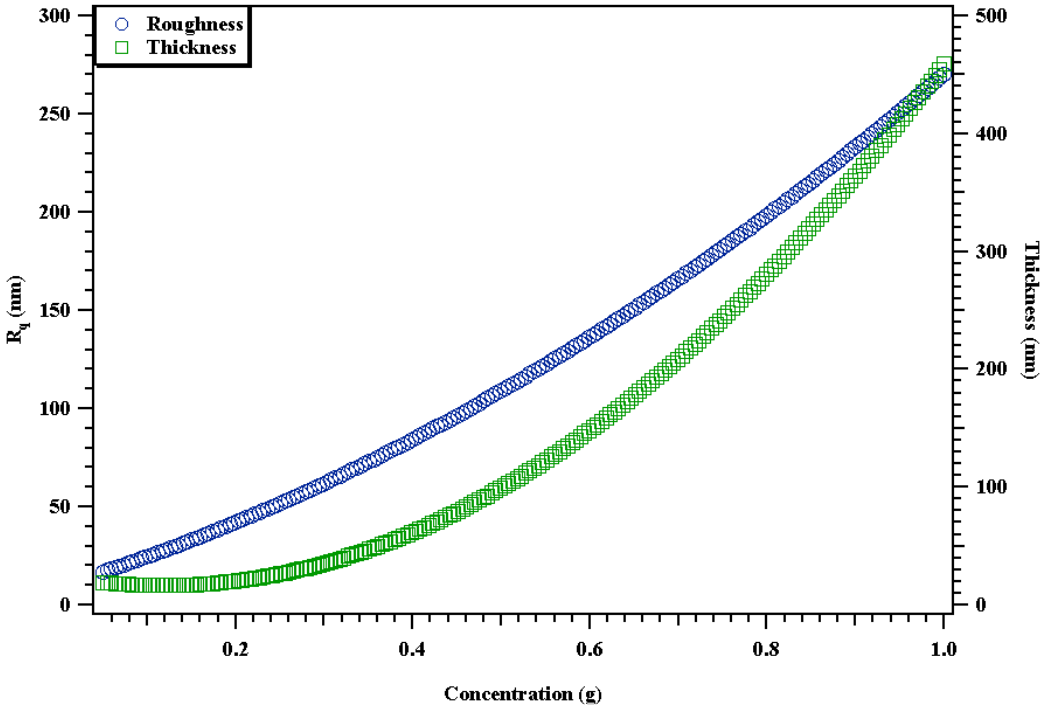

Figure 5.10 Relationship between concentration, thickness and surface roughness of nano-TiO_2 thin film deposited by spin coating

One more point that is left unexplained in this section is the nature of the thin films. 2 out of 3 samples showed prominent peaks that are perpendicular to the surface, indicating an upward oriented nano-TiO_2 particle. It is speculated that this happens due

to the spin coating deposition technique. The substrate is spun on an axis; with the sol-solutionpipetted slowly as it spins. The nano-TiO_2 particles are in the form of agglomerates, as shown in the previous chapter, and when pipetted onto a spinning substrate, the larger particles are prone to be expelled due to the momentum and centrifugal force generated by the spinning. This will forcefully rip the agglomerated nanoparticles apart, and the surface profile will be slightly stilted at an angle. Subsequent annealing will stabilize these tilted particles, orienting them in the most energy efficient orientation, which is clearly shown in the AFM figures above. In some cases, the annealing will merge the nanoparticles to the point that grows without changing phases, thus losing the evident jagged surface, as seen in Fig. 5.7-5.9. Due to the many surfaces that are exposed to its surroundings, these thin films are highly reactive and are suitable for a multitude of applications such as sensors and photocatalysis, which will be discussed in detail in Chapter 6.

5.5 UV-Visible-Near Infrared Spectroscopy (UV-Vis-NIR) Analysis

This section aims to discuss the optical properties of nano-TiO_2 thin films, and analyze the effect of structural properties on the optical properties. A comprehensive summary regarding the optical property of thin films are detailed in the work of Flory and Escoubas (2004).Previous work conducted by researchers such as Bouabid *et al* (2008), Hasan *et al* (2010) and Tanemura *et al* (2003) showed that the best approach in this aspect would be to utilize the UV-Vis-NIR spectrum analysis, regardless of the deposition method of the thin films.

The analysis is conducted using a Shimadzu UV3600UV-Vis-NIR Spectrophotometer. The light source used in the scan has a scanning wavelength of 340 nm.Our scan range was from 200-800 nm, covering the UV and Visible light region. In this work, two modes of operation were used, which are the reflectance mode and the transmission mode. The results of the reflectance mode were converted to absorbance coefficient using the internal software supplied by Shimadzu, via the Kubelka-Munk equation.

Basically, the purpose of the UV-Vis-NIR analysis is to:

- Determine the optical bandgap of nano-TiO_2 thin films
- Determine the optical transmission of the nano-TiO_2 thin films
- Determine the effect of structural properties on the optical properties

Fig. 5.11 shows the absorbance spectrum for the nano-TiO_2 thin films. Generally, all the samples showed absorption edges in the near UV-Vis region of 300-400 nm, although the 1 g sample is red-shifted towards visible light. The absorption edge of samples m_{TiO2} = 1 g and m_{TiO2} = 0.4 g are closer to the visible light region, >380 nm, whereas the m_{TiO2} = 0.05 g is nearer towards the UV region, showing a strong absorption edge at 350 nm.

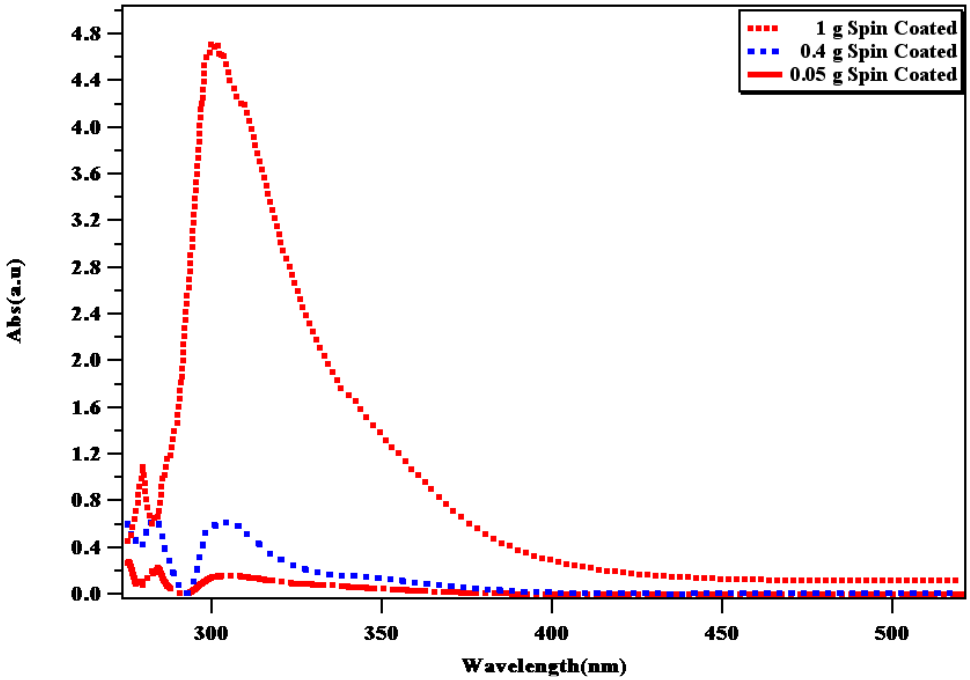

Figure 5.11 Absorbance Spectrum of spin coated nano-TiO_2 thin films

Generally, it is observed that the absorption edge shifted towards lower wavelengths as the concentration of nano-TiO_2 particles is decreased in the sol-solution, decreasing radiation absorption of the samples. Literature points out various factors that might cause absorption edge shifts, such as doping (Lin *et al* 2012) and annealing (Vishwas *et al* 2010). However, studies regarding the effect of precursor concentration on the optical properties of nano-TiO_2 thin films are almost non-existent. The m_{TiO2} = 1 g sample has a very high absorption rates due to the fact that its sol-solution's concentration is higher, and when deposited onto the substrate, forms a network of dense nanoparticles that absorbs a large percentage of light that passes through it. The rougher surface also increases the chance for light scattering, and this also increases the chance for absorption when the light is scattered from one point of the surface to another. A drop in the concentration of nano-TiO_2 particles lowers the absorption rate in the visible region, as seen in both the m_{TiO2} = 0.05 g and m_{TiO2} = 0.4 g. Analogous to the previous sample,

the smaller concentration of nano-TiO_2 particles will form a less dense network of nanoparticles, and the relatively smaller samples is not conducive for high absorption rates due to the fact that the incident light easily passes through the thin films. Decreased surface roughness also decreases light scattering, decreasing the chance for absorption (Ryu *et al* 2004). The transmission of radiation through the samples is also affected by these same structural properties.

Fig. 5.12 shows the optical transmission of UV-Visible light through the nano-TiO_2 thin films. Literature review shows previous work involving optical transmission are the work of Bouabid *et al* (2008), where they studied the effect of the concentration of chemical reagants (HCl) on transmissions, and the work of Janibatar-Darzi *et al* (2009), which studied the effect of calcinations on the transmission of TiO_2 thin films.Generally, the transmission is highest in the UV-Vis region of 400-500 nm for all samples, and lowest in the region of 300-350 nm. The low transmission in these regions is due to the fact that light in this wavelength are being absorbed for the excitation and migration of electron form the valence band to the conduction band of TiO_2. As the energy decrease when the wavelength of incident light increases, absorption ceases, allowing higher percentage of the incident light to pass through the samples. This is clearly evident in Fig. 5.12, as transmission is clearly higher in the visible light region (400-700 nm) and stabilizes at 500-700 nm.Table 5.1 summarizes the average transmission of UV-Visible light through the samples in the range of 400-500 nm.

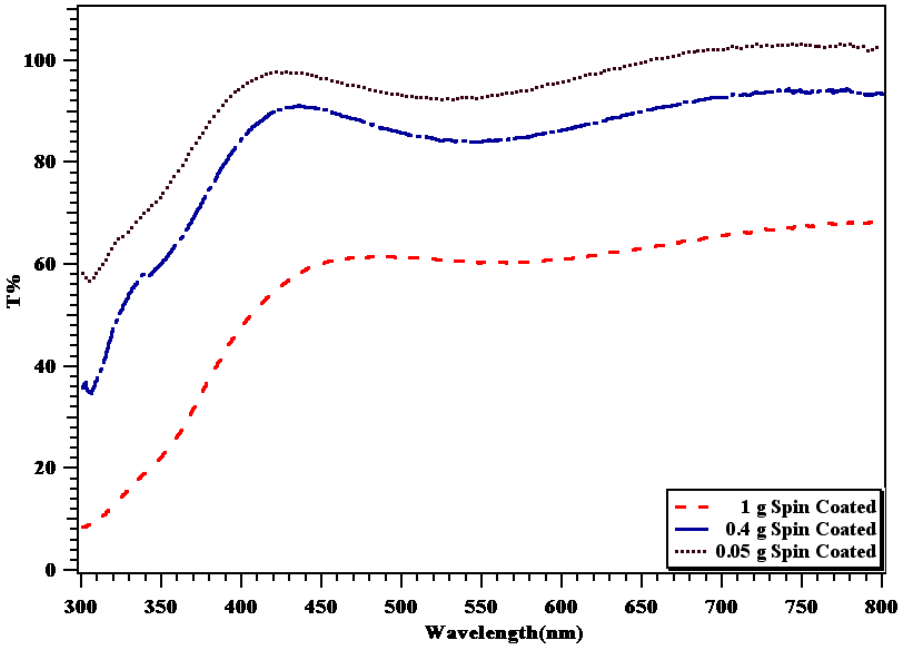

Figure 5.12 Transmission Spectrum of Spin Coated nano-TiO_2 thin films

Table 5.1 Optical Transmission of UV-Visible light through nano-TiO_2 thin film deposited by the spin coating technique

Samples (g)	Transmission (%)
1	~61
0.4	~87
0.05	~95

Fig. 5.12 shows the optical transmittance increasing as the m_{TiO2} increases, from ~ 60% at 550 nm in the m_{TiO2} = 1 g samples, followed by a 90% transmittance in the m_{TiO2} = 0.4 g sample, and finally, an almost 100% transmittance in the m_{TiO2} = 0.05 g sample. Previously, Fig. 5.11 shows a shifting of the absorption edges towards visible light by the m_{TiO2} = 1 g and m_{TiO2} = 0.4 g sample. The absorption of visible light is strongest in

the m_{TiO2} = 1 g sample, and it decreases as the concentration of nano-TiO_2 particles in the sol-solution decreases. When this happens, the absorption edge shifts towards lower wavelengths. The absorption edge is where the excitation and migration of electron from the valence band to the conduction band happens, and this is the region where transmission is the lowest due to the fact that any incident radiation gets absorbed. As the wavelength of the incident light increases and its energy decreases to a level below the required level for TiO_2, the incident radiation will pass through the samples with fewer obstacles. Fig. 5.12 visually depicts this, as the transmission increases with increasing wavelengths. The concentration of nano-TiO_2 particles in the sol-solution also greatly effects the transmission. It is previously established that the higher the concentration of nano-TiO_2 particles is in the sol-solution, the thicker and rougher the films will be. A thicker and rougher film will result in decreased transmission, as shown in Fig. 5.12, where the m_{TiO2} = 1 g have an optical transmission of below 70%, while the m_{TiO2} = 0.05 g has almost 100% transmission. These films, as shown in the previous sections, differ significantly in terms of roughness and thickness, with the m_{TiO2} = 1 g sample being thicker and rougher. Thick and rough films increase the chance of light scattering, and light scattering decreases incident radiation transmission through a sample. From these results, it is surmised that structural properties such as surface roughness, film thickness and precursor concentration directly affects optical transmission.In order to better demonstrate this, the optical bandgap of the samples will be determined using Tauc's Plot.

The Tauc Plot is fitted by plotting $(\alpha h\nu)^2$ against hv, with the linear region extrapolated to intercept the x-axis, and this intercept is the bandgap of the sample. An optical bandgap is the difference of energy between the bottom of the conduction band and the top of the valence band of a material. Generally, conductors have small to no bandgaps,

while insulators have large bandgaps (> 4eV), and semiconductors have bandgaps that are somewhere in between (1.1 eV< x < 4.0 eV). The bandgap is a region where no electron state can be present, and plays a major role in the electrical conductivity of a solid material.

Common phases of TiO_2 has a bandgap of 3.2 eV(anatase) and 3.0eV(rutile) respectively, making it a wide bandgap semiconductor. Wide bandgap semiconductors are material with bandgaps are more than 1.7 eV, examples being AlN (6.3 eV) and ZnO (3.3 eV). They are especially suitable for optoelectronic and power device applications, as well as materials in devices operating at high temperatures. There are also two types of bandgap; direct and indirect. Direct bandgaps are where electrons in the material can emit a photon when excited due to the similarities between the electron and holes in the valence and conduction bands, respectively, while an indirect bandgap cannot do so and must enter an intermediate state before it can emit a photon when excited. Figs. 5.13-5.15show the Tauc Plot for the samples, its optical bandgaps, and the type of bandgaps of each sample.

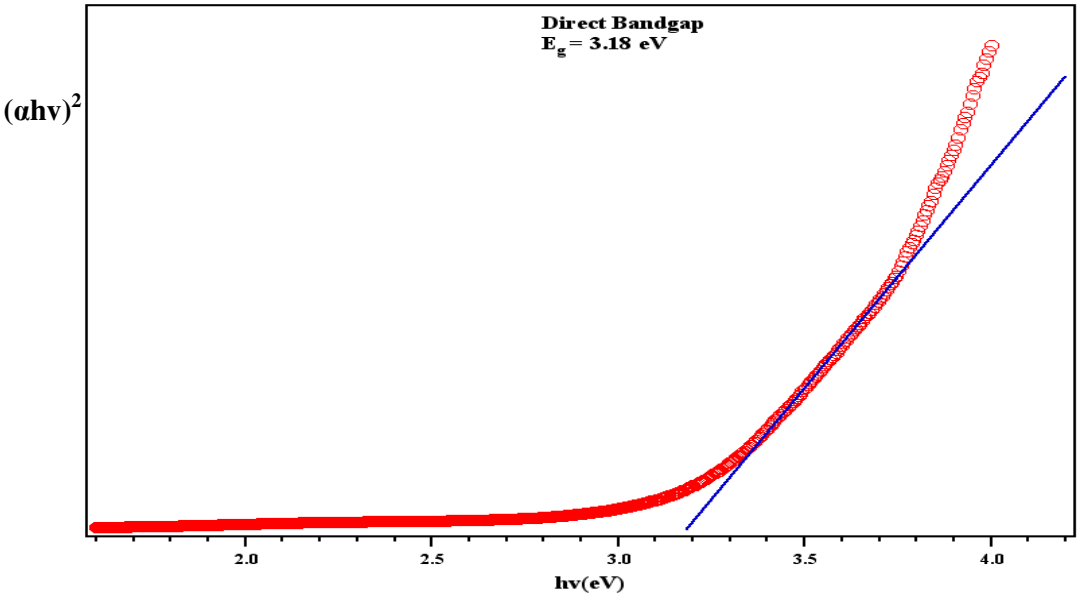

Figure 5.13Tauc Plot for m_{TiO2} = 1 g sample for determination of optical bandgap

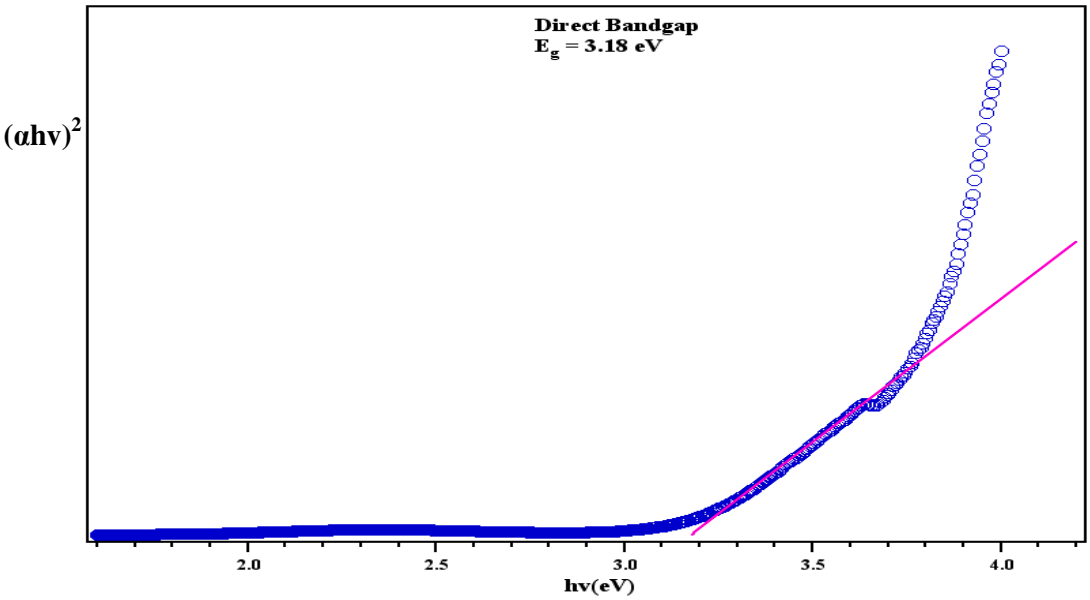

Figure 5.14Tauc Plot for m_{TiO2} = 0.4 g sample for determination of opticalbandgap

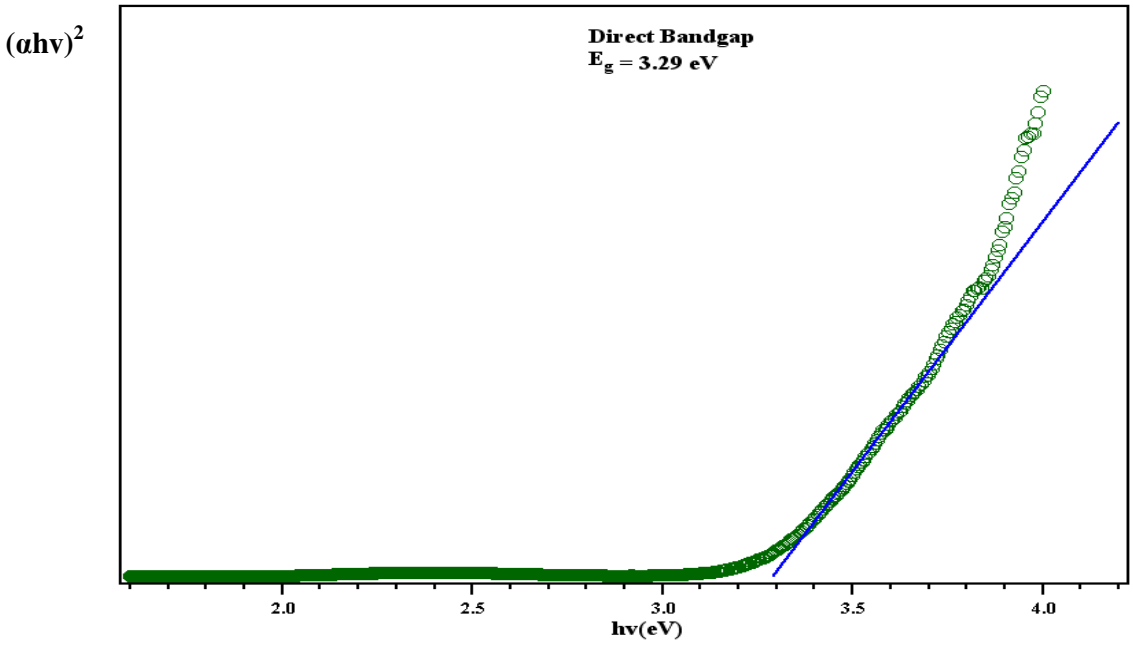

Figure 5.15Tauc Plot for m_{TiO2} = 0.05 g sample for determination of optical bandgap

The optical bandgap of m_{TiO2} = 1 g and m_{TiO2} = 0.4 g is similar (3.18 eV), while the bandgap of the m_{TiO2} = 0.05 g is slightly larger (3.29 eV). Exactly similar work is not found in literature, however, analogous work are available, such as the work of Lin *et al* (2012), that studies the effect of Fe dopant concentration on the optical properties of nanostructured TiO_2 thin films, and the work of Vishwas *et al* (2010), that studied the effect of annealing and surfactant addition to the optical transmittance and reflectance. Boh studies aim to establish a trend with the introduction of external variables that will invariably alter the transmission of the thin films. Similarly, the work here aims to study the effect of nano-TiO_2 particles' concentration on the optical transmittance of the thin films.The optical bandgap gleamed from this study showed that a concentration within 0.1 – 1 g of nano-TiO_2 particles is best when used as thin film sol-solution precursors, due to the fact that it reduces the optical bandgap to a level below what is reported in the literature (3.2 eV), and according to literature, further annealing the samples might

decrease the optical bandgap. Using a smaller amount, as shown by m_{TiO2} = 0.05 g, will increase the optical bandgap, thus affecting the various optical and electrical properties that is inherent in the thin films. This value is very close to the optical bandgap of bulk anatase TiO_2, which is 3.2 eV.

The optical bandgaps of the samples are directly related to the transmission and absorption of the samples. From the explanation in the previous section, it is deduced that transmission is inversely related to absorbance in the case of UV-Vis analysis. The term $(\alpha h\nu)^2$ is derived from transmission, and is therefore directly proportional to transmission. This means that samples with lower transmission will have lower bandgaps, while samples with higher transmission will have higher optical bandgaps, and this is proven in Figs. 5.13 – 5.15. The only anomaly is the similarities between the optical bandgap of the m_{TiO2} = 1 g and m_{TiO2} = 0.4 g sample, which can be attributed to mathematical error margins. During the linearization of the region in the Tauc Plot, the straight line equation of y = mx+ c gave values with error margins, in both cases, quite large due to the fact that the region is not as linear, especially in the case of m_{TiO2} = 0.4 g, thus, resulting in a near similar value of optical bandgap with m_{TiO2} = 1 g. The difference, however, is not major, and the subsequent rounding up of the values to two significant figures will put forth similar values of optical bandgaps (3.18 eV).

5.6. Chapter Summary

This chapter discusses the characterization of the thin film nano-TiO_2 using the XRD, SEM/EDX, AFM and UV-Vis techniques. It is established that the thin films were of the anatase phase of TiO_2, with no impurities, except the m_{TiO2} = 0.05 g sample having a mixture of anatase and rutile, the films thickness and roughness vary with the

concentration of the nano-TiO_2 particles in the sol-solution, and the optical properties such as the absorbance, transmittance and bandgaps are very much influenced by the structural properties of the nano-TiO_2 thin films. The surfaces are generally uniform although with particles perpendicular to the surface being clearly visible, and the thickness is still well below 1 μm. The properties that is determined during the course of this study gives rise to some interesting potential applications for the nano-TiO_2 thin films, which will be discussed in detail in chapter 6.

CHAPTER 6: POTENTIAL APPLICATIONS

6.1 Introduction

The previous chapter discusses the characteristic of nano-TiO_2 thin films fabricated using nano-TiO_2 particles synthesized from low grade mineral precursors. The results showed considerable improvement of the structural and optical properties of both the thin films and nanoparticles, based on comparison with literature. This chapter aims to explore potential applications of both the nano-TiO_2 thin films and nano-TiO_2 particles. Three potential applications have been identified based on the structural and optical properties; electrochromic devices, photovoltaic cells/DSSC, and photocatalysis. The potential role of nano-TiO_2 particles of nano-TiO_2 thin films in these deveices/systems will be discussed and explained in depth. We hope to establish the viability of the nanoparticles and thin films to be used in these devices, by comparing our structural and optical properties to the ones used in these devices/systems.

6.2 Photocatalysis

Photocatalysis essentially means a reaction that is induced by the introduction of light. Photocatalysis is commonly seen in literature dealing with the decomposition of hazardous gases and compounds, and TiO_2, in many forms, have been identified as one of the most viable photocatalyst due to its environmentally friendly nature and efficiency. Numerous studies, conducted by Kang *et al* (2001), Wu *et al* (2005), and Lee *et al* (2004) studied the effect of structural and optical properties on the photocatalytic rate of TiO_2, and its relation

to the decomposition and elimination of bacteria and hazardous compounds such as *E. Coli* and $CHCl_3$.

The mechanism of photocatalysis is relatively simple, and is explained in depth in the work of Fujishima *et al* (2000) and Chen and Mao (2007). Basically, a photocatalyst that is exposed to photons with higher energies than its bandgap energywill cause excitation of its electron and induce migration of the electron from the valence band to the conduction band, creating electron-hole pairs that travels through the optical bandgap energy region in order to reach the surface of the material. These electron-hole pair creates radicals, which will be released upon its arrival at the surface of the materials, to its surroundings. Common radicals include OH^- and O^{2-}. Due to its instability, these radicals will seek out other unstable molecules in order to stabilize itself, and most of the time, toxic and hazardous molecules are unstable, prompting the radicals produced from a photocatalyst to specifically seek out them out and neutralize them. The neutralization will render these formerly toxic and hazardous molecules inert.

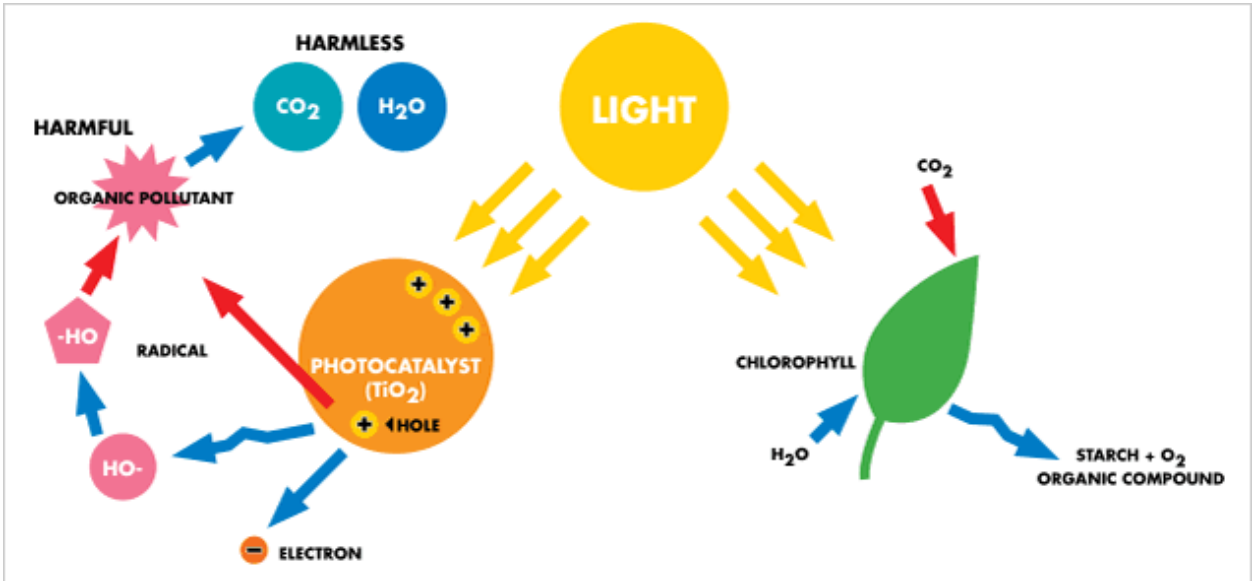

Figure 6.1 The mechanism of photocatalysis of TiO_2 (taken from www.airrevolution.co.za/research)

Two properties play a crucial role in ensuring an efficient and successful photocatalytic process, which are the optical bandgap energy and the specific surface area of the photocatalyst. In order for photocatalysis to be initiated, the absorption of photons with energy higher than the optical band gap energy needs to occur. Any energy that is lower than the optical bandgap is insufficient to initiate photocatalysis. The works of Khan *et al* (2010) and Rizzo *et al* (2009) points out UV rays is the most effective stimulant to induce photocataysis in TiO_2, due to the fact that the optical bandgap energy of anatase is 3.2 eV and rutile 3.0 eV, which corresponds to the wavelengths of 387.5 nm and 413.3 nm, respectively. This puts the energy it is able to absorb to initiate photocataylsis squarely in the UV-region of the electromagnetic spectrum (300-400 nm), with the rutile phase slightly passing this region and venturing into the visible light region. Basically, the lower the bandgap energy is, the wider the range of energy it can absorb to initiate photocatalysis, which makes it viable for activation using visible light, as sunlight, the main source of radiation on earth, consist of only 3-5% of UV light, which makes the probability of activation and photocatalytic efficiency quite low, compared to if the process is initiate by visible light, which constitute of about 95% of the sunlight on earth.

This work has managed to produce nano-TiO_2 particles that has an optical bandgap energy of 3.23 eV, which corresponds to a wavelength of 383.9 nm, making it viable for initiation by UV-Vis light sources for photocatalytic applications. The energy activation range is on the borderline of the visible region, which makes activation viable with visible light in certain conditions. The nano-TiO_2 thin films has smaller average bandgap, with two samples having a bandgap of 3.18 eV, corresponding to a wavelength of 389.9 nm, and is closer to the visible light region compared to the nanoparticles, which also makes it a viable photocatalysis.

Another factor that plays a major role in photocatalysis is the specific surface area of TiO_2. As explained previously, the electron-hole pair will travel to the surface in order to release radicals into the surroundings which will neutralize hazardous compounds. This means that the larger the specific surface area, the more radicals that are released, thus increasing the reaction rate and the efficiency of the photocatalyst. The nano-TiO_2 particles produced in this work has a specific surface area of 186.8 m^2/g, which is comparatively large to the nano-TiO_2 particles produced in the works of He *et al* (2007), and Choi *et al* (2007), which were 90 m^2/g and 146 m^2/g, respectively. Their work aims to degrade methylene blue (He *et al* 2007), and wastewater treatment (Choi *et al* 2007). Even at their relatively smaller surface areas, the decomposition and neutralization results of their product are quite promising. Following this line of reasoning, if we were to use our nano-TiO_2 particles as photocatalyst, in will most definitely outperform the nano-TiO_2 particles described in those works.

Although it would seem that the properties are almost similar, it should be noted that the nano-TiO_2 particles and thin films are synthesized from low grade local mineral precursors, and is less than pure, in the case of the nano-TiO_2 particles. In contrast, the nano-TiO_2 particles and nano-TiO_2 thin films described in literature (Ye *et al* 2010; He *et al* 2007), are prepared from highly pure and expensive TiO_2 precursors such as Potassium Titanium Oxalate (PTO), and tetrabutyl titanate ($Ti(OBu)_4$) . To be able to produce nano-TiO_2 that is on par or superior to the products described in literature is an achievement in itself, due to the fact that this has not been attempted elsewhere.

6.3 Electrochromic Devices

Electrochromism is defined as the ability of a material to undergo color changes when it is being simultaneously oxidized or reduced. Its application is widespread, and is especially prominent is display devices and smart window. Electrochromism allow the external control of absorbance and transmission, making these intrinsic optical properties extrinsic via the introduction of external factors, such as electrical current or high energy incident light (Chen and Mao, 2007).

A basic schematic of an electrochromic device is shown in Fig. 6.2. A very basic design will have two electrodes separated by an electrolyte. Passing an electrical current through an electrochromic device will induce electrochromism, where one electrode will be colored and the other bleached. Usually, the electrode that is less reactive will be bleached while the more reactive ones are colored. The determination of reactivity of electrodes depends primarily on electrochemical potential of each material.

According to literature, TiO_2 thin films display electrochromic tendencies in two forms, highly crystalline TiO_2 thin films (Hagfeldt *et al* 1994), and viologen-modified nanocrystalline TiO_2 (Campus *et al* 1999). The first type is far more common than the second type, and is usually separated by a Li^+ ion containing electrolyte such as $LiOCl_4$. When activated by current or light, these Li^+ ions will move pass its barriers into the TiO_2 lattices for reduction or oxidation, and will return to its original location once the external activation is deactivated. Two factors are highly critical in the determination of the efficiency of the first type of electrochromic device employing TiO_2, which is the freedom of movement of the Li^+ ions between the lattice of TiO_2 electrodes (Ottaviani *et al* 1986), and the specific surface area of the electrodes (Bonhote *et al* 1999).

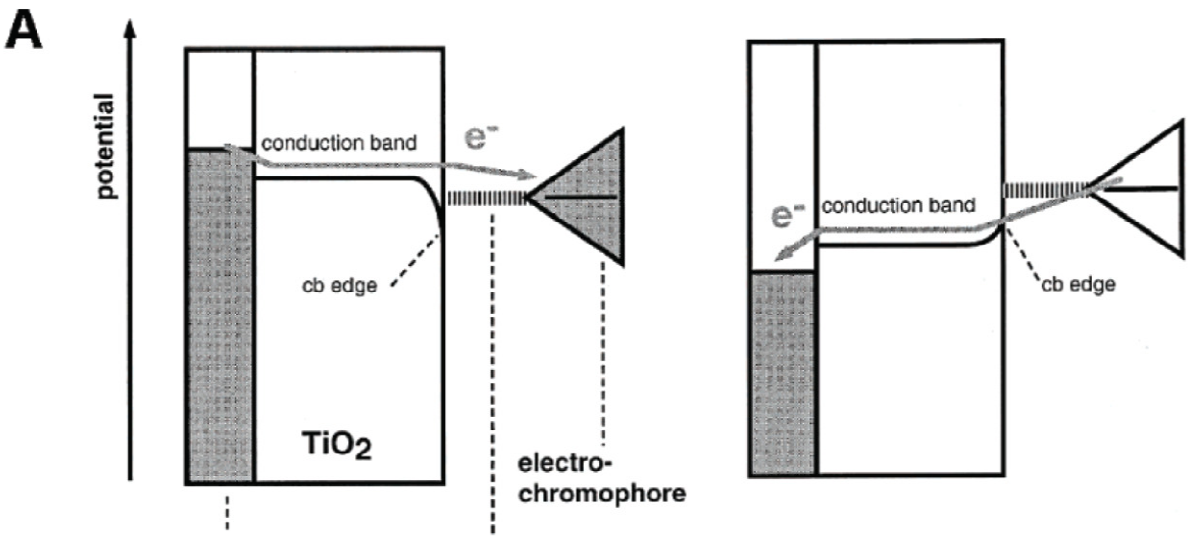

Figure 6.2. The working mechanism of an Electrochromic Device using TiO_2 electrode (from Chen and Mao, 2007)

Having small crystallites and high crystallinity is important due to the fact that the Li^+ ions that is responsible for lattice intercalation needs to move across the boundaries between the electrolyte and electrode with minimal interference in order for it to embed itself in the anatase TiO_2 lattices. Any large, uneven crystallites will impede the movement of Li^+, and slows its rate of intercalation into the TiO_2 lattice. Worse, it might also block the Li^+ when it tries to return to the electrolyte, once the external activation is stopped. If this happens, the efficiency of the device will be severely affected, and in the latter case, the whole system will fail. This work deposited crystallites that are less than 20 nm in size as thin films onto Glass/ITO substrate, and these small crystallites, as shown in the SEM micrographs in Fig. 4.3 and Fig. 5.5, and these small crystallites will in no way impede the movement of Li^+ ions in and out of the lattice of anatase TiO_2. Literature also shows that the anatase phase of TiO_2 is preferred for electrochromic applications, due to the fact that is far more reactive than rutile, and our XRD analysis of the thin film samples showed that it

is 100% anatase, which is a good indicator of its suitability as electrochromic device's electrode(s).

Another structural property that is mentioned in literature regarding TiO_2 as electrochromic device is specific surface area. A high specific surface area is required in order to increase the points of interaction between the electrolyte and electrode. Higher points of contact mean that a higher number of Li^+ ions will be able to interact with the TiO_2 lattice, increasing the electrochromic efficiency of the device. This work manage to produce nano-TiO_2 particles that have a specific surface area of 186.8 m^2/g, which is very high compared to its counterpart in literature, as described in chapter 4. These nanoparticles are then deposited as thin films onto a glass/ITO substrate, and it is assumed that these particles, even as thin films, still maintain its high specific surface area. This makes it highly favorable to be used as electrochrmic device, due to the reasons explained above.

Another factor that is frequently mentioned in works involving electrochromic devices is the absorption of the thin films as electrodes in electrochromic devices (Bonhote et al 1999). In order to lower the energy requirement for the activation of the electrochromic device, it is favorable is the absorbance is quite high, and especially into the visible light region, as its corresponding optical bandgap energy is quite low, thus requiring less power to activate. The thin films produced in this work have high absorption rates in the UV-Vis region (300-450 nm), requiring lower energies for electrochromic activation if it is used as one.

6.4. Photovoltaic Applications

TiO_2 thin films are viable as electrodes in photovoltaic systems such as dye-synthesizes solar cells (DSSC), and other organic solar cells. Solar cells are basically devices that convert photons into electrical energy via the excitation of electrons in the semiconducting materials that makes up the device. Generally, its efficiency is quite low (2-50%, depending on the type of solar cell), but its potential is enormous, in a sense that it is a clean, renewable source of energy that does not emit any pollutants. However, problems such as chemical stability and low efficiency continue to plague the widespread commercialization and applications of solar cells (Gratzel, 2001).

Extensively studied since the 1960s, literature on the subject is abundant, and some researchers such as Gratzel (2000; 2001; 2005) devoted much of their career to the advancement of solar cells technology. Common material for solar cells are Si, and group III and V materials that makes up its dopant, however, recently, oxides and organic dyes are being studied for its feasibility in applications of solar cells, giving way to Dye-Synthesized Solar Cells and Organic Solar Cells. These types of solar cells are cheap, easy to produce, has high mechanical integrity, however, it still has issues regarding efficiency, which is quite low (usually below 10%). However, its potential benefits far outweigh the disadvantages, and extensive studies are currently being conducted on its applications. Works of Pichot and Gregg (2000) and Cahen *et al* (2000), reflects the renewed fervor in this field.

This work produced nano-TiO_2 thin films, and as such, the scope of this work will be the study of DSSC using nanocrystalline TiO_2 thin films as its electrodes. A basic structure and

operating principles of DSSC is shown in Fig. 6.3. Nanocrystalline TiO_2 immersed in a charge transfer dye makes up the core of the system. Photoexcitation of the dye will produce electrons that will be injected into the conduction band of TiO_2; this electron can be conducted to the outer circuit to generate electricity. This is a reversible process, where the electron lost from the dye is replenished by an electron donated from the conducting electrolyte, ensuring that the process is continuous and electricity generation steady. This ensures that no chemical transformation of any part of the DSSC occurs.

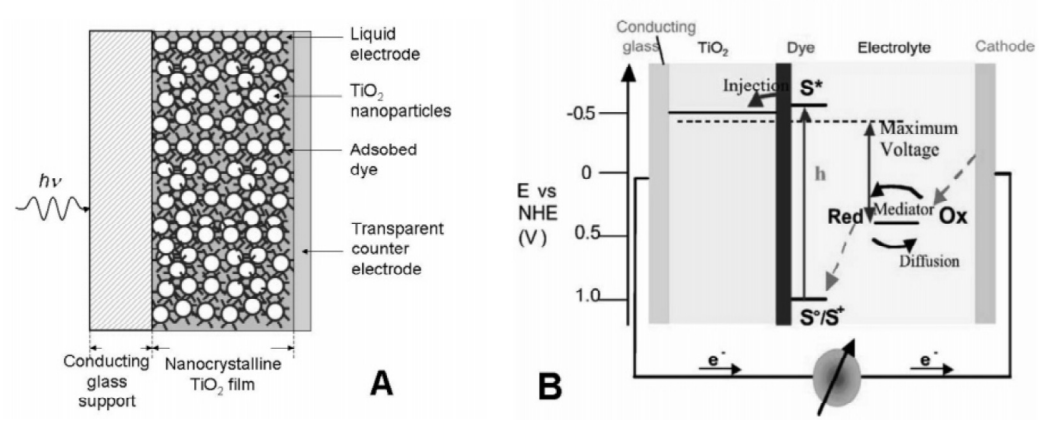

Figure 6.3. DSSC schematics and working mechanisms (from Chen and Mao, 2007)

As such, the electricity generation in a DSSC is controlled by factors such as transport of electronic charges across membranes, and electron-hole recombination rates. As such, the same structural and optical properties that govern the efficiency of electrochromism apply here, such as specific surface area and crystallite sizes.

For DSSC applications, the crystallites need to be small enough so that it would not interfere with the transport of electrons across membranes of DSSCs. The small size and uniformity of distribution will ensure a network of similar sized pores that will allow the electron generated by photoexcitation to be transported across the dye and TiO_2 thin films without being impeded by large crystallites and dense pores. The impediment of movement of these electrons will decrease the efficiency of the DSSC, and it might also degrade the DSSC by chemically changing the nature of the electrodes, as the system depends on the transport of electrons from dye to TiO_2, and from electrolyte to dye to maintain the chemical character of the materials. In this work, the nano-TiO_2 particles produced are crystalline, have crystallites that are smaller than 10 nm, and form a network of pores that is uniform in character, as seen in the SEM micrographs of both the thin films and the nanoparticles. This makes both viable as electrodes in DSSC, although simulations and actual experimentations is the only way to verify this feasibility.

Since the transport of electrons across boundaries is deemed critical to the efficiency of the DSSC, is it important the specific surface area of the TiO_2 is large enough the increase the point of contact between the dye and thin film TiO_2. Higher point of contact between these two surfaces will allow more electrons to be injected into the TiO_2, substantially increasing the efficiency of the DSSC. As mentioned previously, the nano-TiO_2 particles produced in this work has a specific surface area of 186.8 m^2/g, making it viable as an electrode in DSSC applications.

Another factor that is vital in the applications of nano-TiO_2 particles of thin films in DSSC applications is the surface roughness of the thin films. The efficiency of the thin films as electrodes in DSSC depends on the incident light initiating photoexcitation and the electrons getting through to the TiO_2 thin films to drive the load and generate electricity. A

surface with high roughness values will impede the movement of electrons from the dye to the electrodes, thus reducing efficiencies. A rough surface will also have difficulty bonding with the dye, creating a porous, weakly bonded interface between the electrode and dye will cause many of the electrons generated by photoexcitation to be stuck in the dye without being able to cross boundaries in order to generate electricity in DSSC.

The surface roughness of nano-TiO_2 thin films produced in this work is quite small, in the scale of nanometers (15-300 nm). With such low surface roughness, the thin films can be deposited onto the dye with minimal bonding problems, and annealing will increase the integrity of the bonds between the interfaces. The relatively low values of roughness of the nano-TiO_2 thin films will also allow minimal impediment of the transport of charges between the interfaces, increasing the efficiency of the DSSC. Further experimental work needs to be conducted to ensure the viability of the nano-TiO_2 thin films as electrodes in DSSC.

6.5 Chapter Summary

This chapter analyzes and attempts to correlate the structural and optical properties of the nano-TiO_2 particles and nano-TiO_2 thin films for various contemporary applications such as photocatalysis, electrochromic devices and photovoltaic applications. Through literature review it was determined that the products from this work is viable as electrodes/components in these applications, due to the fact that the products are superior in terms such as surface area, crystallite sizes, and optical bandgap energies. Further studies, simulations and experimentation are required in order to determine the actual viability, but

from this preliminary analysis, the application of nano-TiO_2 thin films and nano-TiO_2 particles for these purposes seems very promising.

CHAPTER 7: CONCLUSIONS AND RECOMMENDATIONS

This chapter concludes this work and gives a few recommendations with regards to issues that surfaced potential future work. It will highlight important findings and insight gleamed throughout the completion of this work, and how these facts can be useful in future applications of TiO_2 in the various recommended fields.

The objective and hypothesis of this work outlined and detailed in Chapter 1 has been successfully achieved. Using synthetic rutile, which is a low grade mineral derived precursor, we have managed to produce high quality anatase nano-TiO_2 particles and nano-TiO_2 thin films, using processes modified from conventional means to do so. These precursors and the chemical reagants used in this work are cheap and readily available, mildly toxic, thus requiring no special setup to carry out the experiments, and the process are simple and easy to replicate. The production cost of the nanoparticles and thin films are rather low, which makes it viable for mass production due to the fact that commercial nano-TiO_2 particles and commercial precursors that is used to fabricate TiO_2 thin films are very expensive, and runs into thousands of dollars per kg. In contrast, synthetic rutile only cost RM4.5 per kg, and added up, the whole process to produce 1 kg of nano-TiO_2 particles which serves as a precursor to nano-TiO_2 thin films are less than RM200, which is almost an 80% price reduction. Also, it helps alleviate the problem of ilmenite waste that is generated by the mining industry by converting this waste into high grade materials.

The structural and optical properties of the nano-TiO_2 particles and nano-TiO_2 thin films produced in this work is superior to the commercial products, and certainly superior to certain products that is mentioned in literature, in terms of crystallite size, surface area, crystallinity, optical bandgap energies and absorbance/transmission. The superiority of

these products makes it viable for a number of high end applications such as photovoltaics, electrochromism and photocatalysis.

It is recommended that the next phase of this work involve the extensive study of the viability of these products to be used in high end applications mentioned above. Study in the form of simulation, or actual experimentation is vital in ensuring that these products are actually viable, and will also help us narrow down the kinks and problems that are inherent in their products in order to enable us to rectify it.

Another issue that should be looked into but is outside the scope of this work is the nature of the impurities that is present in the nano-TiO_2 particles. These impurities, although present in significant numbers and showing up in EDXRF and XRD analysis, does not seem to be a detriment to the structural and optical properties of the nanoparticles, and by extension, the thin films. The exact nature of these impurities is still uncertain, and it might be bonded to the Ti-O matrix, or it might just be incorporated into the compound without being actually bonded to the matrix. Either way, if it is actually bonded to the compound, this would present a unique phenomenon because the modified hydrothermal method seems to naturally doped TiO_2, instead of requiring a second process to dope the metallic and nonmetallic impurities to the sample.

REFERENCES

A. Fujishima, T. N. Rao, D. A. Tryk, Titanium dioxide photocatalysis, *J. Photoch. Photobio. C*, 2000, **1,** 1–21

A.Hagfledt, N. Vlachoupoulos, M. Gratzel, Fast Electrochemical Switching with nanocrystalline oxide semiconductor films, *J. Electrochem Soc.* 1994, **141**, L82

A.I. Kontos, I.M. Arabatzis, D.S. Tsoukleris, A.G. Kontos, M.C. Bernard, D.E. Petrakis, P. Falaras, Efficient photocatalysts by hydrothermal treatment of TiO_2, *Catal. Today*, 2005, **101**, 275–281

A.J. Manhique, Walter W. Focke, Carvalho Madivate, Titania recovery from low-grade titanoferrous minerals, *Hydrometallurgy,* 2011, **109,** 230–236

A.L. Castro, M.R. Nunes, A.P. Carvalho, F.M. Costa, M.H. Florencio, Synthesis of anatase TiO_2 nanoparticles with high temperature stability and photocatalytic activity. *Solid State Sci.*, 2008, **10**, 602-606

A.M Gaur, R.Joshi, M.Kumar, Deposition of Doped TiO_2 Thin Film by Sol Gel Technique and its Characterization: A Review. *Proceedings of the World Congress on Engineering 2011*, Vol II, July 6 - 8, 2011, London, U.K.

A. Ogden, J.A. Corno, J.-I. Hong, A.Fedorov, J.L.Gole, Maintaining particle size in the transformation of anatase to rutile titania nanostructures, *J. Phys. Chem. Solids*, 2008, **69,** 2898–2906

B. K. Tanner, T. P. A. Hase, T. A. Lafford and M. S. Goorsky, JCPDS - International Centre for Diffraction Data 2004, *Advances in X-ray Analysis*, **47**

B.N. Akhgar, M. Pazouki, M. Ranjbar, A. Hosseinnia, M. Keyanpour-Rad, Preparation of nanosized synthetic rutile from ilmenite concentrate, *Miner. Eng.*, 2010, **23**, 587–589

C. Garzella, E. Comini, E.Tempesti, C.Frigeri, G.Sberveglieri, TiO_2 thin films by a novel sol–gel processing for gas sensor applications. *Sensor Actuat. B-Chem*, 2000, **68**, 189–196

C. Jonville, Characterisation OF TiO_2Nanoparticles Involving TEM and Image processing analysis. Projet de Fin d'Etudes for ENSPG (France) spent at PUC Rio and CBPF (Brazil)

from 19/04/2004 to 12/09/04

C. Li, B. Liang, L.-h. Guo, Z.-B. Wu, Effect of mechanical activation on the dissolution of Panzhihua ilmenite. *Miner. Eng.*, 2006, **19**, 1430–1438

C.-H. Lu, W.-H. Wu, R. B. Kale, Microemulsion-mediated hydrothermal synthesis of photocatalytic TiO_2 powders, *J. Hazard. Mater.*, 2008, **154**, 649–654

C.S. Kucukkaragoz, R.H. Eric, Solid state reduction of a natural ilmenite. *Miner. Eng.*, 2006, **19**, 334–337

C.Y.W. Lin, D. Channei, P. Koshy, A. Nakaruk, C.C.Sorrell, Effect of Fe Doping on TiO_2 Films Prepared by Spin Coating. *Thin Solid Films*, In Press 2012

D. Cahen, G. Hodes, M. Gratzel, J.F. Guillemoles, I. Riess, Nature of photovoltaic action in dye-synthesized solar cells, *J. Phys. Chem. B*., 1999, **104**, 2053

D. S. Kim, S.-Y. Kwak, The hydrothermal synthesis of mesoporous TiO_2 with high crystallinity, thermal stability, large surface area, and enhanced photocatalytic activity. *Appl. Catal. A-Gen*, 2007, **323**, 110-118

D. Lee, Y. Choi, K. Yong, Morphology and crystal phase evolution of doctor-blade coated $CuInSe_2$ thin films, *J. Cryst. Growth*, 2010, **312**, 3665–3669

E.J. Kumari, K.H. Bhat, S. Sasibhushanan and P.N. M. DAS, Catalytic Removal of Iron from Reduced Ilmenite, *Miner. Eng.*, 2001, **14**, 365-368

E. Morgado Jr., M.A.S. de Abreu, O.R.C. Pravia, B. A. Marinkovic, P. M. Jardim, F. C. Rizzo, A. S. Araújo, A study on the structure and thermal stability of titanate nanotubes as a function of sodium content. *Solid State Sci.*, 2006, 8, 888–900

E. Şayan, M. Bayramoğlu, Statistical modeling of sulfuric acid leaching of TiO_2 from red mud. *Hydrometallurgy*., 2000, **57**, 181-186.

E. Şayan, M. Bayramoğlu, Statistical modeling of sulphuric acid leaching of TiO_2, Fe_2O_3, and Al_2O_3 from red mud. *Trans.IChemE.*, 2001, **79(b)**, 291-296

F. Campus, P. Bonhote, M. Gratzel, S. Heinen, L. Walder, *Sol. Energy Mater. Sol. Cells*, 1999, **56**, 281

F. Flory, L. Escoubas, Optical properties of nanostructured thin films, *Prog. Quant. Electron.*, 2004, **28**, 89–112

F. Pichot, B. Gregg, The Photovoltage Determining Mechanism in Dye-Synthesized Solar Cells, *J. Phys. Chem. B*, 2000, **104**, 6 - 10

F. Sayilkan, M. Asiltürk, S. Erdemoğlu, M. Akarsu, H. Sayilkan,M. Erdemoğlu, E. Arpac, Characterization and photocatalytic properties of TiO_2-nanosols synthesized by hydrothermal process at low temperature. *Mater. Lett.*, 2006, **60**, 230 – 235

G. Mazzocchitti, I. Giannopoulou, D. Panias, Silicon and aluminum removal from ilmenite concentrates by alkaline leaching, *Hydrometallurgy*, 2009, **96**, 327–332

H. Arami, M. Mazloumi, R. Khalifehzadeh, S.K. Sadrnezhaad. Sonochemical preparation of TiO_2 nanoparticles. *Mater. Lett.*, 2007, **61**, 4559–4561

H. Choi, E. Stathatos, D. D. Dionysiou, Photocatalytic TiO_2 films and membranes for the development of efficient wastewater treatment and reuse systems, *Desalination,* 2007, **202**, 199–206

H.-S. Chen, C. Su, C.-K. Lin, Y-F. Hsieh, C.-K. Yang, W.-R. Li, Hydrothermal Preparation of Anatase TiO_2 Nanoparticles for Dye-Sensitized Solar Cells. *J. Chem. Eng. Jpn*, 2009, **42**, 36–42

H. S. Jahromi, H. Taghdisian, S. Afshar, S. Tasharrofi, Effects of pH and polyethylene glycol on surface morphology of TiO_2 thin film, *Surf. & Coat. Tech.*, 2009, **203**, 1991–1996

H.-H. Ou, S.-L. Lo, Review of titania nanotubes synthesized via the hydrothermal treatment: Fabrication, Modification, and Application. *Sep. Purif. Technol.*, 2007, **58**, 179–191

H. P. Shivaraju, K. Byrappa, T. M. S. Vijay Kumar and C. Ranganathaiah, Hydrothermal Synthesis and Characterization of TiO_2 Nanostructures on the Ceramic Support and their Photo-catalysis Performance. *Bulletin of the Catalysis Society of India*, 2010, **9**, 37-50

H.-K. Seo, G.-S. Kim, S.G. Ansari, Y.-S. Kim, H.-S. Shin, K.-H. Shim, E.-K.Suh, A study on the structure/phase transformation of titanate nanotubes synthesized at various hydrothermal temperatures. *Sol. Energ. Mat. Sol. C.*, 2008, **92**, 1533–1539

I. N. Martyanov and K. J. Klabunde, Comparative study of TiO_2 particles in powder form and as a thin nanostructured film on quartz, *J. Catal.*, 2004, **225**, 408–416

I. Strawbridge, P. F. James, Thin Silica Films prepared by Dip Coating, *J. Non-Cryst. Solids*, 1986, **82**, 366 - 372

J. H. Lee, M. Kang, S.-J. Choung, K. Ogino, S. Miyata, M.-S. Kim, J.-Y. Park, J.-B. Kim, The preparation of TiO_2 nanometer photocatalyst film by a hydrothermal method and its sterilization performance for Giardia lamblia, *Water Res.*, 2004, **38**, 713–719

J. M.-Valtierra, M. S.-Cárdenas, C. Fr.-Reyes, S. Calixto, Formation of smooth and rough TiO_2 thin films on fiberglass by sol-gel method. *J. Mex. Chem. Soc.*, 2006, **50(1)**, 8-13

J. Yu, X. Zhao, Q. Zhao, Photocatalytic activity of nanometer TiO_2 thin films prepared by the sol–gel method. *Mater. Chem. Phys.*, 2001, **69**, 25–29

K. Balachandran, Synthesis and characterization of nano TiO_2–peg composite, *International Journal of Engineering Science and Technology (IJEST)*, Vol. **3** No. 5 May 2011, pp.4200-4203

K. Bouabid, A. Ihlal, Y. Amira, A. Sdaq, A. Assabbane, Y. A.-Ichou, A. Outzourhit, E. L. Ameziane, AND G. Nouet, Optical Study of TiO_2 Thin Films Prepared by Sol-Gel, *Ferroelectrics*, 2008, **372**, 69–75, 2008

K. Byrappa, K.M. Lokanatharai, M. Yoshimura, Hydrothermal Preparation of TiO_2 and photocatalytic degradation of hexacyclohexane and dichlorophenyltrichloromethane, *Environ. Technol.*, 2000, **21**, 1085-1090

K. Byrappa, T. Adschiri, Hydrothermal technology for nanotechnology, *Prog. Cryst. Growth Ch.*, 2007, **53**, 117-166

K. Kitsuka, K. Kaneda, M. Ikematsu, M. Iseki,K. Mushiake, T. Ohsaka, Ex situ and in situ characterization studies of spin-coated TiO_2film electrodes for the electrochemical ozone production process. *Electrochim. Acta*, 2009, **55**, 31-36

K. A. Malinger, Aude Maguer, Alain Thorel, Alain Gaunand, Jean-Franc¸ O. Hochepieda Crystallization of anatase nanoparticles from amorphous precipitate by a continuous hydrothermal process. *Chem. Eng. J.*, 2011, **174**, 445– 451

K. Okimura, Low temperature growth of rutile TiO films in modified RF magnetron sputtering, *Surf. Coat. Tech.*, 2001, **135**, 286-290

L. Francioso, D.S. Presicce,A.M. Taurino, R. Rella, P. Siciliano, A. Ficarella, Automotive application of sol–gel TiO_2 thin film-based sensor for lambda measurement. *Sensor Actuat. B-Chem*, 2003, **95**, 66-72

L. Rizzo, S. Meric, D. Kassinos, M. Guida, F. Russo, V. Belgiorno, Degradation of diclofenac by TiO_2 photocatalysis: UV absorbance kinetics and process evaluation through a set of toxicity bioassays, *Water Res.*, 2009, **43**, 979-988

L. Wu, J. C. Yu_, X. Wang, L. Zhang, J. Yu, Characterization of mesoporous nanocrystalline TiO_2 photocatalysts synthesized via a sol-solvothermal process at a low temperature, *J. Solid State Chem.*, 2005, **178**, 321–328

M. Akarsu, M.Asilturk, F. Sayilkan,N. Kiraz, E. Arpac,and H.Sayilkan, A Novel Approach to the Hydrothermal Synthesis of Anatase Titania Nanoparticles and the Photocatalytic Degradation of Rhodamine B. *Turk. J. Chem.*, 2006, **30**, 333-343

M. C. Blount, D. H. Kim, J. L. Falconer, Transparent Thin-Film TiO_2 Photocatalysts with High Activity. *Environ. Sci. Technol.,* 2001, **35 (14)**, 2988–2994

M. Gratzel, Photoelectrochemical Cells, *Nature*, 2001, **414**, 338

M. Gratzel, Perspective for Dye-Synthesized nanocrystalline solar cells, *Prog. Photovolt.* 2000, **8**, 171

M. Gratzel, Dye-Synthesized Solid State Hetereojunction Solar Cell, *MRS Bull.,* 2005, **30**, 23

M. Hussain, R. Ceccarelli, D.L. Marchisio, D. Fino, N. Russo, F. Geobaldo, Synthesis, characterization, and photocatalytic application of novel TiO_2 Nanoparticles. *Chem. Eng. J.*, 2010, **157**, 45–51

M.C. Hidalgo, M. Aguilar, M. Maicu, J.A. Navío, G. Colón, Hydrothermal preparation of highly photoactive TiO_2 nanoparticles. *Catal. Today*, 2007, **129**, 50–58

M.M. Hasan, A.S.M.A. Haseeb, R. Saidur, H.H. Masjuki, M. Hamdi, Influence of substrate and annealing temperatures on optical properties of RF-sputtered TiO_2 thin films, *Opt. Mater.*, 2010, **32**, 690–695

M. Kang, S.-Y. Lee, C.-H. Chung, S. M. Cho, G. Y. Han, B.-W. Kim, K. J. Yoon, Characterization of a TiO_2 photocatalyst synthesized by the solvothermal method and its catalytic performance for $CHCl_3$ decomposition, *J. Photoch Photobio A*, 2001, **144**, 185–191

M. Ottaviani, S. Panero, S. Morzilli, B. Scrosati, M. Lazzari, The Electrochromic Characteristic of Titanium Oxide Thin Film Electrodes, *Solid State Ionics,* 1986, **20**, 197

M. I. Pownceby, G. J. Sparrow, M.J. Fisher-White, Mineralogical Characterisation of Eucla Basin ilmenite concentrates – First results from a new global resource. *Miner. Eng.*, 2008, **21**, 587–597

M. Vishwas, Sudhir Kumar Sharma, K. Narasimha Rao, S. Mohan,K.V. Arjuna Gowda, R.P.S. Chakradhar, Influence of surfactant and annealing temperature on optical properties of sol–gel derived nano-crystalline TiO_2 thin films, *Spectrochim. Acta A.*, 2010, **75**, 1073-1077

M. Ye, Z. Chen, W. Wang, J. Shen, J. Ma, Hydrothermal synthesis of TiO_2 hollow microspheres for the photocatalytic degradation of 4-chloronitrobenzene, *J. Hazard. Mater.*, 2010, 184, 612-619

N. J. Kim, Y. H. La, S. H. Im, B. K. Ryu, Optical and structural properties of Fe–TiO_2 thin films prepared by sol–gel dip coating, *Thin Solid Films*, 2010, **518**, 156-160

N. Saleema, M. Farzaneh, R.W. Paynter, Fabrication of TiO_2 μ-donuts by sol–gel spin coating using a polymer mask, *Appl. Surf. Sci.*, 2009, **255**, 5837–5842

P. Bonhote, E. Gogniat, F. Campus, L. Walder, M. Gratzel, Nanocrystalline Electrochromic Diplays, *Displays*, 1999, **20**, 137

P. Kajitvichyanukula, J. Ananpattarachaia, S. Pongpom, Sol–gel preparation and properties

study of TiO_2 thin film forphotocatalytic reduction of chromium(VI) in photocatalysis process, Sci. Technol. Adv. Mat., 2005, **6**, 352–358

P. Supphasrirongjaroen, P. Praserthdam, J. Panpranot, D.N-Ranong, O. Mekasuwandumrong, Effect of quenching medium on photocatalytic activity of nano-TiO_2 prepared by solvothermal method, *Chem.Eng. J.*, 2008, **138**, 622–627

Q. Chen, Y.Qian, Z. Chen, G. Zhou, Y. Zhang,Preparation of TiO_2 powders with different morphologies by an oxidation-hydrothermal combination method, *Mater. Lett.*, 1995, **22(1-2)**, 77-80

R.Alexandrescu, F.Dumitrache, I.Morjan, I.Sandu, M.Savoiu, I.Voicu, C.Fleaca, TiO_2 nanosized powders by $TiCl_4$ laser pyrolysis, *Nanotechnology,* **15,** 537

R.C.M. Mambote, M.A. Reuter, P. Krijgsman, R.D. Schuiling, Hydrothermal Metallurgy: An Overview of Basic Concepts and Applications. *Miner. Eng.*, 2000, **13**, 803-822

R. Mechiakh, N. Ben Sedrine, R. Chtourou, R. Bensaha, Correlation between microstructure and optical properties of nano-crystalline TiO_2 thin films prepared by sol–gel dip coating, *Appl.Surf. Sci.*, 2010, **257**, 670–676

R. Mechiakh, N. Ben Sedrine, R. Chtourou, Sol–gel synthesis, characterization and optical properties of mercury-doped TiO_2 thin films deposited on ITO glass substrates. *Appl. Surf. Sci.*, 2011, **257**, 9103– 9109

R. Mu, Z. Xu, L. Li, Y. Shao, H. Wan, S. Zheng, On the photocatalytic properties of elongated TiO_2 nanoparticles for phenoldegradation and Cr(VI) reduction, *J. Hazard. Mater.*, 2010, **176**, 495–502

R.S. Sonawane, S.G. Hegde, M.K. Dongare, Preparation of titanium (IV) oxide thin film photocatalyst by sol–gel dip coating. *Mater. Chem. Phys*., 2002, **77**, 744–750

R.S. Sonawane, B.B. Kale, M.K. Dongare, Preparation and photo-catalytic activity of Fe–TiO_2 thin films prepared by sol–gel dip coating. *Mater. Chem. Phys.*, 2004, **85**, 52–57

R. C. Suciu, E. Indrea, T. D. Silipas, S. Dreve, M. C. Rosu, V. Popescu, G. Popescu, H. I. Nascu, TiO_2 thin films prepared by sol - gel method, *J. Phys. Conf. Ser.*, 2009,**182**, 012080

R. K. Wahi, Y. Liu, J. C. Falkner, V. L. Colvin, Solvothermal synthesis and characterization of anatase TiO_2 nanocrystals with ultrahigh surface area, *J. Colloid Interf. Sci.*, 2006, **302**, 530–536

R.A. Zárate, S. Fuentes a, A.L. Cabrera b, V.M. Fuenzalida, Structural characterization of single crystals of sodium titanate nanowires prepared by hydrothermal process. *J.Cryst. Growth*, 2008, **310**, 3630– 3637

S.K. Hazra, S. Roy, S. Basu, Growth of titanium dioxide thin films via a metallurgical route and characterizations for chemical gas sensors, *Mater Sci. Eng. B. Adv.*, 2004, **110**, 195-201

S. Ito, P. Chen, P. Comte, M. K. Nazeeruddin, P. Liska, P.Pe´chy and M. Gra¨tzel, Fabrication of Screen-Printing Pastes From TiO_2 Powders for Dye-Sensitised Solar Cells, *Prog. Photovolt: Res. Appl.* (in press)

S. Janitabar-Darzi, A.R.Mahjoub, A.Nilchi, Investigation of structural, optical and photocatalytic properties of mesoporous TiO_2 thin film synthesized by sol–gel templating technique, *Physica E* 2009, **42**, 176–181

S. Karuppuchamy, J-M. Jeong, D.P. Amalnerkar, H. Minoura, Photoinduced hydrophilicity of titanium dioxide thin films prepared by cathodic electrodeposition. *Vacuum* 2006, **80**, 494–498

S. Karuppuchamy, K. Nonomura, T. Yoshida, T. Sugiura, H. Minoura, Cathodic electrodeposition of oxide semiconductor thin filmsand their application to dye-sensitized solar cells, *Solid State Ionics*, 2002, **151**, 19– 27

S.-H. Nam, S.-J. Cho, C.-K. Jung, J.-H. Boo, J. Šícha, D. Heřman, J. Musil, J. Vlček, Comparison of hydrophilic properties of TiO_2 thin films prepared by sol–gel method and reactive magnetron sputtering system, *Thin Solid Films,* 2011, **519**, 6944–6950

S. W. Oh, S.-H. Park, Y.-K. Sun, Hydrothermal synthesis of nano-sized anatase TiO_2 powders forlithium secondary anode materials. *J.Power Sources*, 2006, **161**, 1314–1318

S. Tanemura, L. Miao, P. Jin, K. Kaneko, A. Terai, N. Nabatova-Gabai, Optical properties of polycrystalline and epitaxial anatase and rutile TiO_2 thin films by RF magnetron sputtering, *Appl. Surf. Sci.*, 2003, **212–213**, 654–660

S. Watanabe, S.Nakagima, K.Uematsu, T.Ishigaki, K. Toda, M. Sato, Low Temperature Synthesis of TiO_2 from acid solutions, *Key Eng. Mat.*, 2010, **421-422**, 498-501

T.A. Lasheen, Soda ash roasting of titania slag product from Rosetta ilmenite, *Hydrometallurgy*, 2008, **93**, 124-128

T. Wen, J. Gao, J. SHEN, Preparation and characterization of TiO_2 thin films by the sol-gel process, *J. Mater. Sci.,* 2001, **36**, 5923 – 5926

U. Khan, N. Benabderrazik, A. J. Bourdelais, D. G. Baden, K. Rein, P. R. Gardinali, L.Arroyo, K. E. O'Shea, UV and solar TiO_2 photocatalysis of brevetoxins (PbTxs), *Toxicon,* 2010, **55**, 1008–1016

Weill, in The Physics and Fabrication of Microstructures and Microdevices, Ed.: Kelly M.J. and C. Weisbuch, Heidelberg 1986

W. Guo, Z. Lin, X. Wanga, G. Song, Sonochemical synthesis of nanocrystalline TiO_2 by hydrolysis of titanium alkoxides, *Microelectron. Eng.*, 2003, **66**, 95–101

X. Chen, S. Mao, Titanium Dioxide Nanomaterials: Synthesis, Properties, Modifications and Applications, *Chem. Rev*., 2007, **107**, 2891-2959

X. Shen, J. Zhang, B. Tian, Microemulsion-mediated solvothermal synthesis and photocatalytic properties of crystalline titania with controllable phases of anatase and rutile, *J. Hazard. Mater.*, 2011, **192**, 651– 657

X. Zhao, M. Liu, Y. Zhu, Fabrication of porous TiO_2 films via hydrothermal method and its photocatalytic performances, *Thin Solid Films*, 2007, **515**, 7127–7134

Y. U. Ahn, E. J. Kim, H. T. Kim, S. H. Hahn, Variation of structural and optical properties of sol-gel TiO_2 thin films with catalyst concentration and calcination temperature, *Mater. Lett.*, 2003, **57**, 4660–4666

Z. He, Z. Zhu, J. Li, J. Zhou, N. Wei, Characterization and activity of mesoporous titanium dioxide beads with high surface areas and controllable pore sizes, *J. Hazard. Mater.*, 2011, **190**,133–139

Z. Liu, B. Guo, L. Hong, H. Jiang, Preparation and characterization of cerium oxide doped TiO_2 nanoparticles, *J. Phys. Chem. Solids*, 2005, **66**, 161–167

Z. Wang, X. Hu, Fabrication and electrochromic properties of spin-coated TiO_2 thin films from peroxo-polytitanic acid, *Thin Solid Films,* 1999, 352, 62-65

Z. Yuan, X. Wang, C. Xu, W. Li, M. Kwauk, A new process for comprehensive utilization of complex titania ore, *Miner. Eng.*, 2006, **19**, 975–978

PUBLICATIONS

ISI Publications

- **Mahdi E. M**. M. Hamdi, Meor Yusoff M. S., The effect of sintering on the physical and optical properties nano-tio_2 synthesized via a modified hydrothermal route, Arabian Journal of Science and Engineering, Major Revision, Resubmitted 26/3/2012 (Q4)

- **Mahdi E. M**., M. Hamdi, Meor Yusoff M.S., Growth of sodium titanate nanobelt from rutile mineral via hydrothermal method, submitted to Journal of Nano Research-SW (Jan 2012), currently under review (Q4)

SCOPUS Indexed publications

- Meor Yusoff M.S., Masliana M., Wilfred P., Parimala D. and **Mahdi M.,** Fabrication of titania Nanotubes by a modified hydrothermal method, Journal of Science and Technology, ISSN: 2229-8460, vol. 2, no.2, Dec. 2010, pp. 15-24 (published in 2011)

- Meor Yusoff, M.S., **Mahmoud, M.E.,** Paulus, W., Annealing of bimetal doped and pure nanotitania: A comparative analysis, IEEE Xplore, ISBN: 978-1-4244-8853-7, 2011

Conference Proceedings

- **Mahdi E. Mahmoud,** Meor Yusoff M. S., Wilfred Paulus, 'The Effect of Annealing and Acid Molarity on the Properties of Bimetal Doped Titania', International Conference of Nanotechnology-Research and Commercialization, 6-9 June 2011, Grand Borneo Hotel, Kota Kinabalu, Sabah.

- Meor Yusoff M.S., **Mahdi Mahmoud**, Masliana M., Wilfred P., Devi P., 2011, A comparative study of fabrication sodium titanate nanowire from commercial chemical and rutile mineral precursors, International Conference of Nanotechnology-Research and Commercialization, 6-9 June 2011, Grand Borneo Hotel, Kota Kinabalu, Sabah.

- Meor Yusoff M.S., **Mahdi Mahmoud**, Masliana M., Wilfred P., Devi P., 2011, 'A comparative study of fabrication sodium titanate nanowire from commercial chemical and rutile mineral precursors' International Conference of Nanotechnology-Research and Commercialization, 6-9 June 2011, Grand Borneo Hotel, Kota Kinabalu, Sabah.

AWARDS

New Formulated Nano Paint for Day and Night Removal of Cigarette Smoke and Odour (Malaysian Technology Expo 2011, Silver Medal, Advance Material category)

APPENDIX

APPENDIX I: BET Raw Data Readings

Quantachrome Corporation
Quantachrome Autosorb Automated Gas Sorption System Report
Autosorb for Windows® Version 1.20

Sample ID 2M TiO_2
Description MTec
Comments
Sample Weight 0.5750 g
Adsorbate NITROGEN
Outgas Temp 300 °C
Operator mhd
Cross-Sec Area 16.2 Å²/molec
Outgas Time 18.0 hrs
Analysis Time 520.8 min
NonIdeality 6.580E-05
P/Po Toler 0
Molecular Wt 28.0134 g/mol
Equil Time 3
File Name 200410.RAW
Station # 1
Bath Temp. 77.40

AREA-VOLUME-PORE SIZE SUMMARY

SURFACE AREA DATA

Multipoint BET..... 1.868E+02 m²/g
Langmuir Surface Area..... 3.095E+02 m²/g
t-Method External Surface Area..... 1.508E+02 m²/g
t-Method Micro Pore Surface Area..... 3.591E+01 m²/g
DR Method Micro Pore Area..... 2.711E+02 m²/g

PORE VOLUME DATA

Total Pore Volume for pores with Diameter
less than 3422.1 Å at P/Po = 0.99437..... 1.645E-01 cc/g
t-Method Micro Pore Volume..... 1.969E-02 cc/g

DR Method Micro Pore Volume..... 9.635E-02 cc/g
HK Method Cumulative Pore Volume..... 8.112E-02 cc/g
SF Method Cumulative Pore Volume..... 8.272E-02 cc/g

PORE SIZE DATA

Average Pore Diameter..... 3.523E+01 Å
DR Method Micro Pore Width ..... 1.044E+02 Å
DA Method Pore Diameter (Mode)..... 1.760E+01 Å
HK Method Pore Width (Mode)..... 1.477E+01 Å
SF Method Pore Diameter (Mode)..... 2.777E+01 Å

DATA REDUCTION PARAMETERS

Thermal Transpiration: OFF
Last Po Acquired 757.41 mm Hg
MaxiDose: OFF
Initial Fill: OFF
DoseWizard: OFF

BJH/DH Moving Average Size: 1

Interaction Constant (K) 2.9600 nm^3 x kJ/mol

Sample ID ilmenite
Description NA
Comments
Sample Weight 2.6070 g
Adsorbate NITROGEN
Outgas Temp 100 °C
Operator mhd
Cross-Sec Area 16.2 Å²/molec
Outgas Time 20.5 hrs
Analysis Time 264.1 min
NonIdeality 6.580E-05
P/Po Toler 0
Molecular Wt 28.0134 g/mol
Equil Time 1
File Name 250811.RAW
Station # 1
Bath Temp. 77.40

AREA-VOLUME-PORE SIZE SUMMARY

SURFACE AREA DATA

Multipoint BET..... 5.938E+00 m²/g
Langmuir Surface Area..... 1.017E+01 m²/g
t-Method External Surface Area..... 5.849E+00 m²/g
t-Method Micro Pore Surface Area..... 8.957E-02 m²/g
DR Method Micro Pore Area..... 8.346E+00 m²/g

PORE VOLUME DATA

Total Pore Volume for pores with Diameter
less than 3261.8 Å at P/Po = 0.99409..... 1.505E-02 cc/g
t-Method Micro Pore Volume..... 1.877E-05 cc/g
DR Method Micro Pore Volume..... 2.966E-03 cc/g
HK Method Cumulative Pore Volume..... 2.388E-03 cc/g
SF Method Cumulative Pore Volume..... 2.448E-03 cc/g

PORE SIZE DATA

Average Pore Diameter..... 1.014E+02 Å
DR Method Micro Pore Width ..... 1.157E+02 Å
DA Method Pore Diameter (Mode)..... 1.780E+01 Å
HK Method Pore Width (Mode)..... 1.483E+01 Å
SF Method Pore Diameter (Mode)..... 2.796E+01 Å

DATA REDUCTION PARAMETERS

Thermal Transpiration: OFF
Last Po Acquired 767.58 mm Hg
MaxiDose: ON

Initial Fill: OFF
DoseWizard: OFF

BJH/DH Moving Average Size: 1

Interaction Constant (K) 2.9600 nm^3 x kJ/mol

Sample ID Synthetic Rutile
Description MTEC
Comments
Sample Weight 0.3390 g
Adsorbate NITROGEN
Outgas Temp 300 °C
Operator MHD
Cross-Sec Area 16.2 Å²/molec
Outgas Time 2.0 hrs
Analysis Time 236.3 min
NonIdeality 6.580E-05
P/Po Toler 0
Molecular Wt 28.0134 g/mol
Equil Time 3
File Name 030310.RAW
Station # 1
Bath Temp. 77.40

AREA-VOLUME-PORE SIZE SUMMARY

SURFACE AREA DATA

Multipoint BET..... 3.932E+00 m²/g
Langmuir Surface Area..... 1.977E+02 m²/g
BJH Method Cumulative Adsorption Surface Area..... 1.064E+01 m²/g
BJH Method Cumulative Desorption Surface Area..... 1.532E+01 m²/g
DH Method Cumulative Adsorption Surface Area..... 1.087E+01 m²/g
DH Method Cumulative Desorption Surface Area..... 1.587E+01 m²/g
t-Method External Surface Area..... 3.932E+00 m²/g
t-Method Micro Pore Surface Area..... 0.000E+00 m²/g
DR Method Micro Pore Area..... 1.549E+01 m²/g

PORE VOLUME DATA

BJH Method Cumulative Adsorption Pore Volume..... 9.883E-02 cc/g
BJH Method Cumulative Desorption Pore Volume..... 9.937E-02 cc/g
DH Method Cumulative Adsorption Pore Volume..... 9.614E-02 cc/g
DH Method Cumulative Desorption Pore Volume..... 9.707E-02 cc/g
t-Method Micro Pore Volume..... 0.000E+00 cc/g
DR Method Micro Pore Volume..... 5.505E-03 cc/g
HK Method Cumulative Pore Volume..... 3.788E-03 cc/g
SF Method Cumulative Pore Volume..... 3.922E-03 cc/g

PORE SIZE DATA

BJH Method Adsorption Pore Diameter (Mode)..... 1.948E+01 Å
BJH Method Desorption Pore Diameter (Mode)..... 2.312E+01 Å
DH Method Adsorption Pore Diameter (Mode)..... 1.948E+01 Å
DH Method Desorption Pore Diameter (Mode)..... 2.312E+01 Å
DR Method Micro Pore Width ..... 1.551E+02 Å
DA Method Pore Diameter (Mode)..... 1.780E+01 Å
HK Method Pore Width (Mode)..... 1.933E+01 Å
SF Method Pore Diameter (Mode)..... 3.866E+01 Å

DATA REDUCTION PARAMETERS

Thermal Transpiration: OFF
Last Po Acquired 757.66 mm Hg
Additional Initialization Information Not Recorded.

BJH/DH Moving Average Size: 1

Interaction Constant (K) 2.9600 nm^3 x kJ/mol

APPENDIX II: PSA RAW DATA

Serial Number: F2395 — MICROTRAC - X100 — Ver:9.1.6 Meas : Original

Particle Size Analysis — Ilmenite — Date: 08/05/11 Meas #: 875 Time: 11:08 Pres #: 1

MALAYSIAN NUCLEAR AGENCY

SAMPLE TESTED USING ASVR AND X-100

USER : MTEC/ MAHDI

Summary		Percentiles		Dia	Vol%	Width
mv = 228.6		10% = 41.29	60% = 251.9	232.5	100%	182.4
mn = 4.394		20% = 160.5	70% = 273.7			
ma = 64.51		30% = 192.2	80% = 302.0			
cs = 0.093		40% = 213.7	90% = 350.7			
sd = 91.20		50% = 232.5	95% = 408.4			

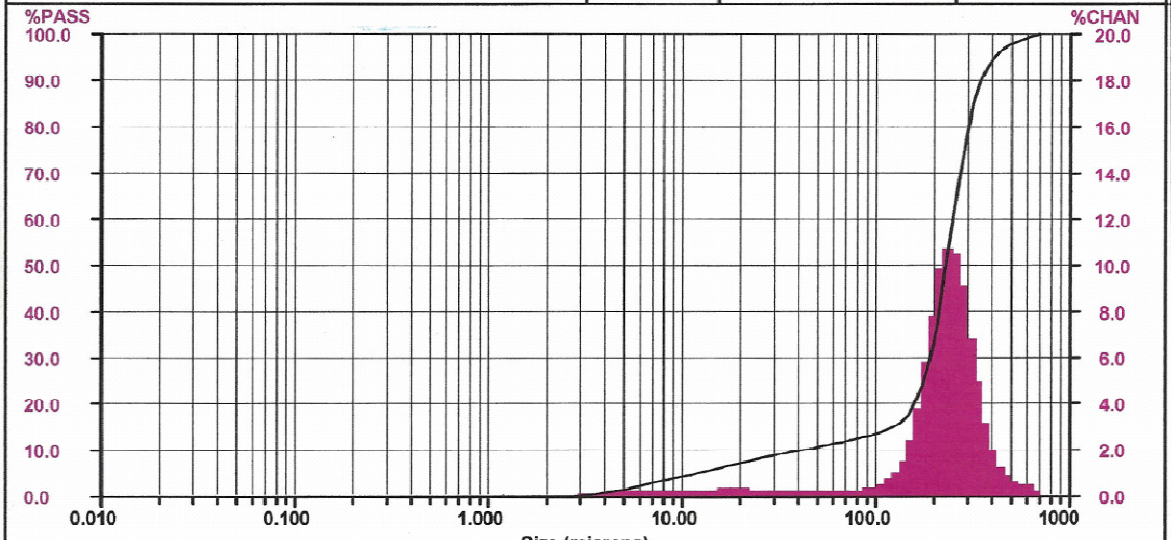

SIZE	%PASS	%CHAN	SIZE	%PASS	%CHAN	SIZE	%PASS	%CHAN	SIZE	%PASS	%CHAN
704.0	100.00	0.34	52.33	10.80	0.30	3.889	0.81	0.23	0.289	0.00	0.00
645.6	99.66	0.52	47.98	10.50	0.29	3.566	0.58	0.20	0.265	0.00	0.00
592.0	99.14	0.57	44.00	10.21	0.29	3.270	0.38	0.15	0.243	0.00	0.00
542.9	98.57	0.70	40.35	9.92	0.28	2.999	0.23	0.11	0.223	0.00	0.00
497.8	97.87	0.94	37.00	9.64	0.29	2.750	0.12	0.08	0.204	0.00	0.00
456.5	96.93	1.39	33.93	9.35	0.30	2.522	0.04	0.04	0.187	0.00	0.00
418.6	95.54	2.09	31.11	9.05	0.32	2.312	0.00	0.00	0.172	0.00	0.00
383.9	93.45	3.25	28.53	8.73	0.33	2.121	0.00	0.00	0.158	0.00	0.00
352.0	90.20	4.97	26.16	8.40	0.36	1.945	0.00	0.00	0.145	0.00	0.00
322.8	85.23	6.93	23.99	8.04	0.37	1.783	0.00	0.00	0.133	0.00	0.00
296.0	78.30	9.22	22.00	7.67	0.39	1.635	0.00	0.00	0.122	0.00	0.00
271.4	69.08	10.54	20.17	7.28	0.39	1.499	0.00	0.00	0.111	0.00	0.00
248.9	58.54	10.85	18.50	6.89	0.39	1.375	0.00	0.00	0.102	0.00	0.00
228.2	47.69	9.96	16.96	6.50	0.38	1.261	0.00	0.00	0.094	0.00	0.00
209.3	37.74	7.85	15.56	6.12	0.37	1.156	0.00	0.00	0.086	0.00	0.00
191.9	29.89	5.84	14.27	5.75	0.37	1.060	0.00	0.00	0.079	0.00	0.00
176.0	24.05	3.87	13.08	5.38	0.36	0.972	0.00	0.00	0.072	0.00	0.00
161.4	20.18	2.49	12.00	5.03	0.35	0.892	0.00	0.00	0.066	0.00	0.00
148.0	17.69	1.63	11.00	4.68	0.35	0.818	0.00	0.00	0.061	0.00	0.00
135.7	16.06	1.07	10.09	4.33	0.34	0.750	0.00	0.00	0.056	0.00	0.00
124.5	14.99	0.76	9.250	3.99	0.34	0.688	0.00	0.00	0.051	0.00	0.00
114.1	14.23	0.56	8.482	3.65	0.35	0.630	0.00	0.00	0.047	0.00	0.00
104.7	13.67	0.46	7.778	3.30	0.35	0.578	0.00	0.00	0.043	0.00	0.00
95.96	13.21	0.40	7.133	2.95	0.35	0.530	0.00	0.00	0.039	0.00	0.00
88.00	12.81	0.36	6.541	2.60	0.34	0.486	0.00	0.00	0.036	0.00	0.00
80.70	12.45	0.35	5.998	2.26	0.33	0.446	0.00	0.00	0.033	0.00	0.00
74.00	12.10	0.34	5.500	1.93	0.31	0.409	0.00	0.00	0.030	0.00	0.00
67.86	11.76	0.33	5.044	1.62	0.29	0.375	0.00	0.00	0.028	0.00	0.00
62.23	11.43	0.32	4.625	1.33	0.27	0.344	0.00	0.00	0.026	0.00	0.00
57.06	11.11	0.31	4.241	1.06	0.26	0.315	0.00	0.00	0.023	0.00	0.00

Distribution: Volume
Progression: Geometric Root8
Upper Edge: 704.0
Lower Edge: 0.021
Residuals: Disabled
Number Of Channels: 120
X100 Extended Range: Yes
Filter: On

RunTime: 30 seconds
Run Number Avg of 3 runs
Particle: DefaultParticle
Particle Transparency: Trans
Particle Refractive Index: 1.81
Particle Shape: Irregular

Database Path: MTWIN.DB

Fluid: Water
Fluid Refractive Index: 1.33
Loading Factor: 0.0539
Transmission: 0.98
Above Residual: 0.00
Below Residual: 0.00

ASVR Flow Rate: 35
Ultrasonic Power: 40 watts
Ultrasonic Time: 60 seconds

PSA analysis of Ilmenite

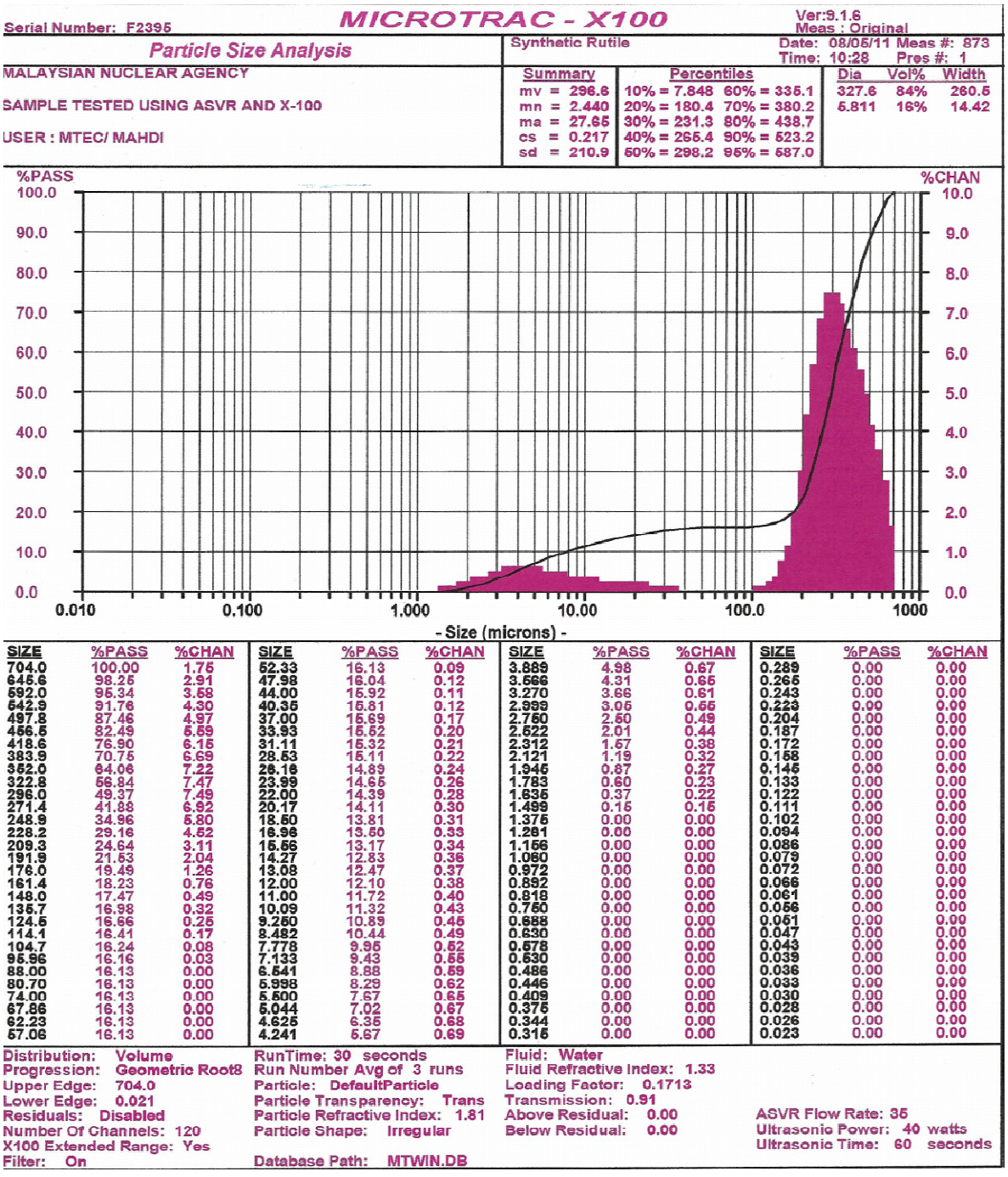

PSA Analysis of Synthetic rutile

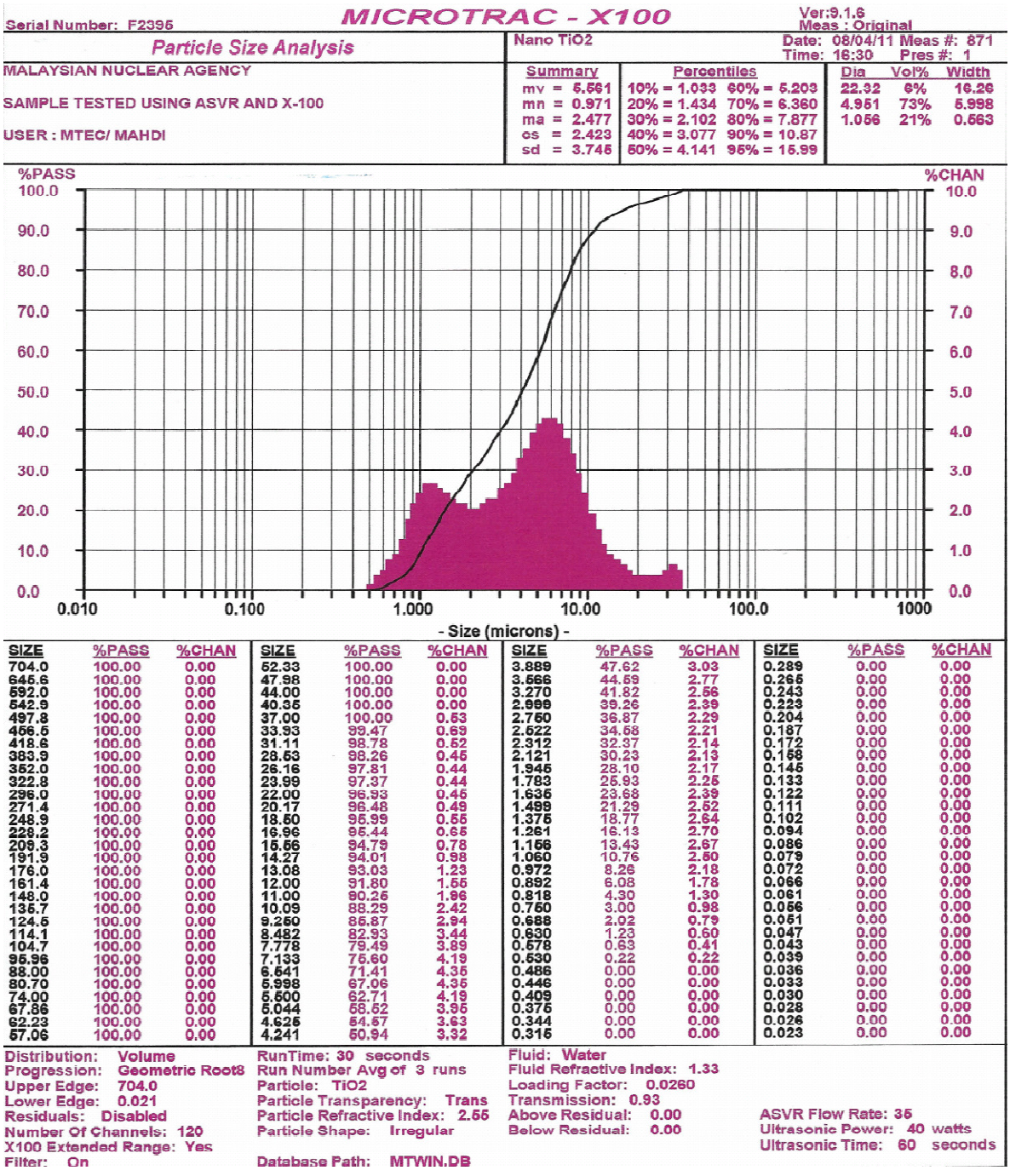

PSA analysis of nano-TiO_2 particles

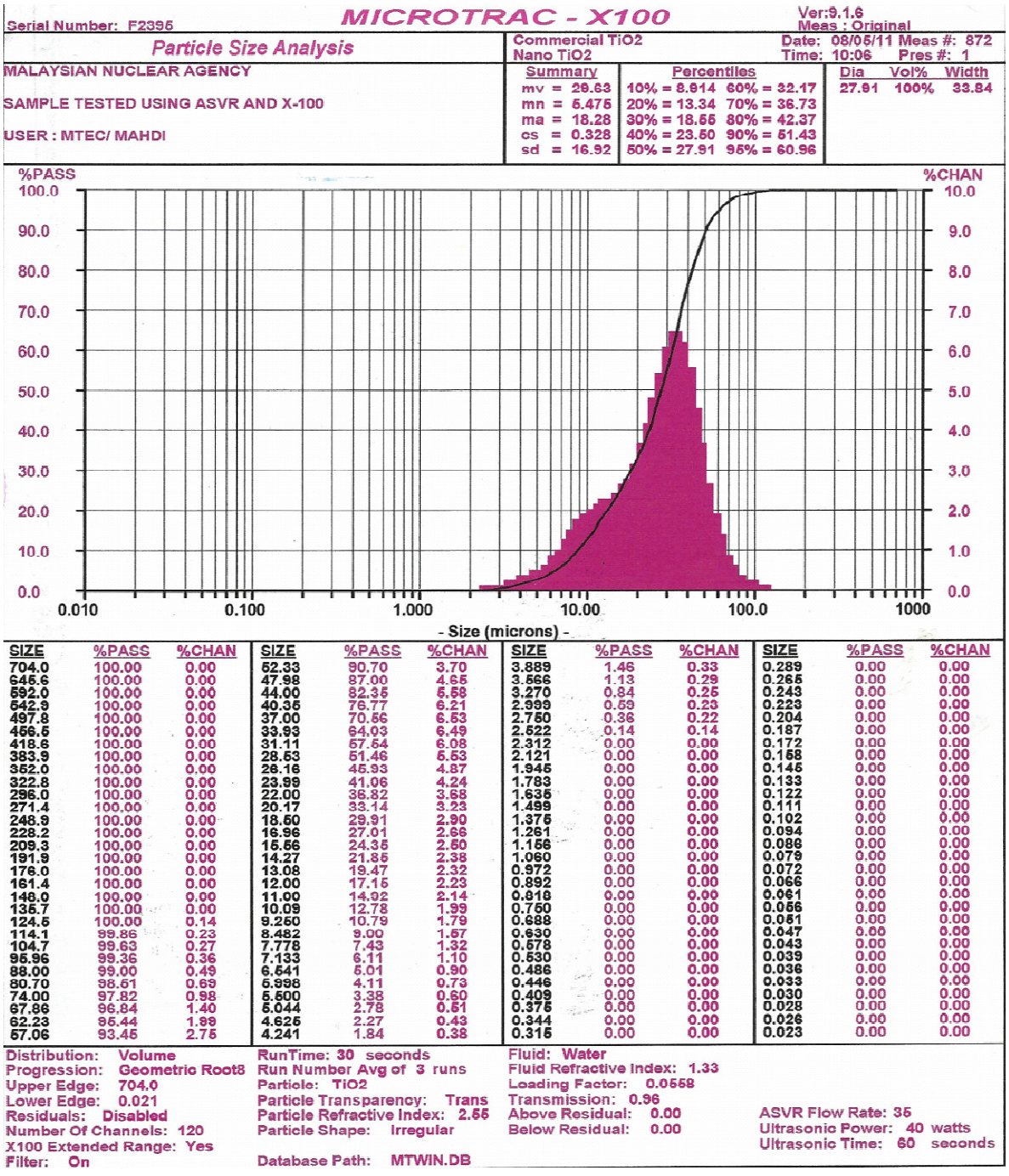

PSA Analysis of Commercial nano-TiO_2 particles

APPENDIX III: EDXRF Results

Quick Report (EDXRF of Nano-TiO_2 particles)

[Sample Image][Sample Information]

No Sample Image

Sample	:	Nano-TiO_2
Operator	:	shimadzu
Comment	:	1ch,100sec
Group	:	easy-100
Meas. Date	:	2011-10-12 15:59:08
Meas. Position(mm)	:	(64.800, 67.638,33.94)
Meas. Diameter	:	50um

[Profile]

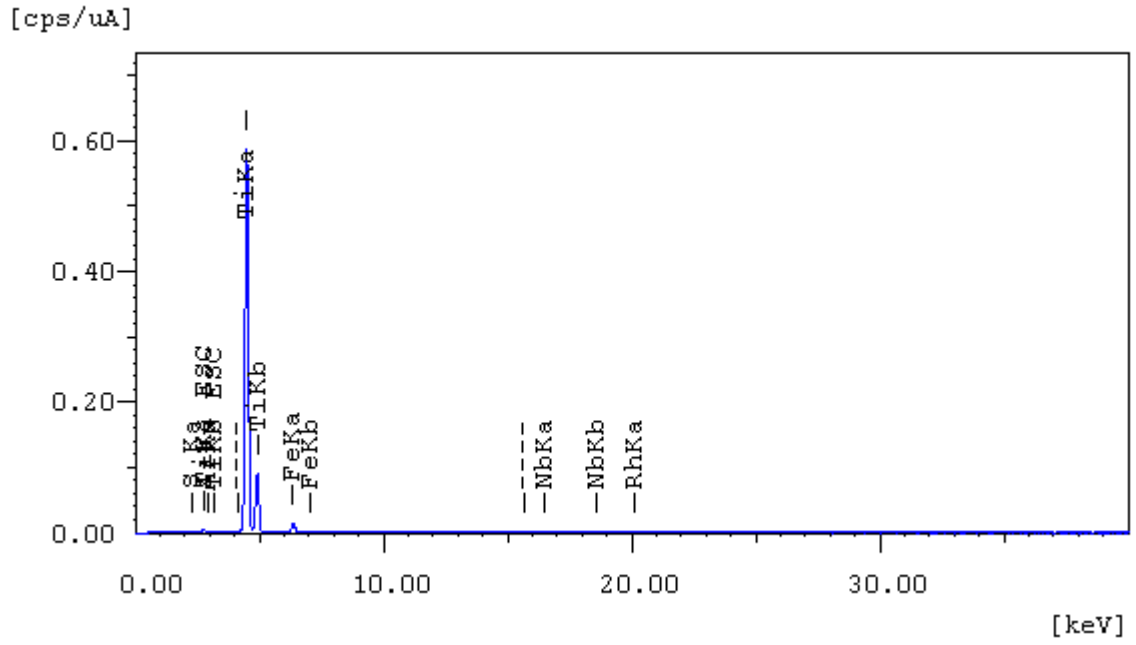

[Meas. Condition]

Instrument :microEDX-1400[SDD:L]		Meas. Diameter:50um				
Channel	TG	kV	uA	Fl	Acq. Anal.(keV)	Time(sec) DT%
Na-U	Rh	50	900	--	0-40 0.00-40.00	RT: 100 2

[Peak List]

Channel	Line	keV	Net (cps/uA)	
Na-U	S Ka	2.31	0.021	QF

TiKaESC	2.76	0.060	
ArKa	2.97	0.026	
TiKbESC	3.17	0.010	
----	4.17	0.015	
TiKa	4.50	9.057	QF
TiKb	4.92	1.428	
FeKa	6.37	0.218	QF
FeKb	7.02	0.035	
----	15.68	0.027	
NbKa	16.51	0.043	QF
NbKb	18.60	0.009	
RhKa	20.09	0.023	

[Quantitative Result]

Analyte	Result	Error	Proc-Calc	Line	Int.(cps/uA)
Ti	91.8634 %	0.1022	Quant.-FP	TiKa	9.057
S	5.2606 %	0.1568	Quant.-FP	S Ka	0.021
Fe	2.2458 %	0.0164	Quant.-FP	FeKa	0.218
Nb	0.6301 %	0.0116	Quant.-FP	NbKa	0.043

Quick Report (EDXRF of Ilmenite)

[Sample Image] **[Sample Information]**

No Sample Image

Sample	: Ilmenite_P004
Operator	: shimadzu
Comment	: 1ch,100sec
Group	: easy-100
Meas. Date	: 2011-10-12 16:30:04
Meas. Position(mm)	: (13.044, 67.988,36.75)
Meas. Diameter	: 50um

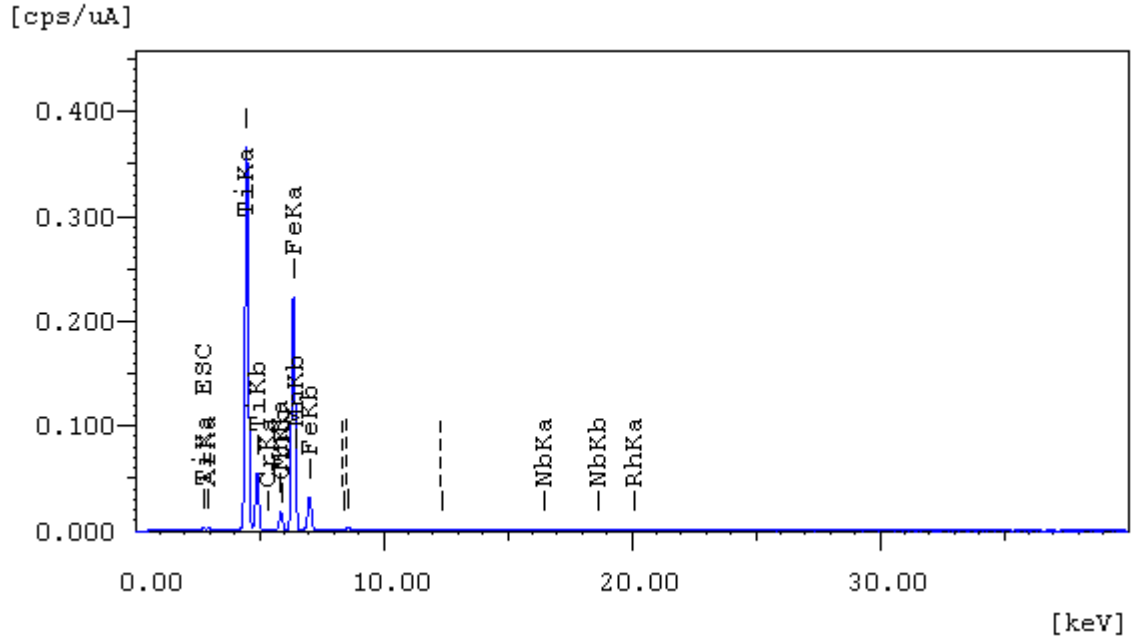

[Meas. Condition]

Instrument: microEDX-1400[SDD:L] Meas. Diameter:50um

Channel	TG	kV	uA	Fl	Acq.	Anal.(keV)	Time(sec)	DT%
Na-U	Rh	50	900	--	0-40	0.00-40.00	RT: 100	2

[Peak List]

Channel	Line	keV	Net(cps/uA)	
Na-U	TiKaESC	2.76	0.037	
	ArKa	2.95	0.028	
	TiKa	4.50	5.622	QF
	TiKb	4.92	0.871	
	CrKa	5.39	0.013	QF
	MnKa	5.88	0.269	QF
	CrKb	5.95	0.002	
	FeKa	6.38	3.817	QF
	MnKb	6.49	0.043	
	FeKb	7.03	0.573	
	----	8.39	0.019	
	----	8.61	0.064	
	----	12.39	0.014	
	NbKa	16.49	0.018	QF
	NbKb	18.70	0.004	
	RhKa	20.12	0.012	

[Quantitative Result]

Analyte	Result	Error	Proc-Calc	Line	Int.(cps/uA)
Ti	58.6037 %	0.0830	Quant.-FP	TiKa	5.622
Fe	37.5794 %	0.0645	Quant.-FP	FeKa	3.817
Mn	3.2524 %	0.0220	Quant.-FP	MnKa	0.269
Nb	0.3758 %	0.0111	Quant.-FP	NbKa	0.018
Cr	0.1886 %	0.0078	Quant.-FP	CrKa	0.013

APPENDIX IV: Sample Raw Data UV-Vis

Wavelength	Reflectance	Absorbance	Transmission
280.5	30.166	0.808	30.245
281	32.031	0.721	31.602
281.5	33.084	0.677	29.547
282	35.208	0.596	30.64
282.5	34.113	0.636	27.98
283	33.145	0.674	27.786
283.5	32.736	0.691	27.778
284	33.601	0.656	28.979
284.5	30.797	0.777	26.404
285	28.229	0.912	25.382
285.5	26.472	1.021	24.775
286	26.742	1.003	26.302
286.5	24.432	1.169	24.427
287	24.468	1.166	24.505
287.5	24.495	1.164	24.269
288	23.649	1.233	22.617
288.5	21.964	1.386	20.141
289	21.748	1.408	19.155
289.5	21.15	1.47	19.093
290	19.928	1.609	17.332
290.5	18.304	1.823	16.366
291	18.352	1.816	15.277
291.5	16.438	2.124	14.203
292	15.322	2.34	13.803
292.5	14.359	2.554	13.582
293	14.158	2.602	12.58
293.5	13.048	2.897	11.684
294	12.753	2.984	11.152
294.5	11.913	3.257	10.535
295	11.319	3.474	10.244
295.5	10.897	3.643	10.507
296	10.209	3.949	9.938
296.5	9.679	4.214	9.315
297	9.718	4.194	9.126
297.5	9.114	4.532	9.317
298	9.04	4.576	9.337
298.5	8.926	4.646	8.808
299	8.946	4.634	8.801

Sample Raw Data from UV-Vis analysis of m_{TiO2} = 1 g nano-TiO_2 thin films